RADIATIVE COOLING BY SPECTRALLY SELECTIVE MATERIALS FOR BUILDINGS

A Dissertation

by

Roxana Family

Submitted to the
Graduate School of Sciences and Engineering
In Partial Fulfillment of the Requirements for
the Degree of

Doctor of Philosophy

in the
Department of Mechanical Engineering

Özyeğin University
...

Copyright © 2018 by Roxana Family

RADIATIVE COOLING BY SPECTRALLY SELECTIVE MATERIALS FOR BUILDINGS

Approved by:

Prof. Dr. M. Pınar Mengüç, Advisor,
Department of Mechanical Engineering
Özyeğin University

Asst. Prof. Zeynep Başaran Bundur,
Department of Civil Engineering
Özyeğin University

Assoc. Prof. Serdar Çelik,
Department of Mechanical Engineering
Southern Illinois University Edwardsville

Prof. Dr. Kürşat Şendur,
Department of Mechatronics Engineering
Sabancı University

Date Approved: 3 October 2018

Asst. Prof. Altuğ Melik Başol,
Department of Mechanical Engineering
Özyeğin University

تقدیم به فرشته ام، مادرم

و قهرمانم، پدرم

وقتی راه رفتن آموختی، دویدن بیاموز و دویدن که آموختی ، پرواز را

راه رفتن بیاموز، زیرا راه هایی که می روی جزیی از تو می شود و سرزمینهایی که می پیمایی بر مساحت تو اضافه می کند. دویدن بیاموز ، چون هر چیز را که بخواهی دور است و هر قدر که زودباشی، دیر و پرواز را یاد بگیر نه برای اینکه از زمین جدا باشی، برای آن که به اندازه فاصله زمین تا آسمان گسترده شوی.

پیشکش به پدر و مادر عزیزم که راه رفتن و دویدن و پرواز کردن را به من آموختند و به من یاد دادند وقتی در دریای زندگی سفر می کنم از توفان ها و امواج نترسم و بگذارم تا از من بگذرند. به من آموختند همیشه به خاطر داشته باشم دریای آرام، ناخدای با تجربه و ماهر نمی سازد، و به من یاد دادند جایی در قلب هر انسان وجود دارد که در آن افکار تبدیل به آرزوها می شوند و آرزوها به اهداف بدل می گردند، جایی که در آن هر غیرممکنی ممکن می شود تنها اگر به اهدافمان ایمان داشته باشیم.

نفس کی توانم زد از شکر دوست

که شکری ندانم که درخورد اوست

To my angel, my mother

and my hero, my father

When you learned to walk, you should learn to run, and when you learned to run, you should learn to fly. You should learn to walk, as the distances that you will pass, will be a part of you. You should learn to run, as whatever you want, will be far, and you should learn to fly, not to be separate of the ground, but to extend your soul in the distance from the Earth to the sky.

To my dear father and mother who taught me how to walk, run and fly. Taught me when I swim in the sea of the life, not to be afraid of the storms and the waves and I should let them pass me. Taught me that I should always keep in mind that a quiet sea does not create a skilled captain, and taught me there is a place in the heart of every human being where thoughts become hopes and wishes become goals, where any impossible thing can happen only if we believe in our goals.

ABSTRACT

Buildings utilize more than one-third of the total energy consumed in counties within the Mediterranean climate zones like in Turkey. Particularly during the summer months, the absorption of solar energy by the buildings increases the required cooling load profoundly. In warmer zones, and in Mediterranean countries, air conditioning applications are becoming more common with every passing year, with their sizable negative impact on energy use. A possible solution to this problem is the radiative cooling of the building surfaces and roofs. This requires tailoring of the radiative properties of surfaces to decrease or increase their natural ability to absorb, emit, or reflect radiant energy. It is favorable to have the utmost emission from the surface with the highest reflection of solar energy and that is for situations where a surface is to be kept cool while exposed to the sun. Note that the Earth's atmosphere is relatively transparent between the wavelength of 8-13 μm; therefore, buildings emitting this is called as "transparency window" for electromagnetic waves. This window allows the radiation emitted by the earth to escape to space with no absorption within the atmosphere. This spectral energy loss, versus the radiation absorbed by the Earth is the reason for the atmospheric radiation cooling. If a building surface emits mostly in this window, than the building can be cooled effectively as well. For daytime radiative cooling which was the goal of this study, coating or painting an object with a strong solar reflector can be considered but significantly mutate its color, which may not be desired. By manufacturing a surface that had an absorptivity large in the spectral region of short wavelengths about the peak solar energy, but small in the spectral region of longer wavelengths where the peak surface emission would occur, it might be possible to absorb almost as a blackbody while emitting very little energy that such surfaces are called "Spectrally selective". Spectrally selective surfaces can also

be useful where it is required to cool an object exposed to incident radiation from any high-temperature source. These situations are objects subjected to the sun, such as the roof of a building. In this study, for the first time sustainable and economically viable materials for radiative cooling in the buildings and the roofs were developed. In the first stage a large group of materials mostly sustainable materials were selected and the morphology and optical properties of them (by optical microscope, UV-Visible, and FTIR) were obtained. For the next stage six sustainable materials were chosen. To evaluate the radiative cooling potential of the samples, the power of cooling was calculated and the results were compared with the selective and broadband emitters. Furthermore, the power of the cooling for the summer and winter time, in daytime and night time cases were also calculated and compared with each other. Heat transfer through most materials is not just a surface phenomenon, but it also needs a volumetric analysis. Therefore, a coupled radiation and conduction heat transfer analysis was solved for all six selected samples. Results are discussed for the selection of the best materials, for different applications on building surfaces. Meanwhile, coupled conduction and radiation was solved for two cases of one layer (concrete roof) and three layers (concrete with soil and the moss on the surface of it) and at last the results were compared with each other.

ÖZETÇE

Binalar, Türkiye'deki gibi Akdeniz iklim bölgelerindeki ilçelerde tüketilen toplam enerjinin üçte birinden fazlasını kullanmaktadır. Özellikle yaz aylarında, güneş enerjisinin binalar tarafından emilmesi, gerekli soğutma yükünü önemli ölçüde artırır. Daha sıcak bölgelerde ve Akdeniz ülkelerinde, iklimlendirme uygulamaları her geçen yıl daha da yaygınlaşmakta ve enerji kullanımı üzerindeki olumsuz etkileri oldukça artmaktadır. Bu soruna olası bir çözüm, bina yüzeylerinin ve çatıların radyal soğutmasıdır. Bu, radyan enerjiyi emmesi, yayması veya yansıtması için doğal yeteneklerini azaltmak veya arttırmak için yüzeylerin ışıma özelliklerinin uyarlanmasını gerektirir. Güneş enerjisinin en yüksek yansımasıyla yüzeyden en yüksek emisyona sahip olmak ve güneşe maruz kaldığında bir yüzeyin serin tutulduğu durumlar için uygundur. Dünya atmosferinin 8-13 μm dalga boyu arasında nispeten şeffaf olduğunu unutmayın; bu nedenle, bunu yayan binalar elektromanyetik dalgalar için "saydamlık penceresi" olarak adlandırılır. Bu pencere, atmosfer tarafından yayılan radyasyonun, atmosferin içinde hiçbir emilim olmaksızın uzaya kaçmasına izin verir. Bu kaybı, Dünya tarafından emilen radyasyona karşı, atmosferik radyasyon soğutmasının sebebidir. Bir bina yüzeyi çoğunlukla bu pencerede ortaya çıkarsa, binadan da etkili bir şekilde soğutulabilir.

Bu çalışmanın amacı olan gündüz ışıma soğutması için, güçlü bir güneş reflektörü olan bir objenin kaplanması veya boyanması düşünülebilir, ancak arzu edilmeyen rengi değiştirebilir. Zirve güneş enerjisi ile ilgili kısa dalga boylarının spektral bölgesinde büyük bir emiciliğe sahip bir yüzey üreterek, ancak pik yüzey emisyonunun meydana geleceği daha uzun dalga boylarının spektral bölgesinde küçükken, bir kara cisim olarak neredeyse absorbe etmek mümkün olabilir. Bu tür yüzeylere 'Spectrally selective 'denen çok az enerji yayarlar. Spektral seçici yüzeyler, herhangi bir yüksek sıcaklık kaynağından gelen radyasyona maruz kalan bir

nesneyi soğutmak gerektiğinde de yararlı olabilir. Bu durumlar, bir binanın çatısı gibi güneşe maruz kalan nesnelerdir. Bu çalışmada, ilk kez binalarda radyasyon soğutması için sürdürülebilir ve ekonomik olarak uygulanabilir malzemeler ve çatılar geliştirilmiştir. İlk aşamada büyük bir malzeme grubu çoğunlukla sürdürülebilir malzemeler seçilmiş ve bunların morfolojisi ve optik özellikleri (optik mikroskop, UV-Görünür ve FTIR) elde edilmiştir. Bir sonraki aşama için altı sürdürülebilir malzeme seçildi. Örneklerin ışıma potansiyelini değerlendirmek için soğutma gücü hesaplanmış ve sonuçlar seçici ve geniş bantlı yayıcılar ile karşılaştırılmıştır. Ayrıca, yaz ve kış dönemi için soğutmanın gücü, gündüz ve gece saatlerinde de hesaplanmış ve birbirleriyle karşılaştırılmıştır. Çoğu malzemeden ısı transferi sadece yüzeysel bir fenomen değil, aynı zamanda volumetrik bir analize de ihtiyaç duyar. Bu nedenle, seçilen altı numunenin tümü için bir birleştirilmiş radyasyon ve iletim ısı transferi analizi çözüldü. Bina yüzeyleri üzerinde farklı uygulamalar için en iyi malzemelerin seçimi için sonuçlar tartışılmıştır. Bu esnada, iki katmanlı bir katman (beton çatı) ve üç katman (toprakla birlikte beton ve yosun) üzerinde eşleşmiş iletim ve radyasyon çözülmüş ve sonuçta sonuçlar birbiriyle karşılaştırılmıştır.

ACKNOWLEDGEMENTS

I would like to express my deepest gratitude to my supervisor Prof. M. Pinar Menguc for giving me this chance to join his group (ECEM/CEEE) and work under his supervision. Over the years I have worked with him he always motivated me and pushed me in my work which helped me develop professionally.

I would like to thank Dr. Serdar Celik, (Associate Professor in Southern Illinois University, Edwardsville, USA), who we worked on a joint project in 2014 and we had a very good research collaboration in whole of these years. I am also grateful to him for accepting to be a committee member in my dissertation.

Gratitude is also due to Dr. Altug M. Basol and Dr. Zeynep Basaran Bundur for serving on my committee, and providing assistance with their comments during my research.

Also, I would like to thank Dr. Kursat Sendur for accepting to be as a committee member in my dissertation.

I am grateful to Mr. Ulas Yildirim for his technical support during my Ph.D. studies.

I would like to sincerely thank to Prof. Cleva W. Ow-Yang for her support at SUNUM Facilities of Sabanci University.

My special thanks to my dear friend Fatin Alani. She was not just a friend for me but closer than a sister who made Turkey feel like home during my Ph.D.

My aunt Parivash Family and my brother Amirreza Family deserve my undying appreciation for their valuable support during all my life.

Finally my deepest gratitude is to my mother Ahang Family, and my father Changiz family. They trained me in the way to be an independent person and not to abandon my dreams at all. In whole of my life they stood in my back and supported me and encouraged me in my education and other aspects of the life.

They are so precious for me and I am thankful everyday for having them.

Contents

List of Tables

List of Figures

Chapter I

INTRODUCTION

1.1 Energy efficiency in buildings

There has been an increase demand in the use of air conditioning system in the buildings for cooling all around the world. In the last two decades has reported an energy crisis during summertime in developing countries due to cooling load requirements in the buildings. Environmental pollution was the reason of increasing consumption of energy in global warming and ozone layer depletion [1].

Global energy demand in buildings increases by 60% from the year 2007 to 2050 as predicted by IEA, so there will be higher ownership rates for existing energy-consuming devices and also increasing demand for new types of energy services. This increase in using energy in buildings is mainly due to the growing demand for energy used for cooling and heating in buildings [2].

The western and most developed countries that are considered responsible for consuming the most of the world's energy, achieved to the conclusion on four main aspects in the following for conserving energy resources which are based on the issue to minimize the effects of the present crises and future energy demands.

1. Lowering energy consumption in the buildings by energy management and efficient buildings.

2. The urgent requirement for renewable and alternatives energy sources of lower price.

3. The design of buildings for the achievement of thermal efficiency such as better insulation.

4. Conserving energy sources, water, and materials.

As without energy, buildings could not be operated, therefore various improvements have been made in lighting, plant, insulation, and controls that help towards

achieving an energy efficient building, but the significant thing is to know what is meant by “Energy Efficiency”. Utilizing the minimum amount of energy for cooling, heating, and lighting which is required to maintain the comfort conditions in building, is “Energy Efficiency”. The building envelope is an important factor in energy efficiency which includes all of the building elements such as roofs, windows, walls, doors, and foundations. To preserve the building cool in the summer and warm in the winter, all of these components should work well together [3].

The cooling and heating systems use up the most energy in a building, nevertheless some controls and building energy management systems might reduce the energy usage of these systems, but cooling by using air conditioning consumes a higher proportion of energy in comparison with heating in consumption of energy in tropical buildings [4].

Space cooling which means an electric powered fan or air conditioning system is growing increasingly in global energy demand. Global sales of air conditioning systems have been growing steadily and annual sales of more than tripled to 135 million units have been reported since 1990· Approximately one-fifth of all the electricity used in the buildings is for cooling, and the increase in the demand for space cooling is already putting a massive strain on electricity systems in many countries, as well as driving up emissions.

Space cooling can show more than 70% of peak residential electrical demand on severely hot days in countries like the Middle East and parts of the United States. Averaged across all countries, space cooling accounted for around 14% of peak demand in 2016· Operating, building, and maintaining the electricity capacity to meet this peak demand is very expensive as it is used only for limited periods which drives up the total costs.

Carbon dioxide (CO_2) emissions from cooling have tripled since 1990 up to now too and caused grow of the local air pollutants. If energy efficient buildings are well maintained and manage energy effectively, so they do not cost inevitably more to build rather than normal buildings, and also, they are set to be very

comfortable, reliable, and as productive as a normal building [2].

People kept cool in buildings by using natural methods before refrigeration technology adventure. These natural methods were:

1. Breezes flowing through windows.

2. Water evaporating from fountains and springs.

3. Large amounts of earth and stone for absorbing daytime heat.

By employing passive cooling techniques which are now considered as an "alternative" to mechanical cooling, it would be possible to eliminate air conditioning or mechanical cooling. Passive cooling will be explained more with details in the following.

1.2 What is Passive Cooling?

Passive cooling mentions design or technologies features which developed to cool buildings without or with minimal energy consumption in order to alter their energy efficiency. These techniques or technologies might be used to minimize or eliminate mechanical air conditioning requirements in areas in which cooling is a dominant problem. In many modern buildings, thermal comfort in summer is related principally to a balance of temperature and humidity, more than simply maintaining the indoor air temperature below 24°C [5].

Passive cooling systems are key factors in discounting the impact of buildings on the environment, and these systems use non-mechanical methods to maintain a comfortable indoor temperature. Furthermore, passive cooling techniques can mitigate the peak cooling load in buildings, therefore reducing the size of the air conditioning equipment and the period for that it is usually required. In the following several passive cooling techniques will be reviewed, and their role in providing thermal comfort and its significance in energy conservation will be analyzed [1].

1. Natural Ventilation: This technique depends on air movement for cooling. Window openings on the opposite sides of the building can raise the cross ventilation driven by breezes. Designers often decide to enhance natural ventilation by

using tall spaces called chimney or stacks, while natural breezes cannot be scheduled. Since warm air could escape by openings near the stack, cooler air enters into the building from openings near the ground. For the flow of the air, ventilation requires the building to be open in the daytime.

2. High Thermal Mass: This technique is based on the capability of materials in the building to absorb heat in the daytime. Each night the mass releases heat, making it ready to absorb heat again the next day.

3. High Thermal Mass with Night Ventilation: This technique relies on the daily heat storage of thermal mass in addition to night ventilation that cools the mass. The building should be closed in the daytime and opened in the nighttime to flush the heat away.

4. Evaporative Cooling: In evaporative cooling, the indoor air temperature will decrease by evaporating water. This is regularly done directly in the space in dry places, but on the other hand, indirect methods, such as roof ponds, permit evaporative cooling to be used in more temperate climates too. Evaporative and ventilation and are frequently supplemented with mechanical means like fans. They use less amount of energy to maintain comfort in comparing with the refrigeration systems. The usage of these strategies in completely passive systems which require no energy to operate or additional machinery would always be possible [6].

Theoretical studies have depicted that the application of all the above techniques in buildings might reduce their cooling load up to 50%-70% [1].

Passive radiative cooling is based on the reality that the sky is like a heat sink within the atmospheric window.

The transparency window of Earth's atmosphere for electromagnetic waves is between the wavelength of 8-13 μm which coincides with peak thermal radiation wavelengths at terrestrial temperatures. This range is called "Atmospheric window" which is that portion of the electromagnetic spectrum that without any distortion or absorption can be transmitted through the atmosphere.

Therefore if the energy transfer is limited to this waveband, cooling can be

possible without any energy consumption [7].

Some of the attempts for passive radiative cooling until the past decade or two are seen in the cover foils and optimization of selective surfaces to explore possibilities for both diurnal (daytime) and nocturnal (nighttime) radiative cooling [8].

The ongoing increase of energy consumption of air conditioning offers a more significant impact on buildings and examination of the urban environment as well as to an extended application of passive cooling techniques [1].

Appropriate research should aim to describe and understand comfort requirements under transient conditions during the summertime.

There is a strong solar heat flux at the 0·2 to 2 μm waveband during the day, which makes the passive radiative cooling very difficult [7].

Actually, passive radiative cooling is very attractive since it is environmentally friendly and requires no electricity [9].

The first aim of any building designer should be passive solar energy-efficient building design, as in most cases, it would be a relatively low-cost exercise. Nowadays incorporating passive cooling techniques in buildings as an architectural expression and inherent part of design is crucial for architects and building engineers. Interpolation of these passive cooling techniques would definitely decrease the dependency on artificial means for minimizing the environmental problems and thermal comfort owing to extreme consumption of energy and other natural resources. Accordingly, there will be a built form which is more sustainable, more environment friendly, and more climate responsive of tomorrow [1].

In this study, the principal focus will be the structural optimization of sustainable materials to achieve desirable spectral radiative properties for passive radiative cooling at day and night time.

1.3 Radiative Cooling

Passive cooling systems propose essential impact as energy saving devices because of their ability to operate without external energy. Radiative cooling is such a method with the potential of offering a high cooling power with optimizes design in the device and under proper atmospheric conditions. The importance of radiative cooling and its capable application was emphasized a few decades ago [10].

Radiative cooling with its highly efficient passive cooling potential, promises a fundamental impact. Modern demonstrations for daytime radiative cooling below the ambient temperature represent their potential for practical energy saving applications [10].

Part 1:

It is often desirable to tailor the radiative properties of surfaces to decrease or increase their natural ability to reflect, absorb, or emit radiant energy. The objective might be to provide a desired directional or spectral performance. For situations where a surface is to be kept cool while exposed to the sun, it is desired to have the maximum reflection of solar energy with maximum radiative emission from the surface [11].

The purpose of radiative cooling is to modify the structure of materials to increase their spectral emissivity in the atmospheric window and decrease it in other regimes [11]. It is described in Figure 1.

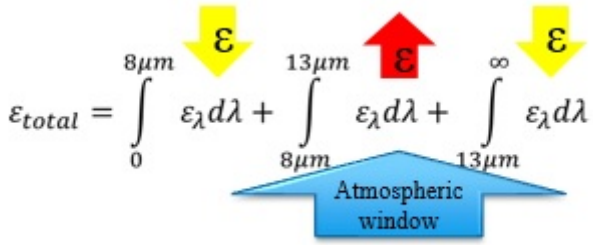

Figure 1: A schematic of increasing and decreasing the spectral emissivity in the atmospheric window and other ranges for the potential of radiative cooling.

A selective emissive radiator with solar reflectance (97%) can deliver a fundamental passive cooling during the daytime, which causes temperatures as low as 15° below the ambient temperature. Nevertheless, the realization of such selective radiators with essential solar reflection is still a major challenge. In addition, the atmospheric conditions in a special geographical location would play a substantial role for significant radiative cooling efficiency. Moreover, the cooling efficiency might be enhanced while radiative cooling combining with other passive cooling devices like phase change materials. (Phase change material is a substance with a high heat of fusion which releases or stores significant amounts of thermal energy while solidifying or melting at a certain temperature, will be explained more in section 2.2.4) [10].

For a given object, creating an imbalance between the absorbed radiation from the environment, and the heat radiated outwards through the transparency window is significant to have radiative cooling. There have been many studies about radiative cooling below ambient temperatures at night time, however for daytime cooling, one must also take into account solar absorption. It is important to attain up to 88% solar radiation reflection, in order to get an equilibrium temperature below the ambient in daytime radiative cooling. However covering an object with a good solar reflector definitely changes its color, that might not be favorable [12].

A highly reflecting coating like a polished metal might be useful for some applications too. This may reflect most of the incident energy, however, be poor for radiating away the energy which was generated or absorbed within an enclosure, such as by electronic equipment. This behavior is significant for the energy balance in the vacuum of outer space, but on the other hand is not significant when there is appreciable convective cooling which dominates over radiant emission. Some metals might not work well as they have a tendency toward lower reflectivity at the shorter wavelengths characteristic of the incident solar energy [13].

Common thin plastic sheets used for solar reflection are Teflon, Kapton, and Mylar with Aluminium or silver coated on the backside [11]. Polished metals and

Fused-silica second-surface mirrors are essentially stable in orbit against to Aluminized Kapton, Metalized Teflon, and some light colored paints which darken over a long period of time and degrading their performance [14]. Figure 2 shows one of the solar reflectors schematic.

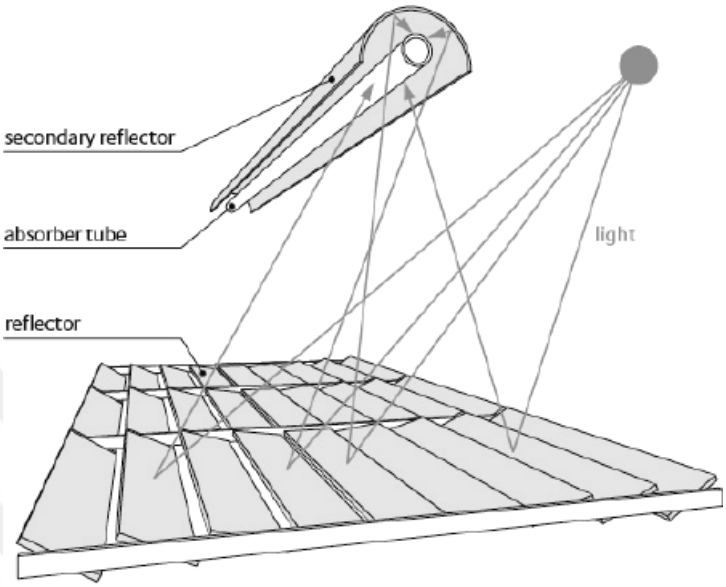

Figure 2: A schematic of a solar reflector [15].

If a surface can be manufactured with a large absorptivity in the short wavelengths spectral region about the peak solar energy, yet small in the longer wavelengths spectral region where the peak surface emission would happen, so it might be possible to absorb like a blackbody while emitting very little energy. These surfaces are called "spectrally selective". Such spectral selective surfaces might be useful where it is desirable to cool an object exposed to incident radiation. Current situations are objects exposed to the sun, such as a cryogenic fuel tank in space, a hydrocarbon storage tank, or the roof of a building. White paint is an example of the spectrally selective surface [13]. Paints not only reflect the incident solar radiation which is dominant at short wavelengths, but also radiate well at the longer wavelengths [11]. Titanium dioxide white paint is also a superior example of eternal solar-selective coating, to polyvinyl fluoride film with an aluminized coating on the underside that is used for spacecraft thermal control [16].

Different spectrally selective surfaces have been defined for thermal control in outer space. Among these surfaces, the optical solar reflector or OSR is a mirror composed of a glass layer silvered on the back side. The reason for selecting the glass is that the glass becomes transparent in the short wavelength region (visible range), and lets the silver reflect incident radiation in this spectral region. The energy absorbed by the glass at longer wavelengths, and that small fraction of short-wavelength energy which is absorbed by the silver, are radiated away by the glass in the longer-wavelength (infrared region) where glass emits well [11].

A mathematical relationship formulated by Max Planck to explain the spectral-energy distribution of radiation emitted by a blackbody (a hypothetical body that absorbs all radiant energy falling upon it, reaches some equilibrium temperature, and then re-emits that energy as quickly as it absorbs it).

Planck supposed that the radiation sources are atoms in a state of oscillation and that the vibrational energy of each oscillator might have any of a series of discrete values but never any value between. Planck also assumed that while an oscillator changing from a state of energy E_1 to E_2 (a state of lower energy), the quantum of radiation or $E_1 - E_2$ would be equal to the product of the frequency of the radiation (υ) and a Planck's constant (h), which he defined from blackbody radiation data that $E_1 - E_2 = h\upsilon$.

The law for the energy radiated per unit volume (Eλ) by a cavity of a blackbody in the wavelength interval λ to $\lambda + \Delta\lambda$ ($\Delta\lambda$ is an increment of wavelength) might be written in terms of Planck's constant that is hc, c is the speed of light, k is the Boltzmann constant, and T is the absolute temperature [11]. In Figure 3 Planck's law is shown.

$$E_\lambda = \frac{8\pi h_c}{\lambda^5} \frac{1}{\exp(^{h_c}/_{\lambda kT}) - 1} \tag{1}$$

Part 2:

To be able to explain radiative cooling, we need to perform radiative transfer equation on a surface. As seen in Figure 4 and equations in the following, we can

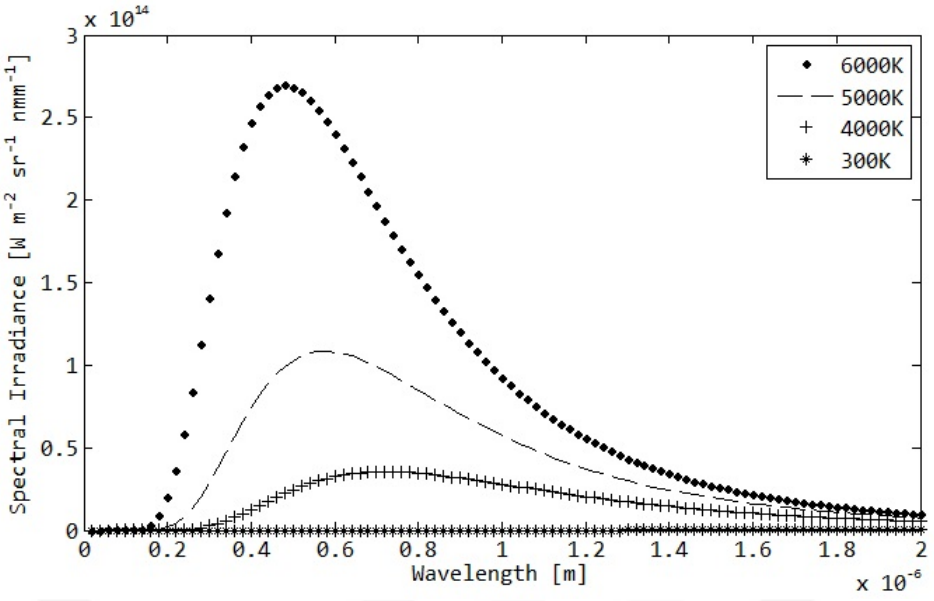

Figure 3: Planck Radiation Law plotted by Matlab and based on Equation 1.

define the explanation of radiative cooling like this:

$$Q_{in} = Q_{solar,absorbed}(T_{Sun}) + Q_{atm,absorbed}(T_{amb}) \tag{2}$$

$$Q_{out} = Q_{emitted}(T_s) + Q_{convected} \tag{3}$$

$$Q_{in} = G_{Sun}(T_{Sun})\alpha_s(T_s) + G_{atm}(T_{amb})\alpha_s(T_s) \tag{4}$$

$$Q_{out} = \varepsilon_s \sigma T_s^4 + h_c(T_s - T_{amb}) \tag{5}$$

$$Q_{net} = Q_{out} - Q_{\,in} \tag{6}$$

In day time if $Q_{out} > Q_{in}$ so we have radiative cooling. In space the radiative cooling will be as explained in Figure 5 and equation (7).

$$Q_{net} = Q_{out} - Q_{in} > 0 \tag{7}$$

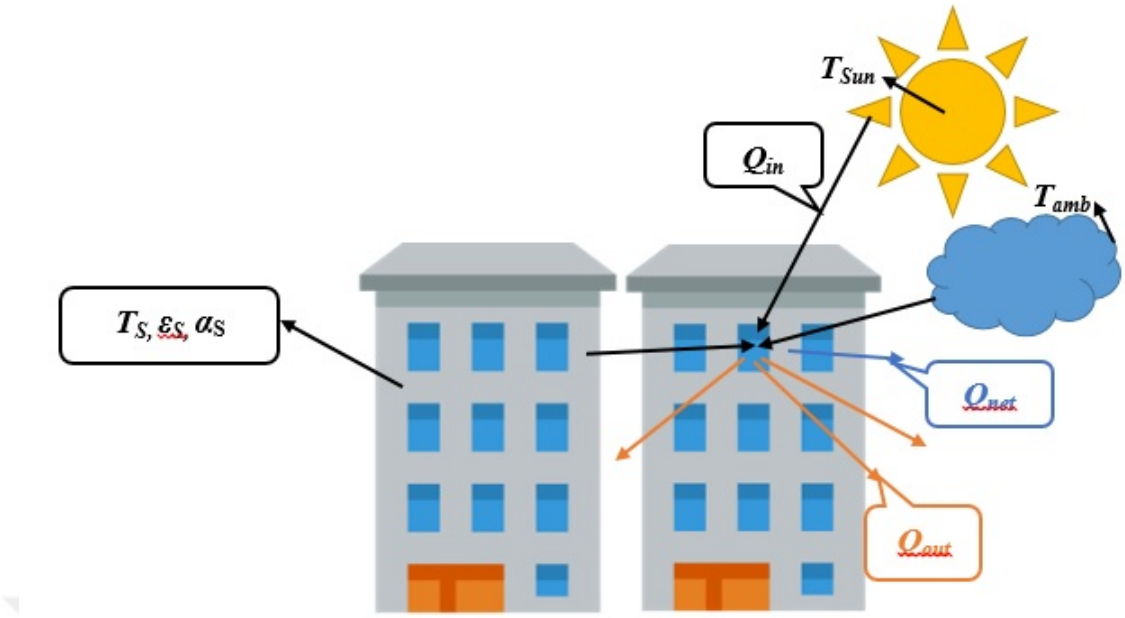

Figure 4: Day time Radiative Cooling.

This happens until T_S reaches to 0 K. One of the other situations is night time radiative cooling that we have to consider it in two states of clear sky and dusty or humid sky. In clear sky, we assume clear night with no dust and humidity so we have night time radiative cooling generally as shown in Figure 6 and equation (8).

$$Q_{in} \ll Q_{out} \tag{8}$$

But if we have dust and humidity in the night time, so it will be like Figure 7 and equation (9). Therefore we do not have night time radiative cooling in this case.

$$Q_{in} \approx Q_{out} \tag{9}$$

1.4 Statement of the problem

Climate change or global warming is observed century-scale rise in the average temperature of the Earth's climate system [17].

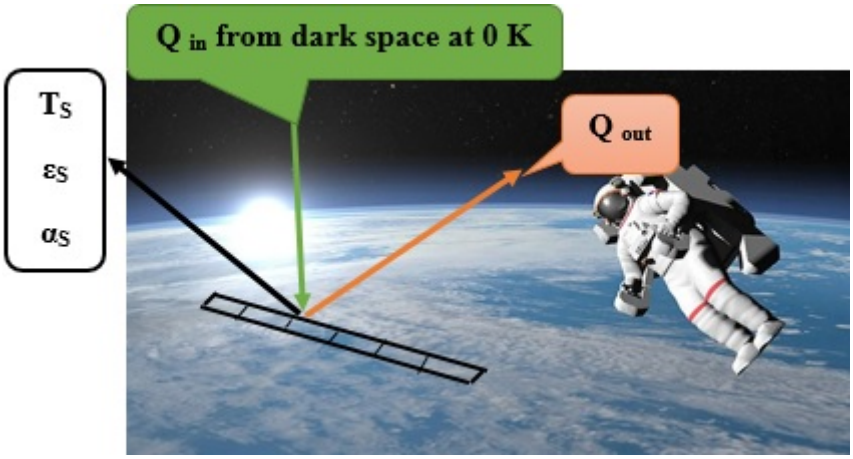

Figure 5: A schematic for Radiative Cooling in Space.

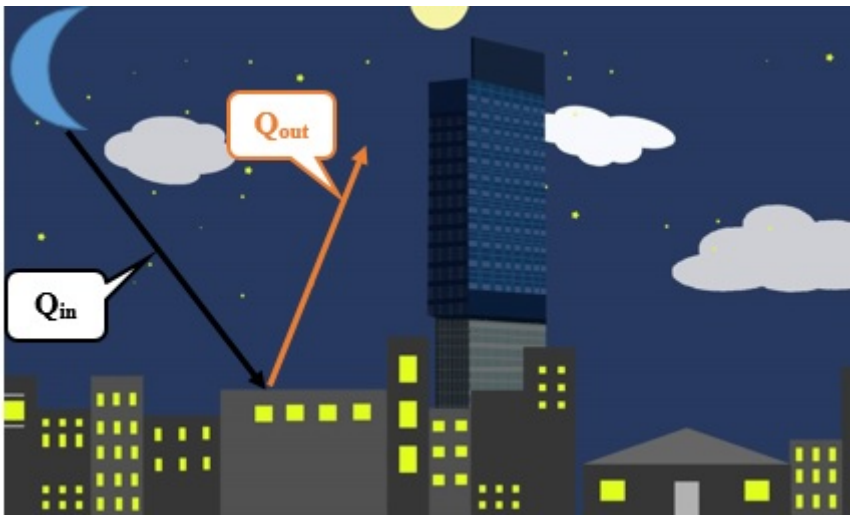

Figure 6: A schematic for Night time Radiative Cooling.

Heat is transferred to a house via roof, floor, doors, windows, and walls. The percentage heat transferred through these components is illustrated in Figure 8.

Figure 8 shows that the roof transfers the highest heat load. Roof is one of the significant contributors to heat gain and loss in a house. Roof structures, materials, and colors are different factors that affect heat transfer through a roof of the house. Other factors are the spectral properties like reflectivity and emissivity. For our case that is radiative cooling, spectral emissivity must be high in atmospheric window band which is explained before and low in the other bands [18].

Approximately 50% of the heat load comes from the roof, therefore radiative

Figure 7: Night time Radiative Cooling (dusty or humid sky).

cooling in the buildings and especially roofs has been studied in this project.

Radiative cooling was often limited at nighttime as proper materials with high IR emission within the atmospheric window and yet delivering powerful solar reflection at daytime was not achieved.

Daytime cooling below the ambient temperature could not be achieved as the absorbed solar energy exceeded the emitted energy by radiation.

Photonic radiative coolers and microstructure based thermal emitters can propose highly efficient cooling power with their selective IR emission within the atmospheric window [10].

The purpose of this dissertation is to identify new group of materials that can be replaced by old materials in radiative cooling applications in the roofs. These materials would be cheaper and the fabrication process of them would be easier rather than the old materials, and would be explained in the following chapters. To evaluate radiative cooling in the roofs, we have to evaluate the heat transfer through it. Heat transfer through the roof would be through radiation and conduction. For the radiation part that is a surface phenomenon, Power of

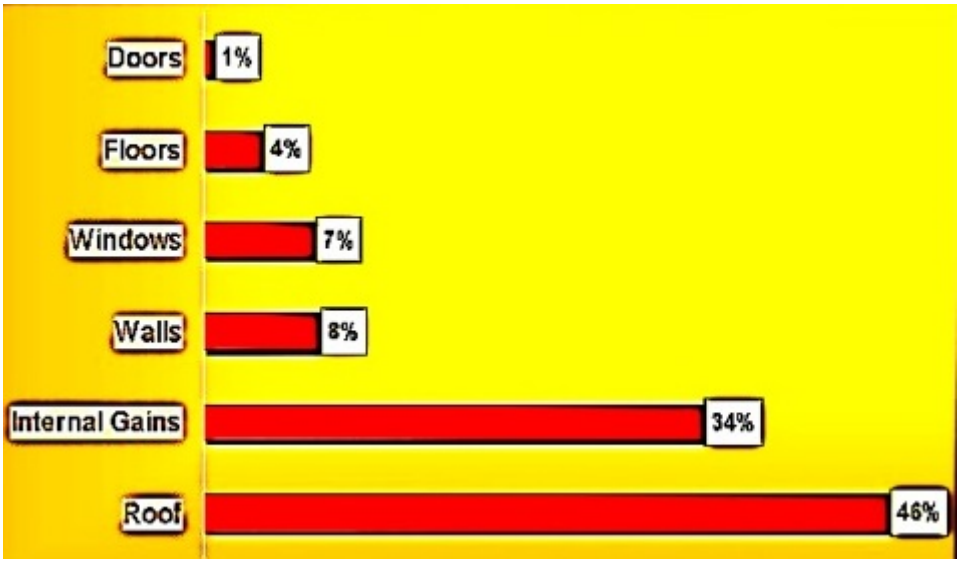

Figure 8: Percentage of heat transferred at different components of the house (ASHRAE Model).

the cooling has been calculated numerically. Since the materials in this project had not been used for radiative cooling in the past, so for getting the properties of them experimental work have been done (UV-visible and FTIR for radiation part and RHLM for conduction part). And for evaluating the total heat transfer through the roofs conduction also should be added, and here coupled conduction and radiation was solved.

The radiation energy within a medium is tracked by solving the radiative transfer equation (RTE). Furthermore, the conservation of energy or the first law of thermodynamics must be satisfied, resulting in the overall energy equation (EE). The EE and RTE are coupled in a participating medium. The divergence of the radiative flux, enters as the sink or the source term in the EE, so long as the temperature that is obtained by solving the EE at any point, influences local emission and radiative properties affecting the solution of the RTE [11][19].

As mentioned before, our objective in this study is to evaluate radiative cooling at the roofs and walls of buildings, by using inexpensive sustainable materials which have not been used up to now. In Figure 9, a schematic for building-related radiative cooling applications is presented; the primary goal of the present study

is highlighted by bold lines.

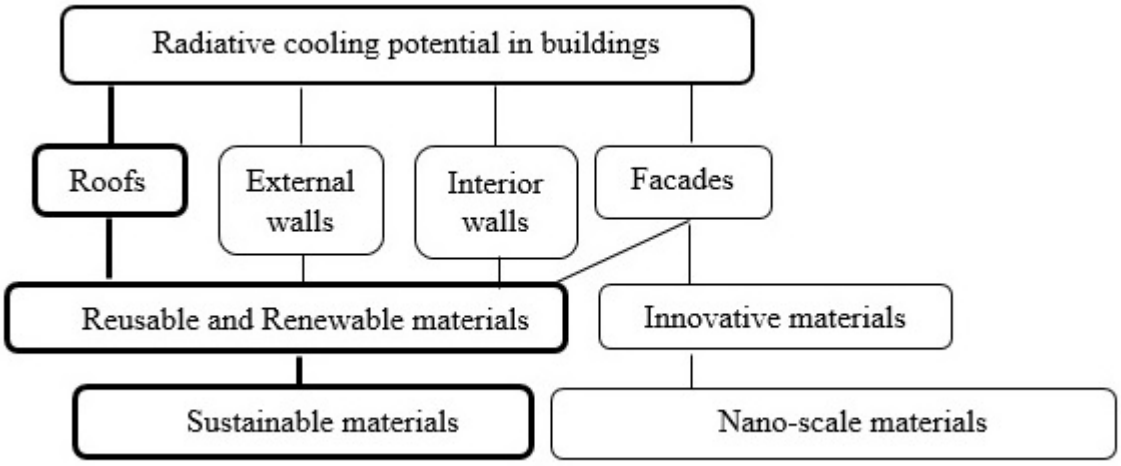

Figure 9: A schematic to show different materials, which can be used for radiative cooling applications in the built environment.

This study for the first time looks at a new group of materials in radiative cooling and also investigates the total heat transfer through the roofs of the buildings via radiation and conduction.

Chapter II

LITERATURE REVIEW

2.1 Historical Developments and Different Attempts for Radiative Cooling

2.1.1 Selective Materials

There are different materials that have absorption peaks at different wavelengths. Rare earth metals might be used as selective emitters in the infrared region due to their high absorption in this region. Recently, these metals are used with other materials such as ceramic or titania (Titanium dioxide) by mixing as composites because of the unavailability of these metals. At higher temperatures, gray-body like emission from other constituents' starts to dominate the rare earth metal's selective emission, and this would be the problem with these composites. For applications, which require peaks of various wavelengths the absorption peaks have to be shifted or tuned and the answer falls in the nanoscale, like nano-sized metal particles embedded in semiconductor matrix or insulators [20][21][22].

There are some material systems depending on the application that can be considered for radiation-cooled rockets. A chamber which fabricated from pure iridium (Ir) although would eliminate the rhenium/iridium diffusion mechanism, on the other hand, there are concerns about its structural integrity as a rocket engine. Woven carbon-carbon fibers and Tantalum-10% tungsten alloy could serve as high-temperature substrates, but for any type of long life applications, requires a suitable oxidation-resistant coating. Grain-stabilized platinum and Platinum-10% rhodium alloy are good oxidation resistant materials that might be considered for very long life, but relatively for a low temperature (1650°C) applications. Intermetallic compounds and cermets have also been considered for high temperature rocket operation, although there is a very limited experience base with them [23].

Designing a "grating" or a regular micro-roughness that will provide selective

emission is another approach for radiative cooling. The roughness dimension is the same size as the radiation wavelengths [24][25].

2.1.2 Coatings and Paints

Goswami et al. [21] in 2012 have a review of radiative cooling by paints and coatings. The purpose of using paints and coatings is their ability of controlling the emission in the structures, and modifying optical properties of coatings or paints to alter the spectral reflectivity or emissivity.

Three optical properties are significant: Absorption coefficient, scattering coefficient, and refractive index.

Paints are solid pigments in one organic resin. The role of pigment in cooling is, contribute color by absorption and reflection of light. The pigments that can be used are metal oxides and semiconductors. The benefits of semiconductors and doped semiconductors are that they allow frequencies lower than their band gap to pass and absorb others, it means that they have selective absorption [21].

Carbon, Zn powder, Silicon, PbS, organic soot and melanin (natural pigment) are other examples. Titanium dioxide (TiO_2), is the best pigment that has been reported for radiative cooling up to now, and Resins are also organic silicones that have strong absorption in the middle infrared region [21]. The resins that can be used in this case are polyethylene, propylene, and polyester.

The techniques that have been reported for paintings are the roll or coin coating, dip coating, spin coating, spray coating, and brush coating.

spray coating and brush coating are preferred among these techniques because they will have higher solar absorption and thermal emission rather than others [21].

For Coatings, metal films are good candidates for using in radiative cooling. They have high reflectivity in the infrared region and are semitransparent in the visible region. Meanwhile, thin coatings (less than 1 μm) of oxides, nitrides, oxynitrides, and sulfides of silisium are good infrared emitters. The common coating techniques are electro plating, chemical vapor deposition, chemical conversion,

vacuum deposition, and spray pyrolysis [21]. Cermets are also a mixture of insulating and metallic components which are used for spectral emittance.

Study on radiative cooling has been started from more than 30 years ago. One of the pioneers who started to work on radiative cooling is Claes-Göran Granqvist. He has worked on different materials for radiative cooling application. In 1981, he used Aluminium coated by SiO with different thicknesses in his work. For coating method, they used evaporation of SiO on smooth Aluminium. They calculated and measured reflectance in their work and the plate of Aluminium coated with SiO places under transparent polyethylene films in a polystyrene box was used for a practical test of radiative cooling. At last comparison with a panel containing blackbody radiator was done. Although this choice was not a practically useful one but it was appropriate as an example of how surfaces should be analyzed for radiative cooling and as different thicknesses were analyzed in this work so the optimum thickness of 0.8-1.8 μm for suitable spectral selectivity was found [26]. In the same year (1981) [27], Granqvist evaluated the radiative cooling of green leaves and showed how the problem of radiative cooling can be solved by nature elegantly and efficiently.

Evaporation of water through the stomata (In botany, stoma or stomata is a tiny pore that is used for gas exchange), is a significant mechanism for cooling, and leaves use spectral selectivity for maintaining low temperature with limited loss of water. This makes green leaves as natural selective surfaces, and in longest wavelengths (over 3 μm), the high water contents in the leaves make them like an ideal emitter, and the result of a green leaf agreed well with the ideal curve. At last this study proved that the green leaf is adapted to its spectral requirements more ideally than transparent heat mirror and man-made selective absorbers [27]. In 1982 [26], Granqvist group used a selective surface of the evaporated Si_3N_4 film for evaluating radiative cooling and this work represented the development of a practically effective surface.

There is a long-term gap (a decade) in working on radiative cooling and there

are not too many references between 1990-2000 about radiative cooling applications.

In 2002, the performance of a polymer-based radiative cooling system was evaluated by Meir et al. experimentally and numerically. It was proved that the system has the potential to cover a profound fraction of the cooling demand. The advantages of the system were the relatively low costs of the radiators, a simple over-all system design, and the complete building integration, that parts could be used for heating and cooling [28].

In 2003, Mastai group used semiconductor films for radiative cooling applications. They used chemical solution deposition of thin semiconductor films of $PbSe$ and PbS onto polyethylene foils for radiative cooling. In addition, they prepared pigmented shields by incorporation of ZnO or ZnS into polyethylene, and also studied the combination of these pigmented foils with thin films of PbS which represented better optical properties for cooling applications [29].

In 2005, Belafhal et al. described the chemical solution deposition of the $CdTe$ as a thin film with the thickness of 9.7 μm onto 1 mm silicon substrate for radiative cooling application. The thin film had high solar band reflectance and was transparent within the atmospheric window that depicts $CdTe$ film might be used as a good radiative cooling material. $CdTe$ thin film has high IR band transmittance (0.62 over 1) and low IR band reflectance (below 0.1 over 1) across the 8-13 μm band. Preparing radiative cooling object based on spectral selectivity would be appropriate [30].

Belafhal et al. in 2006, in another study, reported the possibility of a specific shield CdS for passive cooling. They also used the method of chemical solution deposition of the thin film with the thickness of 1 mm. They demonstrated that CdS thin film is a good candidate for radiative cooling [31].

In 2014, Maruyama group in Japan modeled radiative transfer in the pigmented coating by ray emission model (REM). They measured reflectivity by spectroscopy integrating sphere in the visible and near-infrared. In their work, they used CuO

submicron particles which has high absorptivity in visible region and is high reflectance in the near-infrared region. Particle size control and effects of particle size on spectral behavior in radiative cooling was the key point in their work. The white coating is a good candidate for radiative cooling like TiO_2 but the disadvantage of the white coating is the high reflectance of visible light which produces a high glare which is unpleasant to the eye. The goal of their work was achieving the maximum reflectivity of the solar energy by using cool-pigmented coatings [32].

In similar works Smith et al. in 2003 [33], had used colored paints based on utilization of coated flakes of metal as the pigment. In the same year, Johnson et al. [34] had used ZnO pigment coating on spacecraft wall to maximize reflectance. In 2006 Vargas et al. [35] had used just TiO_2 as white pigment coatings, and In 2007 Levinson et al. [36] had used non-white surfaces to residential roofing materials.

The parameters that Maruyama group considered in their work were particle size, coating thickness, and volume fraction. They compared CuO coating with TiO_2 pigmented coating and for their substrate, they used black and white paper. Their matrix was clear acrylic synthetic resin. For black color pigment, they used three CuO powders with the different nominal sizes and for white pigment, they used TiO_2 powder with particle size of 0.65 μm. For paint making, they used pigment powder plus acrylic resin plus thinner in ultrasonic and they coated by the method of bar coater machine [32].

For the measurement of reflectance, they used two different spectrometers. For 0.3-0.85 μm UV-Visible spectrometer and for 0.85-2.5 μm Fourier transform infrared (FTIR) [32].

In Figure 10 the result of comparing CuO coating on white paper and TiO_2 coating on black paper with the same particle volume fraction (f_v) and coating thickness is represented.

At last, the Maruyama group work showed the results forCuO coating with the results for TiO_2 pigmented coating. The performance of CuO pigment is much higher than that of TiO_2 pigment, although the CuO coating shows a black-color.

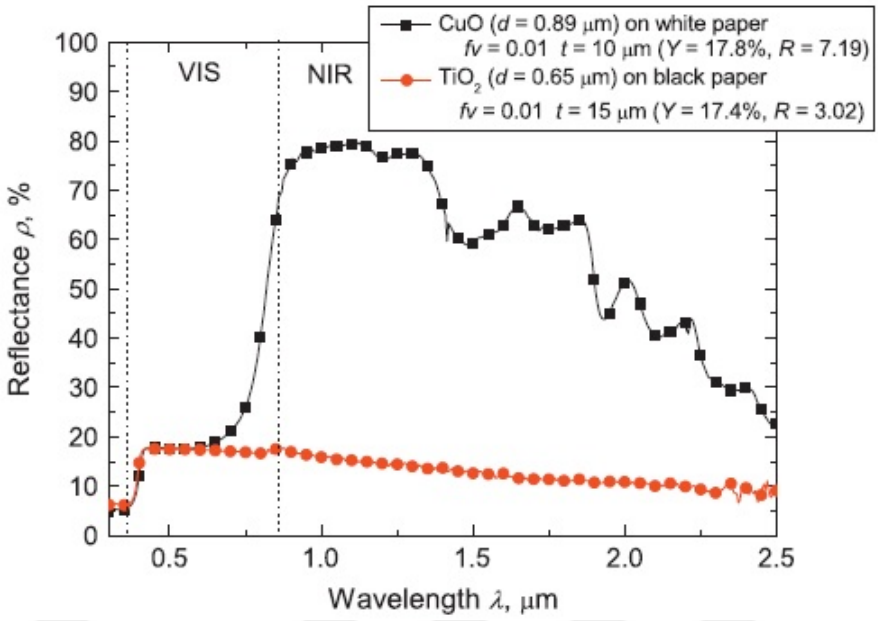

Figure 10: Comparison of the measured reflectance of the TiO_2 coating on black paper and the CuO coating on white paper [37].

In 2015 Hu et al. [38] studied TPET (Titanium-based solar selective absorbing coating plus polyethylene terephthalate) for radiative cooling and also solar heating. PET (polyethylene terephthalate) has high emissivity in atmospheric window and the equilibrium temperature of it is 11°C lower than the ambient temperature but degradation by solar ultraviolet is the disadvantage of it that they decided to use TPET instead of PET. They considered two wavelength ranges. First 0.2-3 μm as solar radiation band for daytime heat collector applications and the second one 8-13 μm (atmospheric window) for nighttime radiative cooling applications. The result for TPET sample is shown in Figure 11.

They also measured the equilibrium temperature of TPET under different inclination angles and different weather conditions at daytime and nighttime. The physical picture of the setup is represented in Figure 12 and the results are shown in Figures 13 and 14. They set the insulating layer at the bottom and around the surface to reduce heat conduction and covered the surface by the windscreen to decrease heat convection.

In 2016, Sydney Taylor et al. proposed an emitter with a lossless dielectric

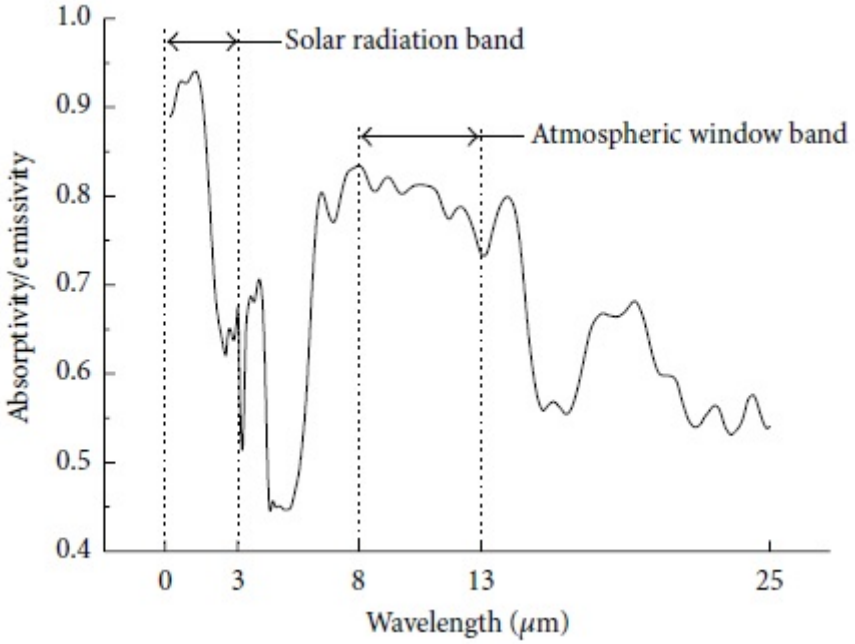

Figure 11: Spectral emissivity of TPET (Polyethylene terephthalate) [38].

spacer sandwiched between a thin film of vanadium oxide (VO_2) and an opaque aluminium substrate. For this emitter, when the temperature is lower than 341 K, the thin film (VO_2) is insulating and leading to high reflectance that is more than 90% in the range of 2-20 μm, but over 345 K, this thin film is metallic and forms a cavity that shows high broadband emittance at 10 μm.

This development of selective coatings has significant implications for applications in spacecraft thermal control, smart windows, and in building cooling.

Different material systems have been studied which may offer more oxidation resistance or thermal margins, such as ceramic oxide-coated iridium/rhenium chambers and hafnium carbide/tantalum carbide matrix composites [23].

2.1.3 Nanostructures

Goswami et al. in their work [21] reported that finding materials with selective emissivity in the nature is hard but creating this selective emissivity with nanotechnology is possible. Nanosized metal particles embeded in insulators or a semiconductor matrix is an example.

In 2009, Lin et al. [39] used nanodiamond powder, multiwall carbon nanotube,

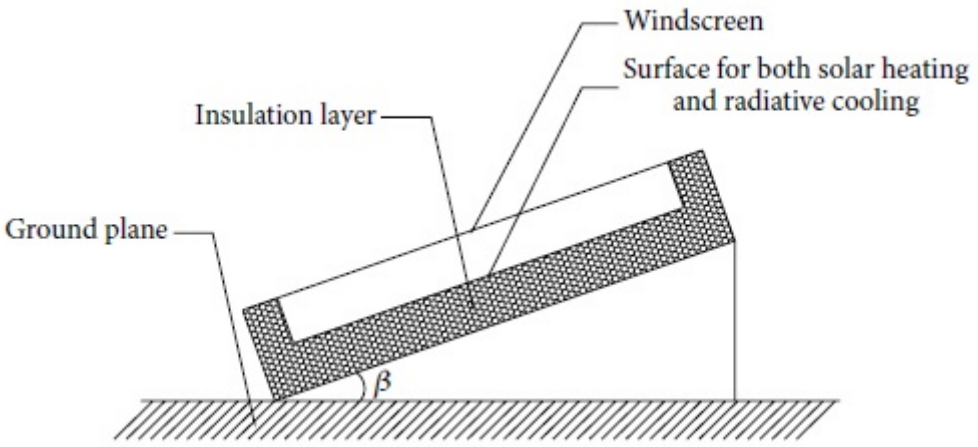

Figure 12: Schematic of radiative cooling and solar heating combined system of TPET (Polyethylene terephthalate) [38].

and carbon black for radiative cooling. They dispersed them in an acrylate emulsion to make composite materials. Then, they coated the materials on Aluminium panels by spray gun to form thin coatings. As surface emissivity of the coatings plays a significant role in releasing heat, the purpose of their work was to process and formulate a coating having strong surface emissivity for the goal of effective heat dissipation. At last they showed multiwall carbon nanotube was the best among others in radiative cooling, and by increasing the percentage of multiwall carbon nanotube, they got better cooling due to lower the equilibrium temperature.

Fan group in Stanford University are one of the pioneers in using nanostructures for radiative cooling applications. In 2013, they compared two materials in original structure and modified structure (nanostructure). For original structure, they used Silicon nanowire on top of an Aluminium layer. Silicon has small extinction coefficient over thermal wavelengths, and for the nanostructure, they used $\propto$-quartz on top of the original structure. This nanostructure which has two phonon-polariton resonances, is transparent over visible wavelengths, and is emissive in the atmospheric transparency window. Their structures are shown in Figure 15.

The modified structure could maintain absorptivity and be highly emissive.

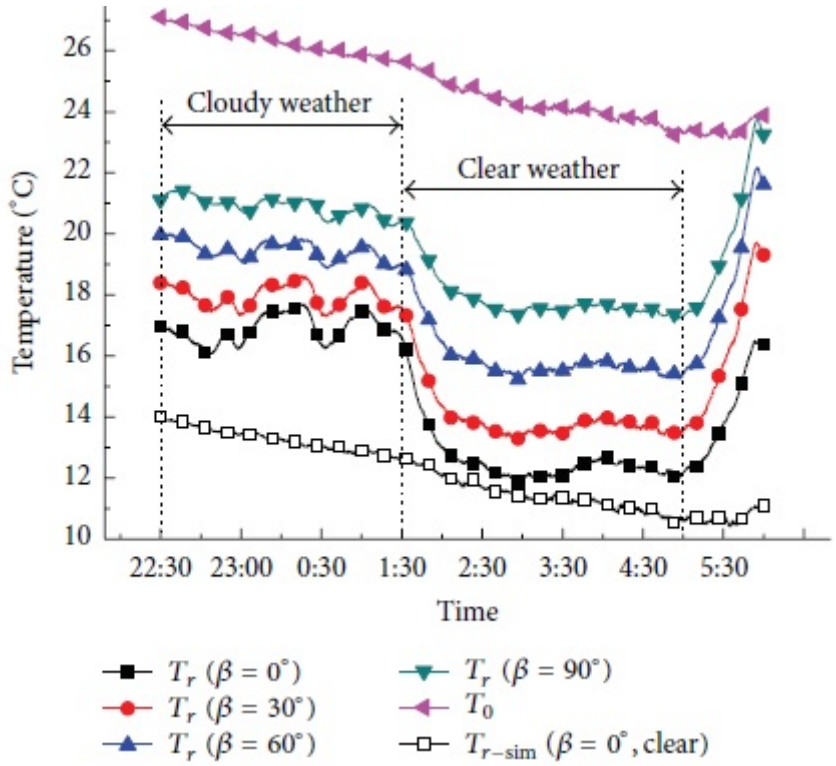

Figure 13: Steady-state temperature results for nighttime radiative cooling applications of TPET (Polyethylene terephthalate) [38].

Their design even with large non-radiative heat exchange could lower the temperature of the structure.

One of the nanostructured metals that can be used in radiative cooling is tungsten (W). In 2013, Takamura et al. [37] investigated the physical properties of tungsten with the helium defect of fiber-form nanostructure on its surface for cooling and thermal characteristics. They obtained the total emissivity quantitatively from Stefan-Boltzmann formula for the black tungsten surface with the fiber-form nanostructure, that was between 0.45 and 0.55 as a lower limit.

In 2017 Bao et al. [40] used double layer nanoparticle coating for radiative cooling. Their coatings composed of TiO_2 with SiC and TiO_2 with SiO_2 on reflective substrates (black and Aluminium). They used spray coating method, and the schematic of the coating is shown in Figure 16.

They calculated the power of the cooling of the system at day and night. Results are shown in Figure 17.

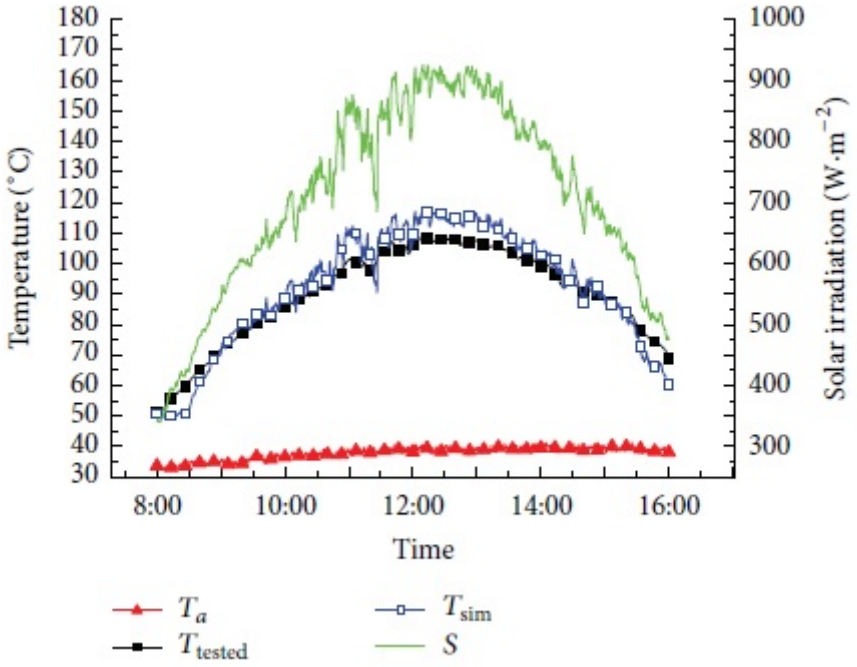

Figure 14: Steady-state temperature results for daytime solar heating applications of TPET (Polyethylene terephthalate) [38].

Their approach was a low-cost design and a significant step toward of achieving large-scale application in radiative cooling.

Personal heating and cooling by thermal management is a strategy for large energy saving. Fan group in another study represented that Nano PE or nano porous polyethylene is transparent to mid-infrared human body radiation, on the other hand is opaque to visible light owing to the pore size distribution that was 50 to 1000 nanometers. They processed the material for developing a textile which promotes effective radiative cooling while having water wicking rate, adequate air permeability, and mechanical strength for wearability. A device for simulating the skin temperature was developed by them which showed temperatures 2.7° and 2° lower while covering with nano porous polyethylene cloth and the processed nano porous polyethylene cloth rather than covered with cotton. Their attempt was a scalable and effective textile for personal thermal management [41]. The schematic of their study is presented in Figure 18.

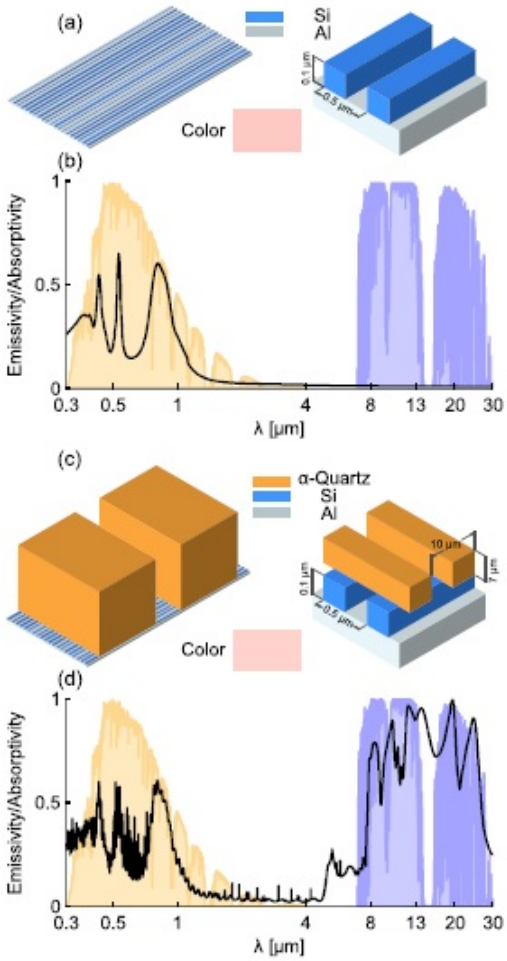

Figure 15: Schematic of original structure and nanostructure for radiative cooling [12].

2.1.4 Effect of Particle Size on Radiative Cooling

In this part, the size effect in radiative cooling was investigated numerically. One of the materials that had high reflectivity in terms of our UV-Visible analysis in visible range which was Titanium dioxide (TiO_2), was selected and then the graph of reflectance versus wavelength was drawn numerically with different sizes. Data was taken from the literatures [42].

As it is obvious from Figure 19, finest particles (less than 2 μm), showed high reflectance in comparing with the other ones but in higher wavelengths (higher than infrared), the effect of particle size is not obvious.

we know $\alpha_\lambda + \tau_\lambda + \rho_\lambda = 1$, and because for opaque samples the spectral

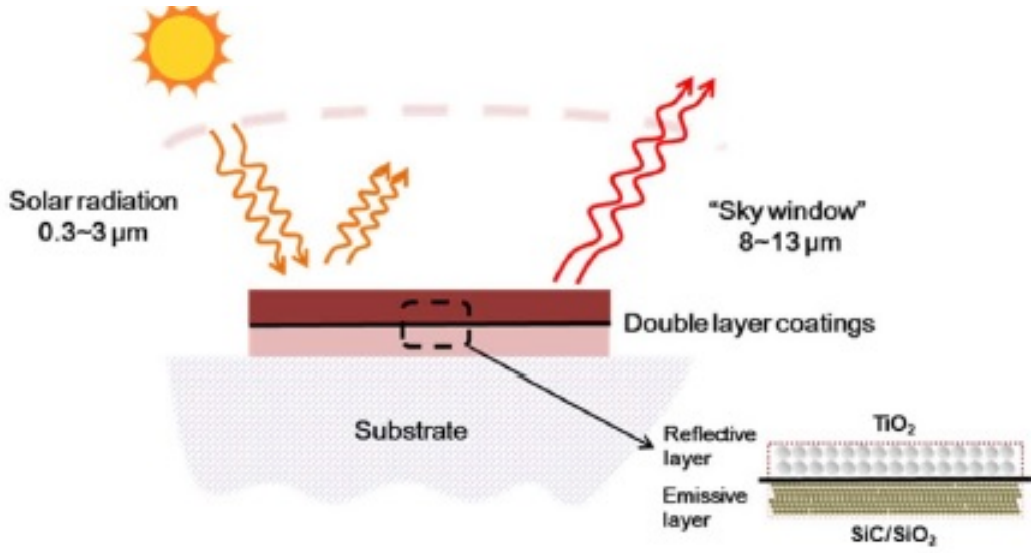

Figure 16: Schematic of a nanoparticle coating system [40].

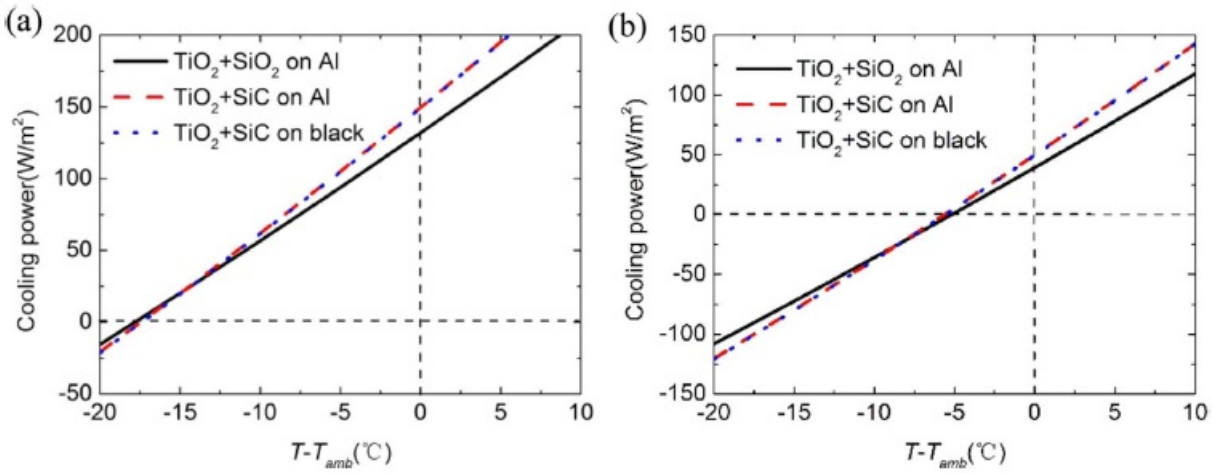

Figure 17: Power of the cooling (a) Nighttime and (b) Daytime [40].

transmissivity is zero. Therefore, $\alpha_\lambda = 1 - \rho_\lambda$ and with Kirchhoff's Law, $\alpha_\lambda = 1 - \rho_\lambda$. Hence, lower reflectivity means higher emissivity. The result shows that by decreasing the size, the reflectance decreased and this is one of the reasons for using nanoparticles in radiative cooling applications.

2.1.5 Photonic Devices

The recent development of radiative coolers based on photonic devices has opened a window to get highly efficient cooling and make them able to operate under the sun and reaching a temperature below the ambient temperature. These approaches

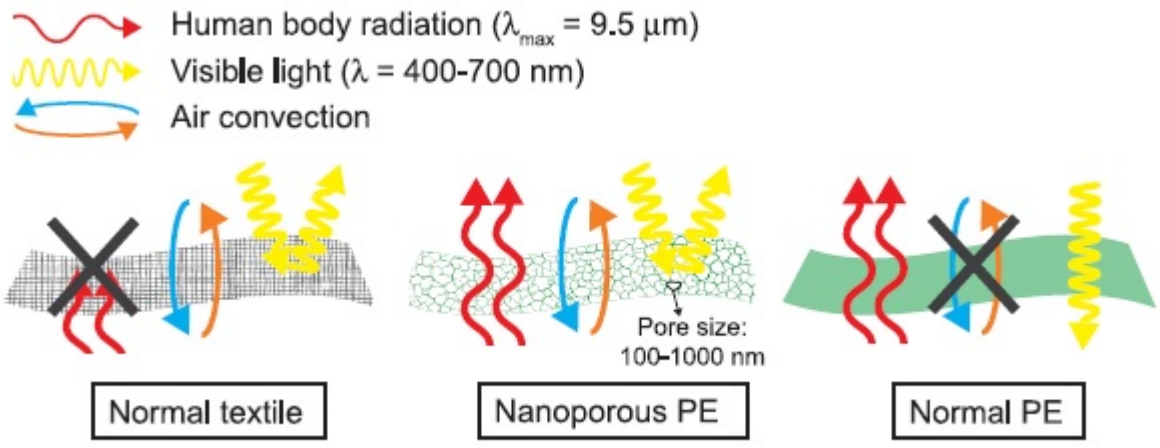

Figure 18: The schematic of comparisons between normal polyethylene, nano polyethylene, and cotton. [41].

use photonic properties combined with the intrinsic properties. These devices can be selective and have strong thermal emission with high solar reflection [10].

Fan group in 2014, for the first time, presented a metal-dielectric photonic structure [43]. It behaved as a broadband mirror for solar light and also emitted strongly in mid-IR. Their structure is shown in Figure 20.

Previous devices had the cover of ZnS or $ZnSe$ and the problem of them was transmitting thermal radiation while reflecting sunlight, but this new structure was the new concept of nanophotonics which suppressed solar absorption and enhanced thermal emission. It had two layer photonic crystal of SiC and quartz that were desirable for this structure because they are weak absorbers in visible and IR Ranges.

In the same year [44], Fan group introduced another thermal emitter and photonic solar reflector consisting of seven layers of SiO_2 and HfO_2 which reflects 97% of the sunlight while emitting selectively and strongly in the atmospheric window.

The schematic of the structure and the scanning electron microscope (SEM) image of it are shown in Figure 21. The four thinner bottom layers which were deposited on Al-coated Si wafer used as chirped photonic crystal and the top three thick layers contributed to the atmospheric window range. The photonic

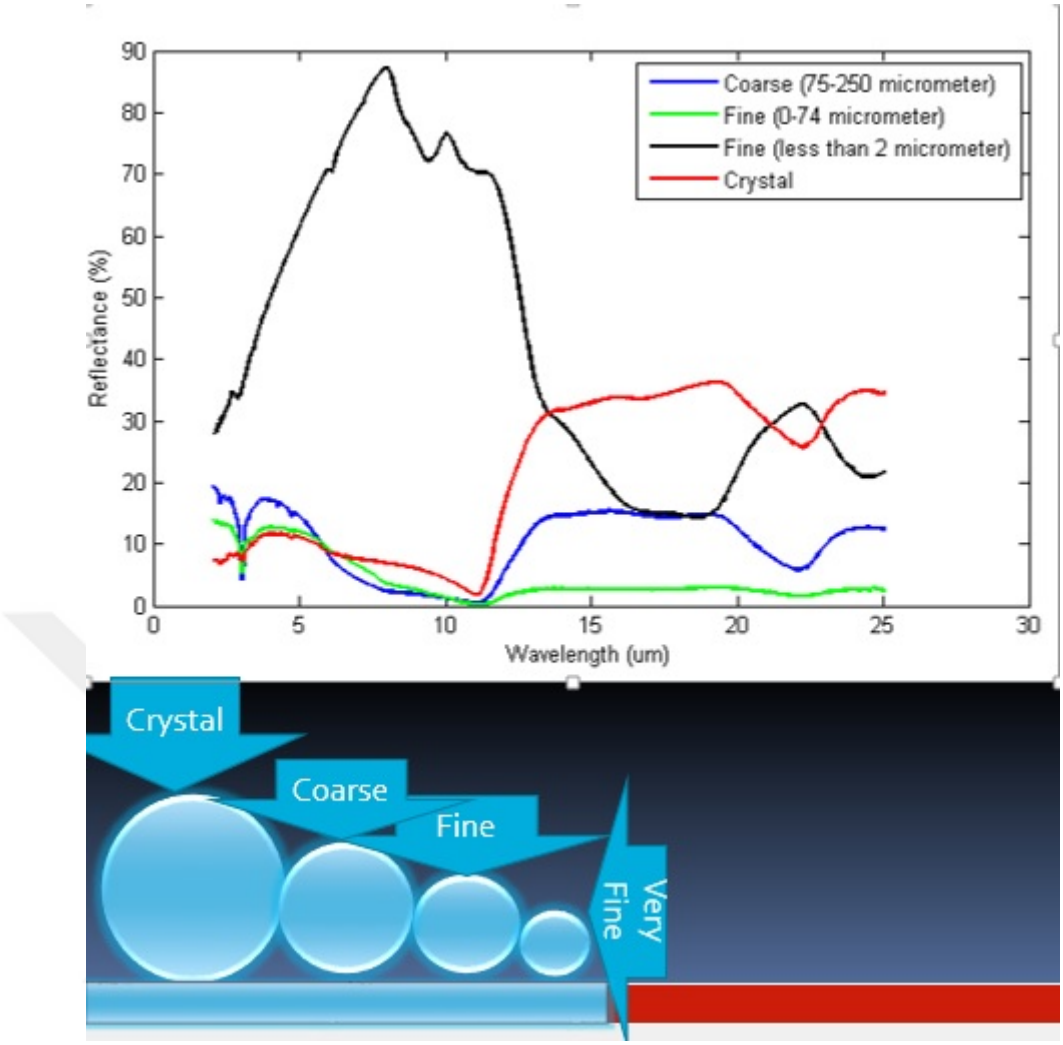

Figure 19: Comparison of particle size of TiO_2 as a pigment and effect of it on radiative cooling (Plotted by Matlab and Data has taken from http://speclib.jpl.nasa.gov/search-1).

device led to a cooling power of around 40 Wm^{-2} at the ambient temperature and enabled the cooling during the daytime. There were two challenges for this device for achieving more cooling. The first one is that the IR emission of the device was not strictly selective because of the intrinsic absorption of the materials and the other one is that the emission in the atmospheric window was not very strong as is shown in Figure 22. Although increasing the thickness of the top three layers might increase the emission, but it could also degrade the selectivity of the IR emission.

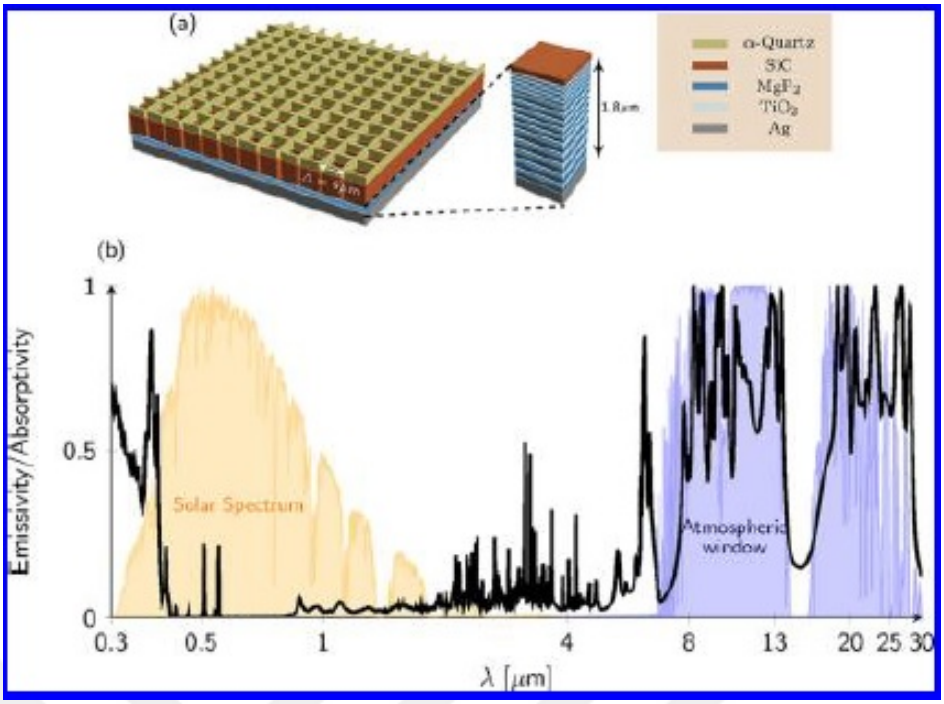

Figure 20: Radiative cooler designed in Stanford university by Fan group [43].

In 2018, Tan et al. proposed a new hybrid radiative cooled-cold storage cooling system which was based on a recently developed novel radiative cooling metamaterial. Their study was a novel work on this radiative cooling metamaterial that can provide cost-effective diurnal cooling to residential buildings. Their system could be conveniently integrated with the conventional air conditioning system which are used in single-family houses.

The main advantages of their study are the followings:

1. The average annual coefficient of performance of the system in this study is increased by more than 39.4 in comparing with the coefficient of performance of the split air conditioner lonely system.

2. A cost effective solution for radiative cooling technology must be provided in residential building applications by the diurnal working hybrid radiative cooled-cold storage cooling system [45].

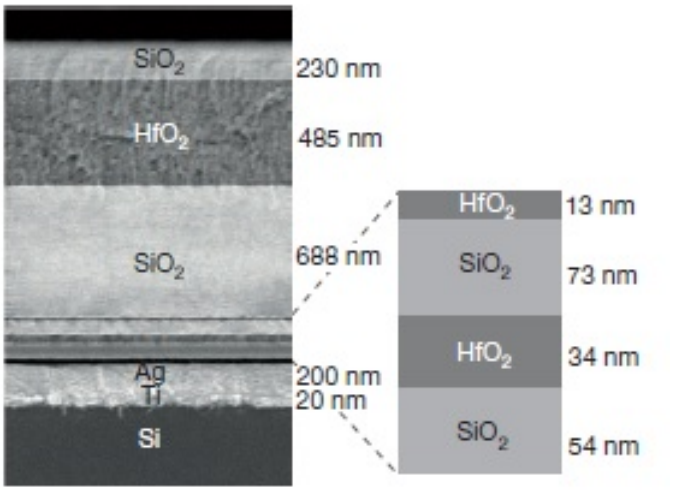

Figure 21: Scanning electron microscope of the radiative cooler device introduced by Fan group [44].

2.2 Materials

2.2.1 Base Materials

Materials for building facades must be designed with a surface which emits strongly in a preferable spectrum (atmospheric window) while decreasing emission into other spectra. Rare Earth metals and composition of them with ceramics are selective emitters as explained before but at high temperatures emission from other constituents dominate these metals [46].

Volcanic soil and their deposits have potential to be used as construction materials. Volcanoes send huge amounts of rocks and other sandy objects to the surface during their eruption. These materials form porous structures by cooling off, that are extensively used as the building materials, because of their desired low-conductance properties. Among these materials, diabase and basalt have been used for crushed stone: roofing granules. The other ones are perlite, pumice, and volcanic ash. In ancient days, volcanic ash and pumice were considered to make cement, but nowadays they are mixed to make cement for large construction projects such as dams. This is more common in places where volcanic activity has been significant such as in Oklahoma and California in the United States, Sicily, and

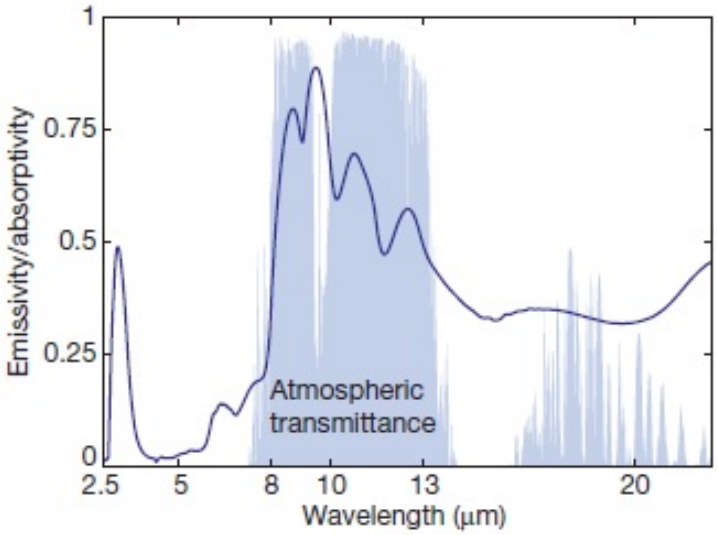

Figure 22: Spectral emissivity of the radiative cooler introduced by Fan group [44].

Southern Italy, as well as in Central and Eastern Turkey. These materials used as lightweight aggregate in concrete too, especially precast concrete blocks. Pozzolans are another examples of alternative building materials, that based on the abundant volcanic ashes in that area used in Uganda. They will be cementitious by activating with lime or cement and by transforming to pozzolan cement, they might be used to produce binders, blocks, and wall panels to manufacture a cheap alternative building [46].

2.2.2 Paints

Paints with zero transparency are coatings on surfaces and combined with pigment and resin. In radiative cooling applications, highly reflective paints are desirable; however, high emission or absorption is also important, so the pigment must have a high emissivity. Pigments are semiconductors and metal oxides. Carbon, FeO_x, $FeMnO_x$, Zn powder, PbS, Silicon, TiO_2, Melanin, and organic soot are the examples of pigments that can be used for radiative cooling. The structure and design of such paints are combined with two-layer structures of infrared selective metal in the bottom and thickness sensitive spectrally selective paints (TSSS) on the top [46].

2.2.3 Coatings

Coatings can be used for controlling the emission as well the paints. Metal films with high reflectance in infrared are good examples for radiative cooling applications. They are also semitransparent in the visible spectrum. Thin film coatings are other examples for radiative cooling like nitrides, oxides, oxinitrides, and sulfides of Silisium (Si_3N_4 or SiO) [46]

2.2.4 Phase-change Materials

Phase-change material (PCM) is a substance with a high heat of fusion which releases or stores significant amounts of thermal energy while solidifying or melting at a certain temperature. Heat can be released or absorbed while the material converts from solid to liquid and vice versa [46]. In Figure 23 classification of PCMs is shown.

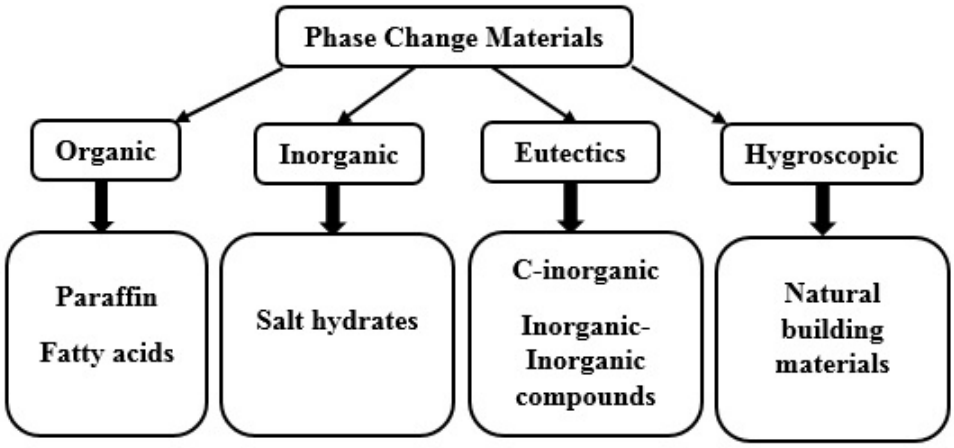

Figure 23: Classification of Phase-Change materials [46].

PCMs have small volume change during phase change, high thermal conductivity, the high latent heat of fusion, and minimum subcooling while freezing. They are stable chemically, non-toxic, inexpensive, and also the melting temperature ranging for PCMs used for free cooling must be from 15° to 30° for the concept of sustainable buildings. PCMs are good candidates for free cooling because if the

phase change temperature of them be in the midrange of diurnal temperature variation, they might increase the performance of free cooling systems. In buildings, PCM's can be used by storing thermal energy through the phase change to reduce the peak cooling demand of the building. Nighttime radiative cooling might release heat by radiation towards the cold nocturnal sky, for example via solar panels, so those two technologies can be mixed, using the cold water produced by radiative cooling to discharge the thermal energy stored in the PCM. In addition, microencapsulated phase change material (MPCM) slurry seems to be a suitable medium for passive cooling technology in air conditioning systems (combined application). In comparing phase change materials, BioPCMTM is derived from salt hydrates or petroleum, unlike other PCM products. BioPCMTM is the trade name for bio-based phase change materials and is cost-effective, sustainable which derived from abundant, bio-based materials [46].

2.2.5 Nanoscale Materials

Required selectivity in emission and absorption spectra needs maxima or minima of the refractive index of a material with respect to the frequency. Finding materials with this characteristic in nature is impossible, but with the recent approaches in nano-technology, they might be designed. However, it should be mentioned that these materials are still quite expensive to find a wide-spread use as sustainable building materials.

2.3 Description of the Materials in this Study

The goal in this dissertation was to to use new sustainable materials to increase radiative cooling by these structures. The materials that have been used and the experimental analysis that have been done on them are listed in Table 1.

2.3.1 Sustainable materials

A Sustainable resource or a sustainable material is something whose production is supported indefinitely by nature, that means, a resource is used up at the same

Table 1: List of the materials that have been used in this project.

Name	*Analysis*
XPS (Extruded Polystyrene Foam)	Optical Microscope, UV-Visible, FTIR
Coated XPS from the factory	Optical Microscope
Coated XPS with nano Titanium dioxide	UV-Visible
TPO (White membrane)	Optical Microscope
EPDM (Black membrane)	Optical Microscope, UV-Visible, FTIR
Red membrane	Optical Microscope, UV-Visible, FTIR
PPC (Perlite Pumice composite material)	UV-Visible, FTIR
White Painted PPC	UV-Visible, FTIR
Painted and coated PPC	UV-Visible
Plant (moss)	Optical Microscope, UV-Visible, FTIR
Cactus	FTIR
Heat insulation plate (Ytong)	Optical Microscope
Styronit Cement	Optical Microscope
Lava	Optical Microscope
Furnace bottom ash	Optical Microscope
Arkalyte	Optical Microscope
Haydite	Optical Microscope
Silisium	UV-Visible
Cappadocia Stone	FTIR
Ephesus Black Stone	FTIR
Ephesus Red Stone	FTIR

speed which it is renewed. A Sustainable product during its entire life protects the environment. That is, from the moment the raw materials are extracted from the source to the time the final product is disposed of, there must be no permanent damage caused to the environment [47].

Sustainable materials have the least amount of energy consumption. Green energy is used first in the sustainable materials, as well as a lack of emissions and assures that the material continues to grow or to be created rather than evacuate its stocks [48].

Recycled rubber, bamboo, adobe, hemp, cork, straw, hay, clay, coconut palm, timber, and textiles are some examples of sustainable construction materials.

Structures and buildings can be made from the mentioned materials. Selecting one of these materials make the home, happier, healthier, and eco-friendly. As an example, by using materials like straw or hay for insulation application, they can be replaced in a few years as it had regrown in fields throughout the country. It means each time of using it, more is being produced. For this, it is natural to see why there is such a huge demand for using sustainable materials for construction [49][48].

Sustainable materials play a significant role in buildings. By using renewable fuel and materials cause much less harm rather than using the non-renewable ones. In building a house even a part of it, like a garage, choosing sustainable materials is beneficial as they not only last for a long time but they are durable, strong, and environmentally-friendly too. Usage of recycled and sustainable materials can help ceasing the devastation which is clear from the gaping holes in the atmosphere, So there is no argument of using non-sustainable materials as construction materials.

The key point in using the sustainable materials is that; how they should be used in construction. Building a house in an interesting time, but when it comes to designing, it is significant to think about the materials and its sustainability when it is the first time that it is created [48].

Currently, within our group Center for Energy, Environment and Economy at Ozyegin University, Istanbul (CEEE), we have been using and developing an economically and sustainable viable materials for building applications. A category of the sustainable materials are shown in Figure 24.

In the following for analyzing numerical work in this study, six of the materials have been selected that their properties will be explained here briefly. XPS, PPC, Painted PPC, Plant or moss, EPDM or black membrane, and red membrane were the materials that have been chosen for further analysis.

XPS: Extruded polystyrene foam contains closed cells, causes meliorate higher stiffness and surface roughness and low thermal conductivity. Density range is

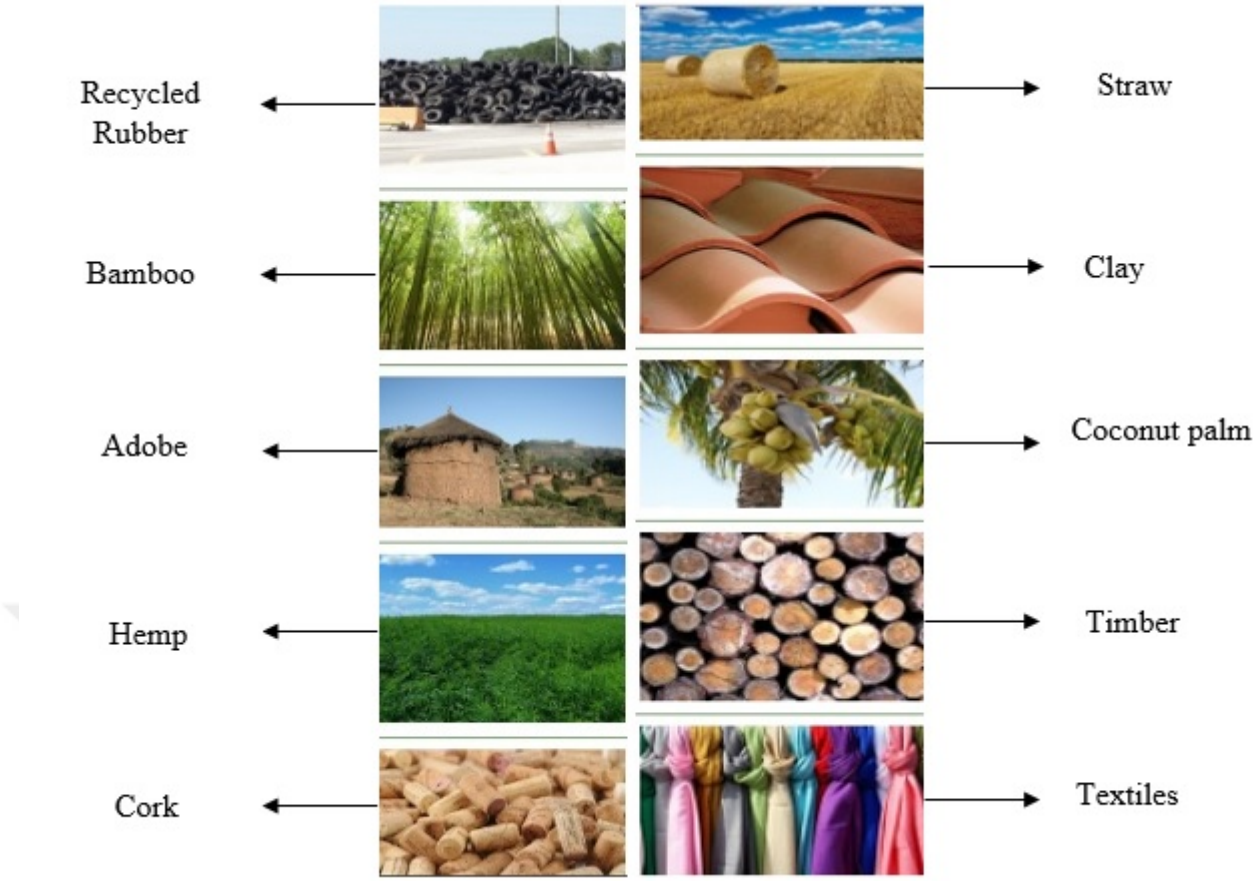

Figure 24: Examples of sustainable materials.

about 28–45 kg/m^3. It absorbs only minimum quantities of moisture, and is resilient and resistant to aging and rotting. Thermal conductivity is between 0.029 to 0.039 W/(m · K) with the average of $\sim$ 0.035 W/(m · K) based on bearing strength/density. Water vapor diffusion resistance (μ) of XPS is around 80–250; therefore, makes it suitable for wetter environments.

Extruded XPS, is in the form of continuous foam billets. Polystyrene is melted inside of the extruder and by adding carbon dioxide (CO_2) or sometimes partially halogenated fluorochlorohydrocarbon as a foaming agent, it extrudes through a nozzle and finally, thicknesses between 20 and 200 mm can be produced. While running through a cooling zone the billet can be cut (by sawing) into panels in a subsequent machine and the edges can be formed. The foam skin stays on the external surfaces of the panels. In the case of using for "insulation under plaster", the foam skin is either removed. Finally, the panels are aged to admit dimensional

consistency [50][51].

There are many applications for XPS such as for roofs (flat roofs, inverted roofs), ceilings (floor insulation with high load-bearing capacity, walls, basements, swimming pool insulation, and load bearing insulation. In Figure 25 scanning electron microscope (SEM) of XPS is shown.

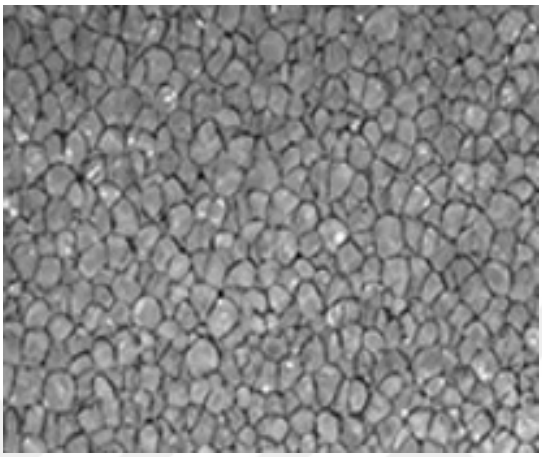

Figure 25: Scanning electron microscope image of XPS **25X** [52].

Perlite pumice composite (PPC): Perlite which has the potential to be utilized as a raw material in geopolymerization technology, is an amorphous aluminosilicate volcanic glass. It has 2–5% combined water and by heating to temperatures between 760°C and 1150°C, expands 10 to 30 times of its original volume depending on the raw material mixture [53][54].

Pumice can be considered as a sustainable building material [55]. Pumice with a sponge-like structure is a lightweight volcanic aluminum silicate which is formed by the expansion of gases when molten lava rapidly cools. It has a low bulk density in the range of 480-960 kg/m^3 and has low thermal conductivity, low sound transmission characteristics, and high strength-to-weight ratio. These properties make it favorable as an additive for lightweight aggregate, bricks, and blocks and aggregate for plaster and concrete [56].

In this study, perlite pumice composite powder (PPC) which is shown in Figure 26 was used. It was mixed with enough water like a slurry and poured into two molds for making the samples. After drying, the surface of one of them was painted

with white paint for the experiments.

Figure 26: Perlite Pumice Composite powder camera image.

Black membrane or EPDM: EPDM rubber (ethylene propylene diene monomer (M-class) rubber) is a kind of synthetic rubber and an elastomer with a lot of applications. EPDM is an extremely durable membrane that widely used in low-slope buildings. Its two primary ingredients, propylene, and ethylene are derived from natural gas and oil. EPDM is existing in both white and black and is sold in a wide variety of widths, ranging from 2.2-15.2 meters, and in two thicknesses of 1.1 and 1.5 millimeters. EPDM may be installed either fully adhered, ballasted or mechanically attached, sealed with liquid adhesives or specially formulated tape with the seams of the roofing system [57]

Red membrane: Red membrane is a type of wall or roof element that uses asphalt for waterproofing. There are two dominant base materials in forming asphalt shingles. First a fiberglass base and second a formerly-living organic base. Both types are made in a similar manner with asphalt or modified-asphalt applied to one or both sides of the asphalt-saturated base, covered with quartz, ceramic granules, stone or vitrified brick and the back side treated with mica, sand or talc to inhibit the shingles from sticking to each other before usage. The top surface granules provide some physical protection of the asphalt and give the shingles their color by blocking ultraviolet light. To avoid shingles from being separated by high winds, self-sealing strips are used as adhesion on shingles. Shingles are commonly

limestone, fly-ash-modified resins, or polymer-modified bitumen element. SBS or a styrene-butadiene-styrene sometimes called rubberized or modified asphalt is sometimes added to the asphalt mixture as an additive to create shingles more resistant to thermal cracking, as well as more resistant to damage from hail strikes [58][59]. In this work, red type was used and it was called red membrane.

Plant or Moss: For modeling a green roof, moss from the yard of the university campus (Ozyegin University) was used. A moss is a plant which is produced of spores and flowerless with the spores produced in small capsules. They typically grow in dense green mats or clumps, frequently in shady or damp locations [60]. The image of the sample is shown in Figure 27.

Figure 27: Moss sample camera image.

Chapter III

EXPERIMENTAL PROCEDURES

3.1 Introduction

Radiative coolers are based on the intrinsic optical properties of bulk materials which improve cooling abilities. Usage of bulk materials consists of intrinsic infrared emissions for significant radiative cooling. The advantage of some bulk materials not only lie in their intrinsic IR absorption but also in their capability to make large-scale films for practical applications like polymers [10].

As intrinsic optical properties of the materials in this study were not available, firstly, experimental analysis were done. Optical microscope was used to analyze the morphology of the surface of a group of sustainable materials, although just six of these materials were selected for further analysis, but these results are beneficial for future work in this area. These materials are used on the surface of the roofs (as a coating), so the surface morphology of them is significant. More accurate surface morphology can be done by Scanning electron microscopy (SEM) or Transmission electron microscopy (TEM).

Reflection measurements were undertaken using the UV-visible spectrometer, but this data proved not to be useful, as only showed a small portion of the wavelength and not the range of the atmospheric window, but it included the solar band, so this range would use to evaluate the samples in the term of solar absorbers.

Fourier Transform Infrared Spectroscopy (FTIR) was also used for measuring infrared spectrum of emission or absorption of the samples in the atmospheric window range which shows the best sample as a radiative cooler.

3.2 Optical microscope description and results

Since the samples will be used in roofs as a coating, in the first stage, surface morphology of some of the samples were analyzed by the optical microscope (Metkon 200X).

In optical microscope or optical light microscope, light from a mirror is reflected up through the object to be viewed or the specimen, into the powerful objective lens, that produces the first magnification. Then the objective lens produced image is magnified again by the eyepiece lens that acts as a simple magnifying glass. By using a light microscope, one can view cell walls, nucleus and cell membrane of the samples. Light microscopes use light and lenses to magnify cell parts, although they usually can gain a maximum of 2000x magnification that is not adequate to see other tiny organelles [61]. Optical microscope images of some selected samples are shown from Figures 28 to 38.

In Figure 28 the XPS and in Figure 29, the XPS with a coating on the surface of it are obvious. The brightness of the coating which is from the factory and is like a nylon is obvious in Figure 29. The white spots relate to the brominated fire retardant that used in the XPS process. The lack of material during foam expansion caused some holes as open cell wall which are obvious in the figures. The percentage of these open cells affect both the radiation and conduction properties [62].

A heat insulation material is a construction material which provides excellent thermal energy efficiency for the building. Optical microscope image of it is shown in Figure 30 [63]. The surface was found to be rough and irregular. The existence of pores and impurities is also noted in the Figure, which proves that coating on the surface of this sample may not be homogeneous too much [64].

Styronit cement is a natural thermal insulation plaster, which is applied externally and internally instead of classic rough plaster. It is a thermal insulation with excellent adhesion, breathable, environmentally friendly product, easy to prepare, flexible, long lasting and economic for using that its morphology is shown in Figure

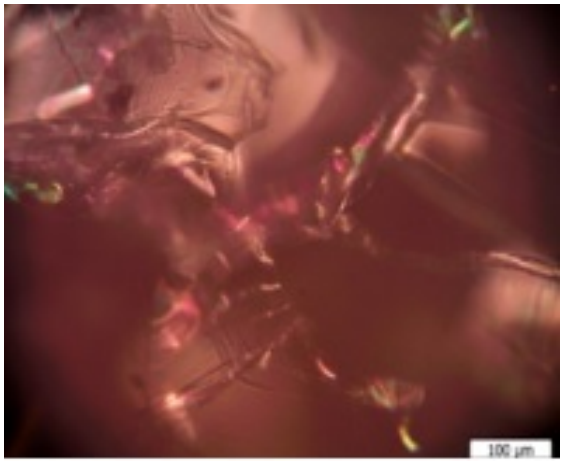

Figure 28: Optical microscope image of XPS obtained at Ozyegin University.

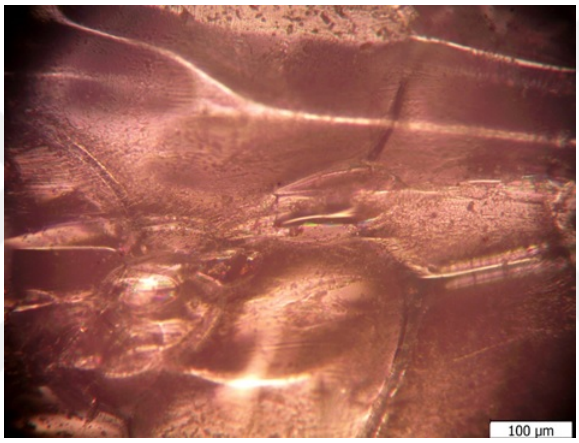

Figure 29: Optical microscope image of coated XPS from the company obtained at Ozyegin University.

31 [65].

Lava Stone, lava rock, or Basalt is an igneous volcanic rock [66]. It is shown in Figure 32. Irregular protrusions that look like cauliflowers occur on the surface of the lava which is obvious in the Figure 32. At first, protrusions are attached under the massive lava. Later they break and create loose debris on the flow surface. Generally the surface of the cauliflower is broad with smoothly undulating zones and clinker surfaces which is presented in Figure 32 [67].

Figures 33 and 34 are related to Black (EPDM) and White (TPO or Thermoplastic Polyolefin) Membrane. As is clear in the images the morphology of the white membrane is more homogeneous rather than the black one.

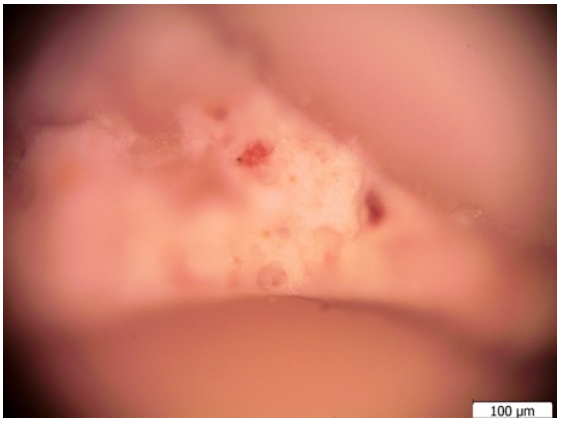

Figure 30: Optical microscope image of Heat Insulation Plate (Ytong) obtained at Ozyegin University.

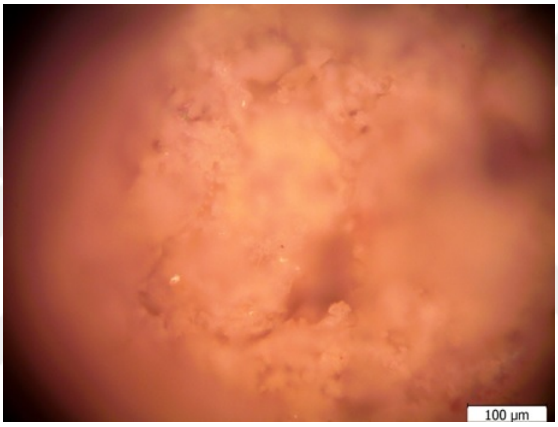

Figure 31: Optical microscope image of Styronit Cement obtained at Ozyegin University.

Structure of moss under Optical microscope is presented in Figure 35. Bottom ash refers to coal combustion and comprises traces of combustibles which are embedded in making sticking and clinkers to hot side walls of a coal-burning furnace in the duration of its operation. Morphology of it is represented in Figure 36 [68].

Bottom ash has a large variation in shape and grain size with angular and sub angular particles of translucent and opaque materials. Spherical bodies are mainly opaque which are equally frequent with the translucent ones, and point contact are preferable in the grains [69]. Arkalyte is an expanded clay and Haydite is a concrete block which are shown in Figures 37 and 38.

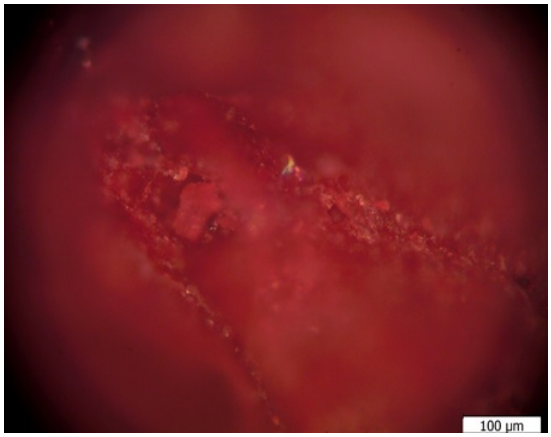

Figure 32: Optical microscope image of red lava obtained at Ozyegin University.

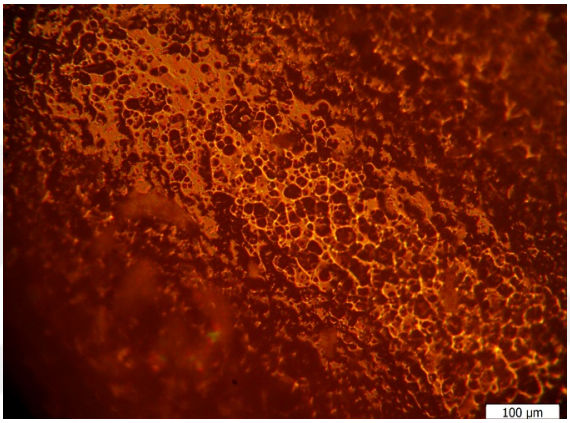

Figure 33: Optical microscope image of black membrane or EPDM obtained at Ozyegin University.

Red lava, Arkalyte, bottom ash and haydite are four growth media which are used for green roofs [70]. Since most of the materials which were introduced in this study have to be used as a coating, for this the morphology of them was presented, but for further analysis Scanning electron microscopy (SEM) must be used.

3.3 Description of the UV-Visible spectroscopy and results

Firstly, the experimental results were provided as measured from the UV-Visible spectrophotometer and FTIR spectroscopy, which correspond to the solar window of 0.2-2 μm and the atmospheric window of 8-13 μm wavelength intervals. A system with high emissivity in both solar radiation and atmospheric window bands can

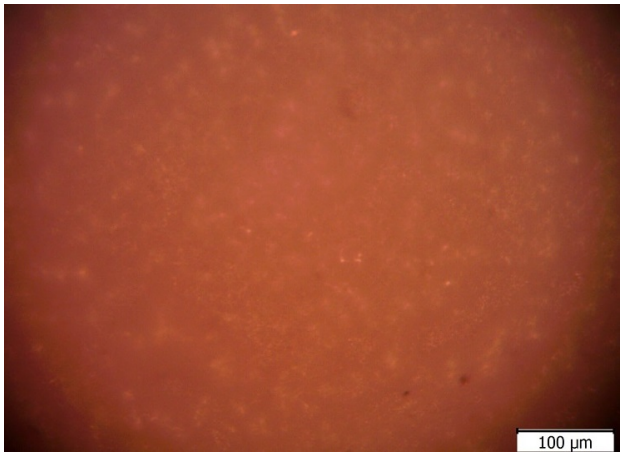

Figure 34: Optical microscope image of white membrane or TPO obtained at Ozyegin University.

Figure 35: Structure of moss under Optical microscope.

act as a solar heating system during daytime, and also a radiative cooling system at night time [71][72].

In UV-Visible, a beam of light from a visible light source (UV) is separated into its ingredient wavelengths by the diffraction grating. A half mirrored device split each single wavelength beam (monochromatic) into two equal intensity beams. The sample beam or colored magenta passes through a tiny transparent container which is containing a solution of the compound in a transparent solvent. The reference beam or colored blue passes through an identical container which is containing only the solvent. Then electronic detectors measure the intensities of these light beams and they are compared [73]. Schematic of the UV- visible spectrophotometer is

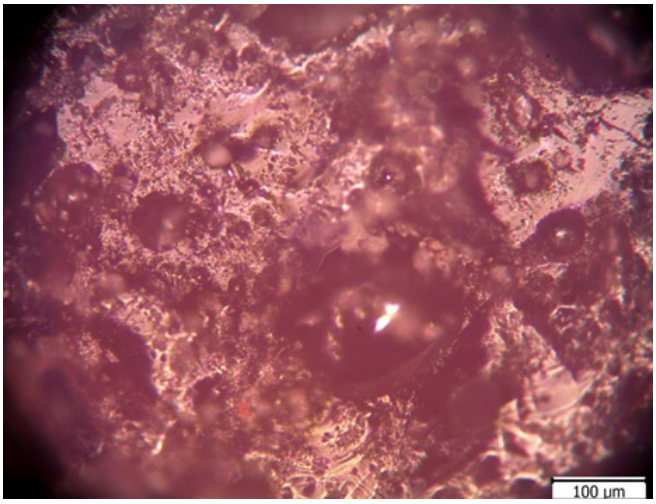

Figure 36: Optical microscope image of Furnace Bottom Ash obtained at Ozyegin University.

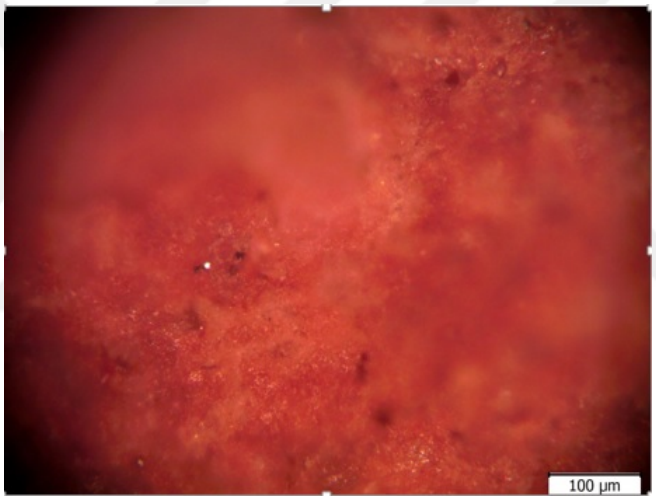

Figure 37: Optical microscope image of Arkalyte obtained at Ozyegin University.

shown in Figure 39. It is effectively an ideal surface for this application; its expected spectrum is shown in Figure 40.

In the first step of investigating radiative cooling on the samples, a group of the samples were analyzed with the UV-Visible spectrophotometer. The first group constituted of XPS, Coated XPS, PPC, Painted PPC, Painted and Coated PPC, and Silicium (Silicon powder). XPS is extruded polystyrene foam which was explained before. PPC is perlite pumice composite as explained in the past, and Painted PPC was the white painted PPC one.

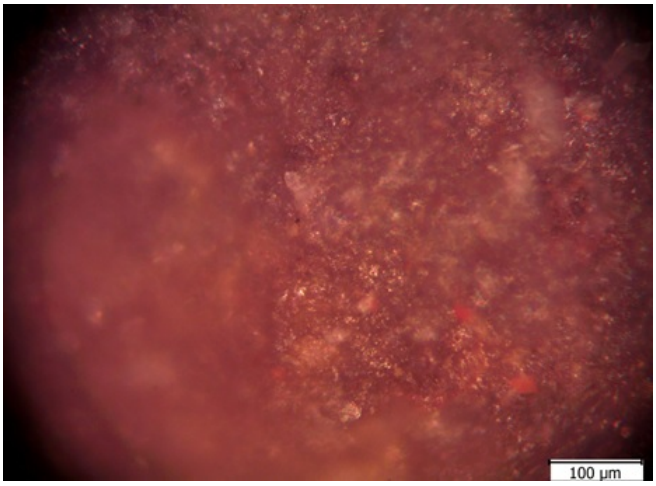

Figure 38: Optical microscope image of Haydite obtained at Ozyegin University.

Silicon is generally present as a silicate, which can be discovered in many clays, rocks, and soils. By reducing the (SiO_2) and silica by carbon, silicon can be obtained. For high purity silicon, zone refining might be done as well. Silicon is available in two allotropic form; powder brown silicon and crystalline or metallic silicon which is grey and is more abundantly used. Bulk silicon is unreactive towards acids (HF), water, although it is soluble in hot alkalis.

Silicon has a variety in its application like ultra-high purity silicon with its semiconducting properties is mostly used in the semiconductor industry. In the manufacture of alloys also silicon can be used. Furthermore, it is also in the manufacture of glass [74].

Painted and coated PPC and coated XPS were coated with nano Titanium dioxide (TiO_2) by sol-gel method. Sol-gel process is a method for fabrication of solid materials from tiny molecules. This method is mainly used for producing metal oxides like titanium and silicon. The process imports monomers into the sol which is a colloidal solution and acts as the precursor for the gel that is the integrated network. Metal alkoxides are typical precursors. The process is shown in Figure 41.

Sol-Gel protective coatings have shown excellent chemical stability, oxidation control and enhanced corrosion resistance for substrates [75]. For this, one of the

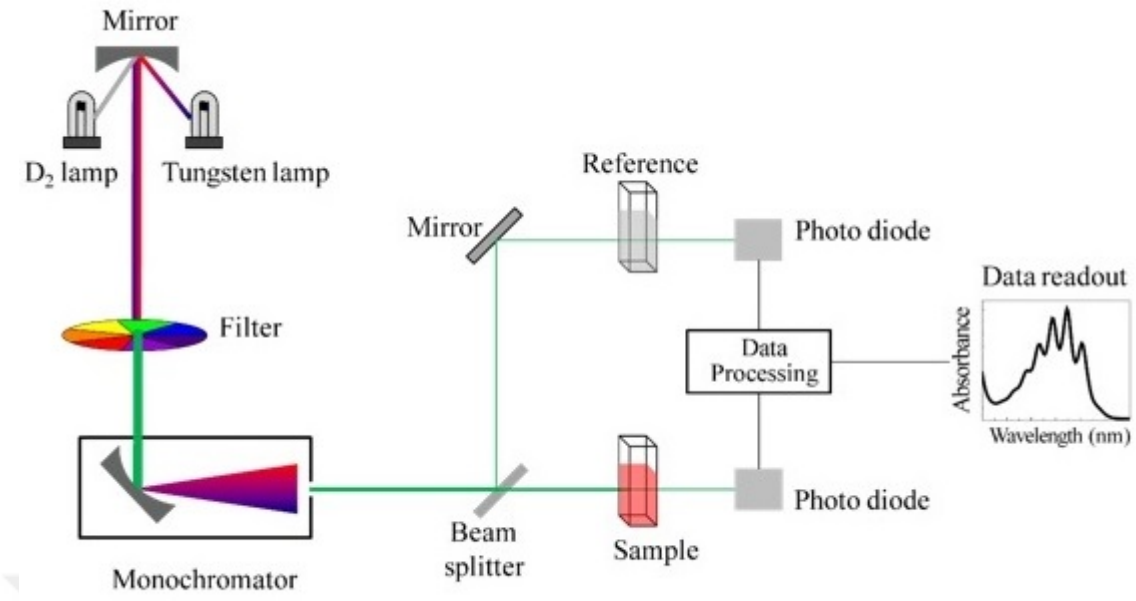

Figure 39: Schematic of UV- visible spectrophotometer [73].

PPC samples was painted and then coated. One of the XPS panels was also coated with $nano - TiO_2$ by sol-gel method. $Nano - TiO_2$ (15 g) and distilled water (∼500 mL) were added to a 1000-mL beaker and stirred by mechanical agitation to prepare a $nano - TiO_2$ suspension. The solution was aged under stirring for 24 hours and then the panels were coated by the solution and print screen method. They were dried at 80°C and analyzed with UV-Visible. The results are shown in Figure 42.

This wavelength range (0.2-0.8 μm) in Figure 42 was not adequate for analyzing radiative cooling so later FTIR was used, but this wavelength range can be considered as solar radiation band (0.2-2 μm) and the samples are analyzed as solar absorbers.

Capturing sunlight as a heat source efficiently is beneficial for many application like solar heating, solar thermal electricity, solar thermophotovoltaic, and solar thermoelectrics. More efficient benefits can be gained in this process just if the selective solar absorbers be used to absorb most of the solar wavelengths at the surface of the earth and under the standard atmospheric conditions This

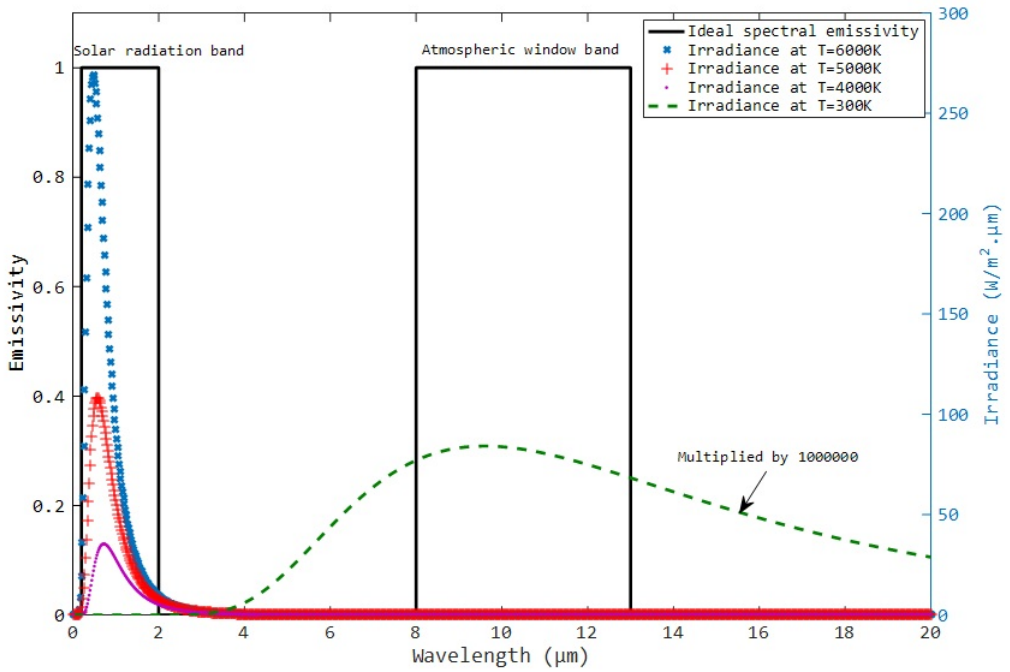

Figure 40: Ideal surface spectral emissivity, for solar heating and radiative cooling applications. The rectangular boxes show the desired spectral bands for the ideal case. Irradiance for T = 300 K is drawn after multiplying by 10^6.

atmospheric condition corresponds to absorbing most in the solar radiation band (0.2-2 μm) and reflecting everything else [76].

Because the samples considered were opaque; their spectral transmissivity was zero. We know α_λ+τ_λ+ρ_λ=1, and therefore, α_λ=1-ρ_λ. Based on Kirchhoff's Law, $\alpha_\lambda = \epsilon_\lambda$. Hence, the results provided below for lower reflectivity, correspond to higher emissivity.

A material for solar heating or solar absorber would have a high spectral emissivity or absorptivity in the solar radiation band (0.2-2 μm) and a low emissivity or absorptivity in other bands.

Painted and coated with $nano - TiO_2$ PPC sample, shows the highest reflectivity in the visible range (0.4-0.7 μm) and higher wavelengths and the painted sample (Painted with white paint as explained before) has the second rank as expected.

PPC and Silicium had high reflectivity in the 0.2-0.8 μm range. XPS is a green

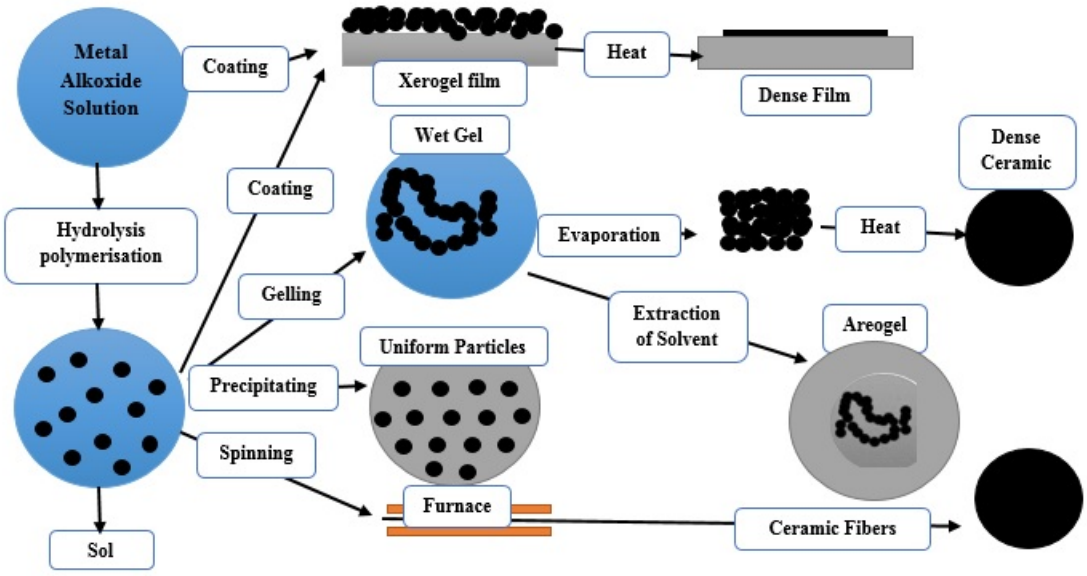

Figure 41: Schematic of sol-gel method.

foam that was used and it did not showed any regular behaviors in its spectral reflectivity but for both PPC and XPS samples, it can be seen that the titanium dioxide coating did a fairly good job on increasing the reflectivity, but as using nano coating did not change the reflectivity too much and coating the samples is not easy at all it can be concluded that the usage of this coating would not be logical in this application that is related to apply radiative cooling in the roofs.

As this project is based on using sustainable materials, coated samples were eliminated from the group of samples, so PPC, Painted PPC and XPS were kept for further analysis.

In the following, UV-Visible were done on XPS, PPC, Painted PPC, Red membrane, Black membrane and moss samples to evaluate them in the case of solar absorbers. Figure 43 shows the results.

For effectively capturing sunlight as heat source, selective solar absorbers are a critical technology. It was found that the highest performance for solar heating is the black membrane based on Figure 43. The capacity for performing at high temperature is significant, since the highest theoretical efficiency for converting the heat into electricity is at the high operating temperatures for fixing cold-side

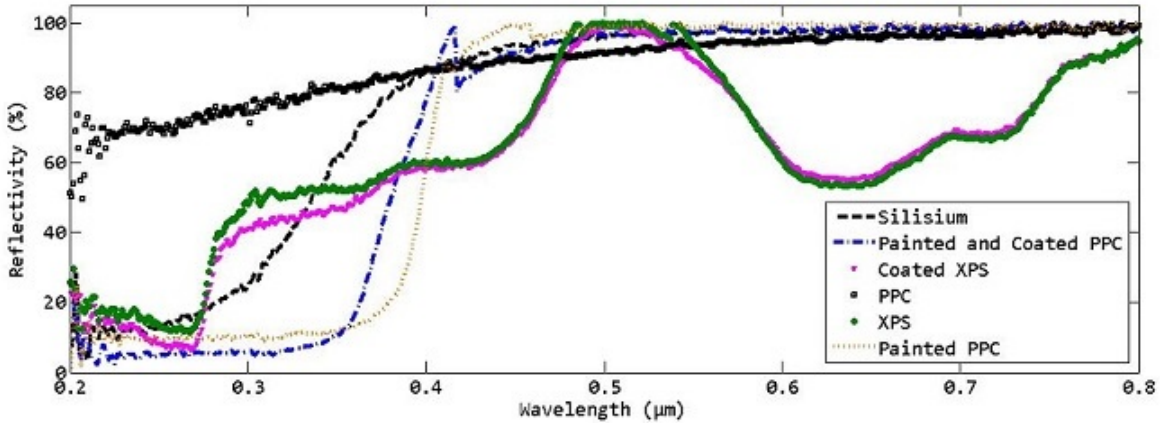

Figure 42: Near Field Reflectivity, Measurements were made using a Shimadzu 3150 UV-Visible-NIR Spectrophotometer (Performed at Sabanci University, Istanbul, Turkey).

temperature [76].

The results in Figure 43, show the black membrane is the only sample that has low reflectivity and high emissivity in the solar radiation band. Black membrane showed no reflection peak in UV light range, so based on the mentioned formulations above, it showed high absorption peak at UV. It can be noted from its spectra, that the absorption characteristic of the black membrane has a broader absorption wavelength compared to the other samples. If the samples were evaluated for a solar heating model or solar collector, black membrane would be the best candidate to be used.

3.4 Fourier-transform Infrared Spectroscopy (FTIR) description and results

As UV-Visible spectral range was not enough for evaluating radiative cooling, FTIR was done on the samples. FTIR is the technique used to obtain the spectrum of absorption, emission, and the main aim is to measure the amount of light absorbed by a sample each wavelength. In infrared spectroscopy, IR radiation is passed through a sample, so some of the infrared radiation is absorbed by the sample and some of it is passed through (transmitted). The resulting spectrum represents the molecular absorption and transmission [77]. Figure 44 shows

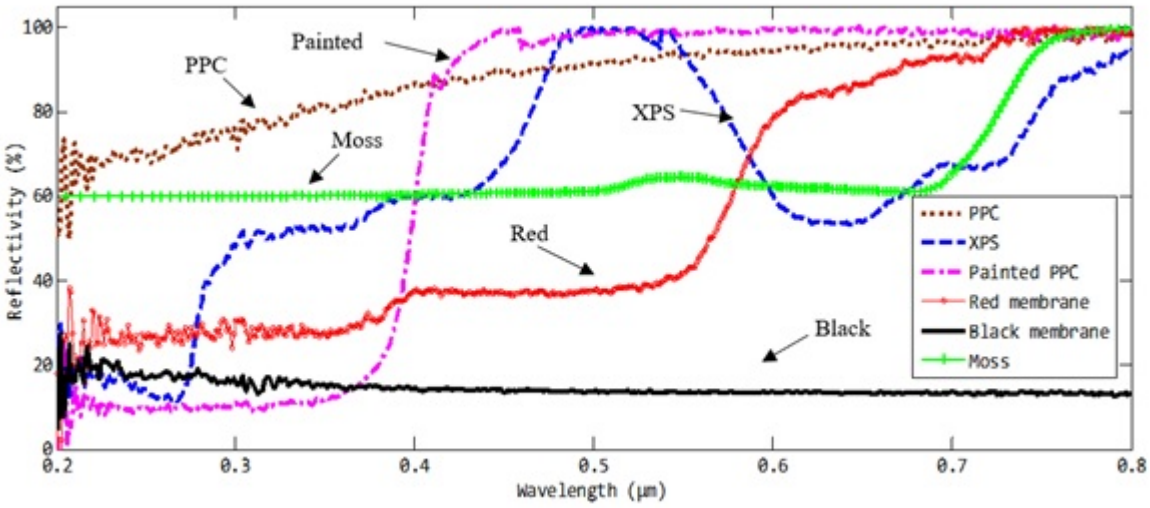

Figure 43: Near Field Reflectivity, Shimadzu 3150 , UV-Visible-NIR, Spectrophotometer (Performed at Sabanci University, Istanbul, Turkey).

a schematic of the FTIR device operation.

All FTIR (Fourier transform infrared) spectroscopy spectra were recorded as direct (specular) absorbance or transmittance. Diffuse absorbance and transmittance spectroscopy measurements in the UV/ Vis/ near IR region were carried out on a Nicolet iS10 FTIR Spectrometer (Figure 45) equipped with an integrating sphere that is shown in Figure 44. Spectra were recorded at room temperature between 4000 and 400 $cm^{-}1$. For sample preparation in hard solids like the samples in this study, if the solid is a hard inorganic solid, it should be like a powder before applying it to the crystal [71].

For evaluating the characteristics of the samples in atmospheric window, FTIR was used for the six selected samples (XPS, PPC, Painted PPC, Red membrane, Black membrane, and moss) which were explained in the previous section and the results are shown in Figure 46. From spectral emissivity, we can see the position of the two critical points (8 and 13) which are the beginning and end of the atmospheric window range (8-13 μm).

Based on Kirchhoff's law, the spectral emissivity is the same as the spectral absorptivity $\alpha_\lambda = \epsilon_\lambda$; for that reason, the results shown in Figure 43 are referred

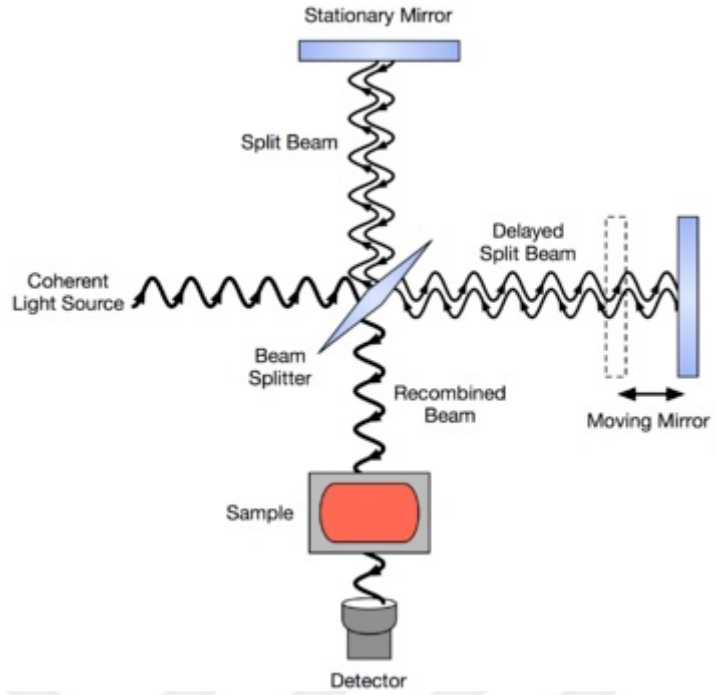

Figure 44: Schematic of the FTIR device [78].

as the spectral emissivity. It is noted from the data given in Figure 46 that moss, PPC, and Painted PPC have high spectral emissivity in the atmospheric window range of 8-13 mum, whereas their spectral emissivity is low within the other bands. This means that they can be good candidates as radiative emitters in the long wavelengths and for radiative cooling applications in daytime. On the other hand, XPS, black membrane, and red membrane had low spectral emissivity in the atmospheric window, so they do not have the potential to be used as a radiative cooler.

In plants for preventing water loss from internal tissues, cuticular has been developed as a barrier and can cover the epidermis leaves, fruits, petals of fruits, and non-lignified stems. Cuticles include mostly intracuticular waxes that are embedded in the cutin matrix and epicuticular waxes that are deposited on the surface [79].

Figure 45: Thermo-Nicolet iS10 FTIR, Sabanci University.

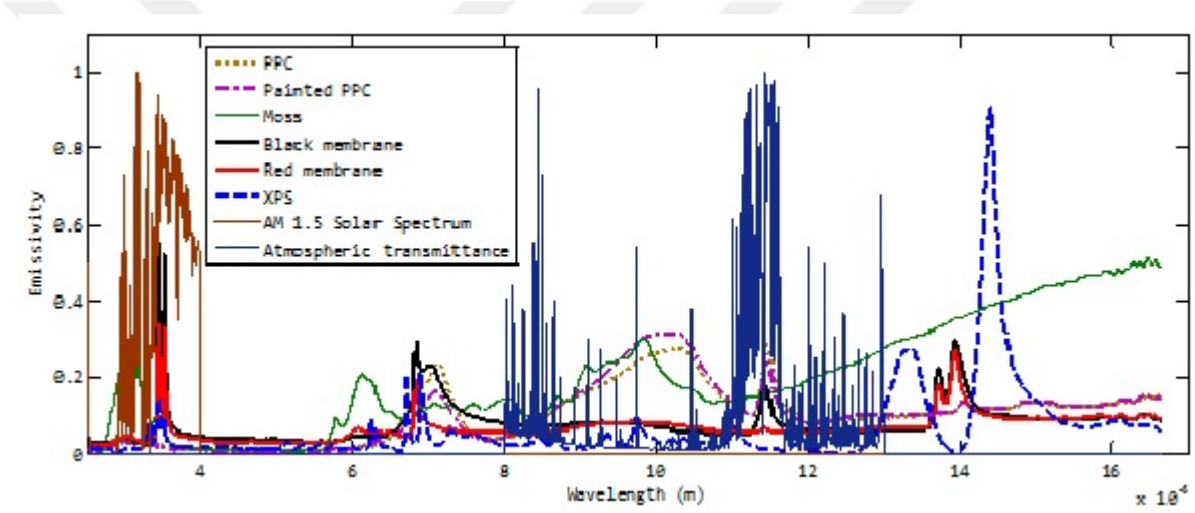

Figure 46: Spectral emissivity of the samples measured by Thermo-Nicolet iS10 FTIR spectrometer. (Performed at Sabanci University, Istanbul, Turkey).

3.4.1 Spectral emissivity of various samples taken by FTIR

Figure 47 shows the effect of titanium dioxide on increasing the radiative cooling. Titanium dioxide is the most significant white pigment currently produced which is used as IR radiator [10]. For this, adding a titanium dioxide as a coating on the surface of XPS improves the radiative properties of the surface.

It should be noted that in the examples of this section, abrorbance is equal to absorptivity and based on Kirchhoff's Law which is described before, spectral emissivity and spectral absorptivity are equal to each other.

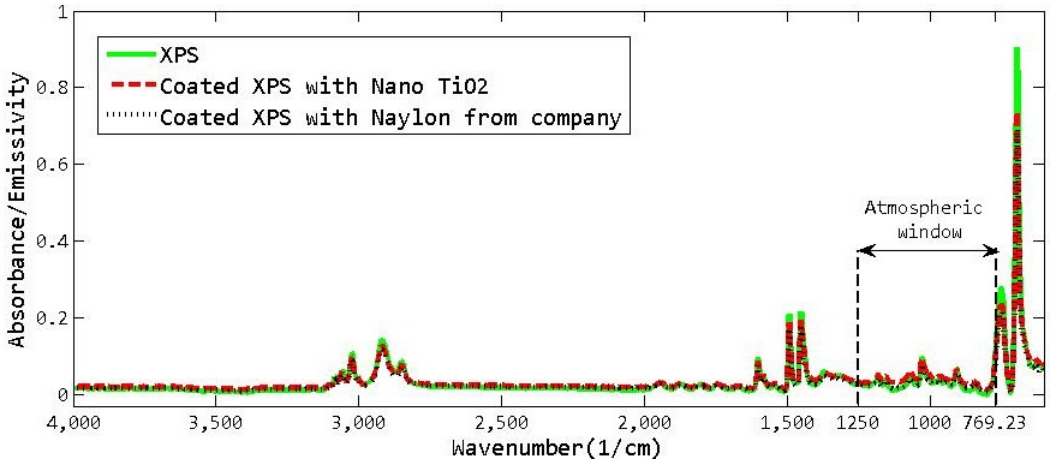

Figure 47: Effect of coating on spectral absorbance of the XPS measured by Thermo-Nicolet iS10 FTIR spectrometer. (Performed at Sabanci University, Istanbul, Turkey).

Figure 48 shows the effect of titanium dioxide as a coating and white paint as a paint on increasing the radiative cooling of PPC. Titanium dioxide as a good radiative cooler increases the abrorbance of PPC. White paint also has this capability to increase the radiative cooling of PPC but as it is obvious from the Figure 48 and in the other figures, does not increase the radiative cooling potential too much so painting the surface as it increases the cost will be rejected as a candidate in this study.

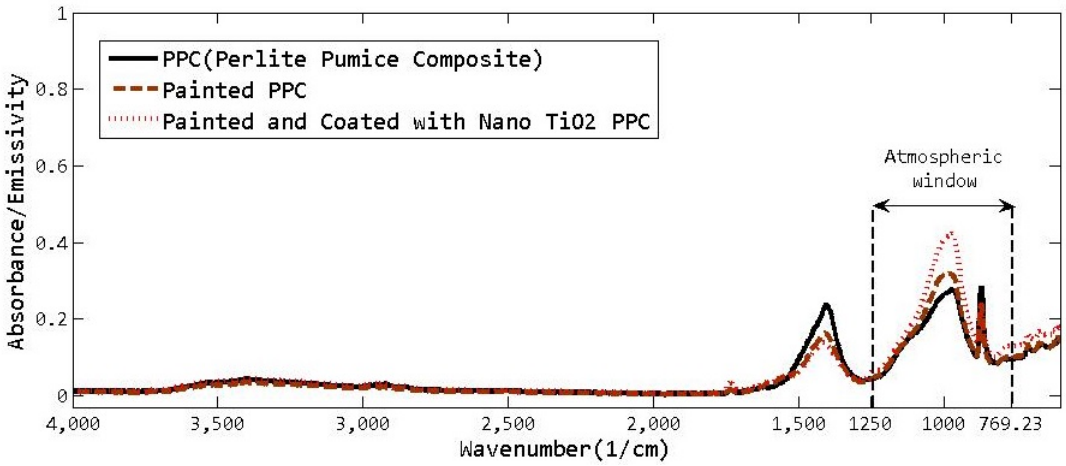

Figure 48: Effect of coating and paint on spectral absorbance of PPC measured by Thermo-Nicolet iS10 FTIR spectrometer. (Performed at Sabanci University, Istanbul, Turkey).

Titanium dioxide which was used in this study was nanopowder, however nano Titanium dioxide depicted improving the radiative cooling on the surface of the samples, but as the goal of this study is the evaluation of radiative cooling in the roofs of the buildings and nanomaterials are expensive so nano Titanium dioxide will also be rejected among the candidates as radiative coolers.

The concentration of this study was on the application of inexpensive materials in radiative cooling such as sustainable materials, but the other materials were also added to the experiments for further analysis.

Figure 49 represents that among building facades (black membrane, red membrane and moss), moss effects the better role as radiative cooler. Both black membrane and red membrane are so weak as radiative cooler.

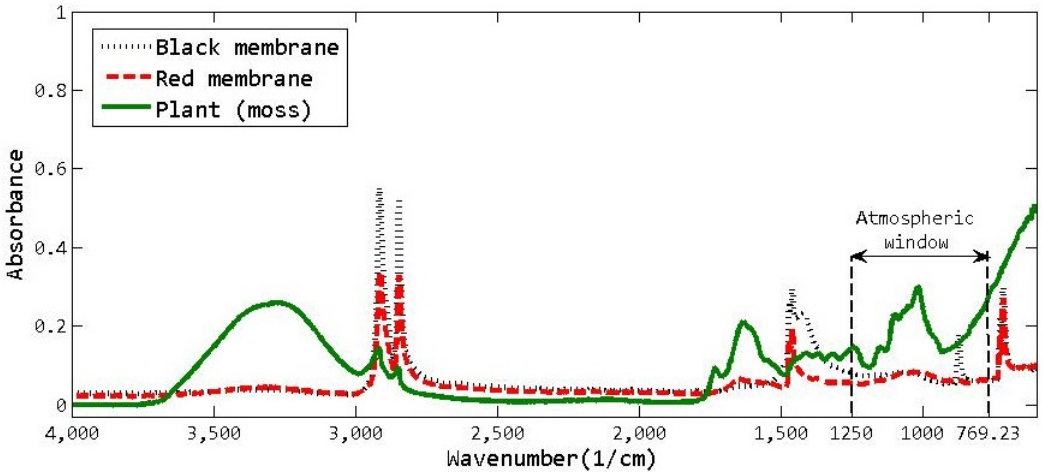

Figure 49: Building facades spectral absorbance measured by Thermo-Nicolet iS10 FTIR spectrometer. (Performed at Sabanci University, Istanbul, Turkey).

Figure 50 shows that among XPS, PPC, Painted PPC and moss, moss is the best one for radiative cooling applications. PPC and Painted PPC have the same behaviour as radiative cooler and XPS is a very weak radiative cooler.

The comparison between the radiative cooling performance of mussel (white part and purple part of it) and pistachio shell is presented in Figure 51. As it is obvious from the figure, mussel does not have high spectral absorbance or emissivity in the atmospheric window in both sides of it, but on the other hand it seems

that pistachio may be a good candidate as a radiative cooler.

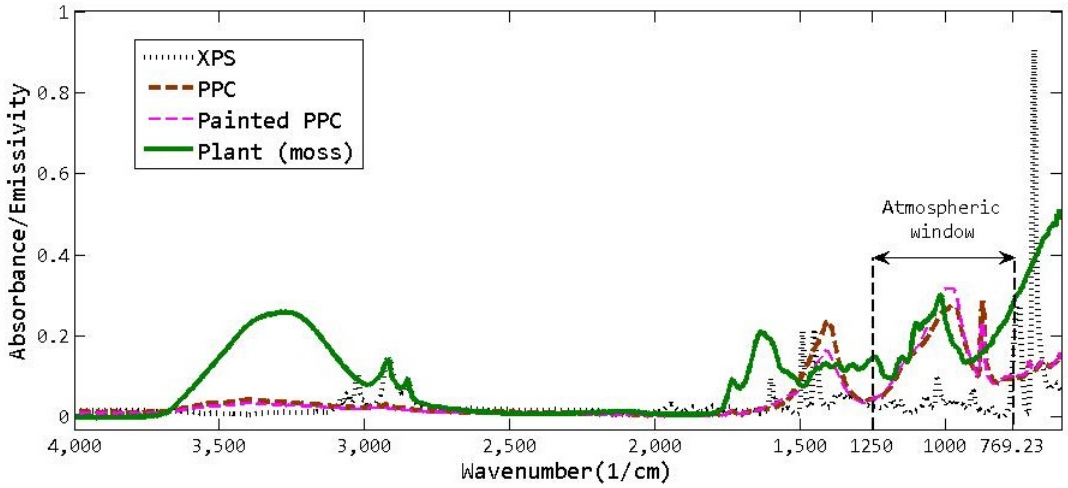

Figure 50: Spectral absorbance of building materials measured by Thermo-Nicolet iS10 FTIR spectrometer. (Performed at Sabanci University, Istanbul, Turkey).

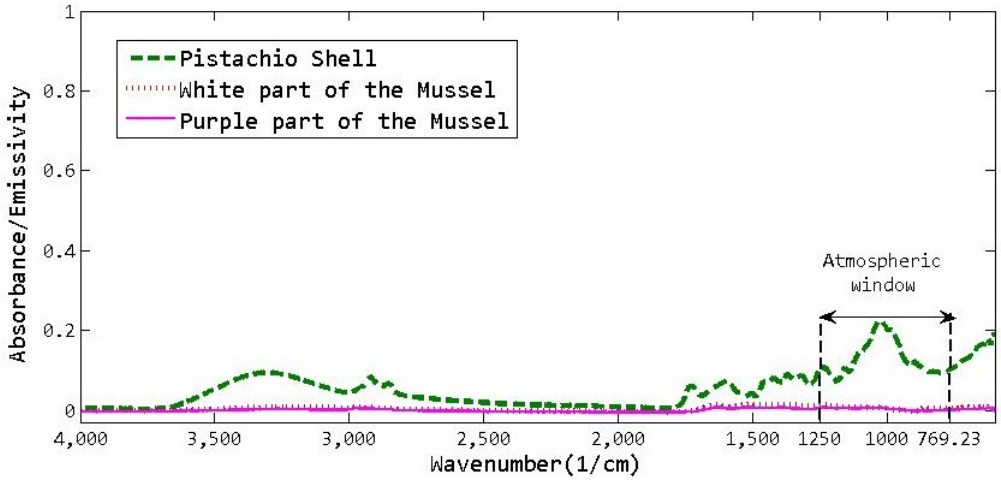

Figure 51: Spectral absorbance of mussel and pistachio measured by Thermo-Nicolet iS10 FTIR spectrometer. (Performed at Sabanci University, Istanbul, Turkey).

Figure 52 shows the comparison of different plant types on radiative cooling. Among moss, leaf, and cactus, moss increase the radiative cooling of the green roofs more. The usage of these three types of plants as green roofs on the surface of the PPC or concrete and soil will be evaluated with more details in the last chapter.

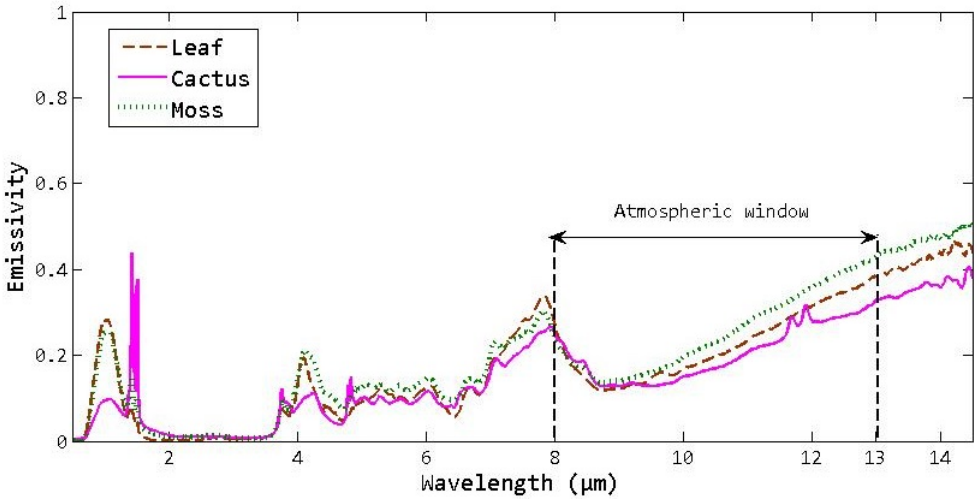

Figure 52: Spectral emissivity of of Green Roof Samples measured by Thermo-Nicolet iS10 FTIR spectrometer. (Performed at Sabanci University, Istanbul, Turkey)

Figure 53 shows the comparison of different stone types on radiative cooling. Among Cappadocia stone, Black and Red Ephesus stones, Red Ephesus stone increase the radiative cooling to some extent more than other for stone roof applications.

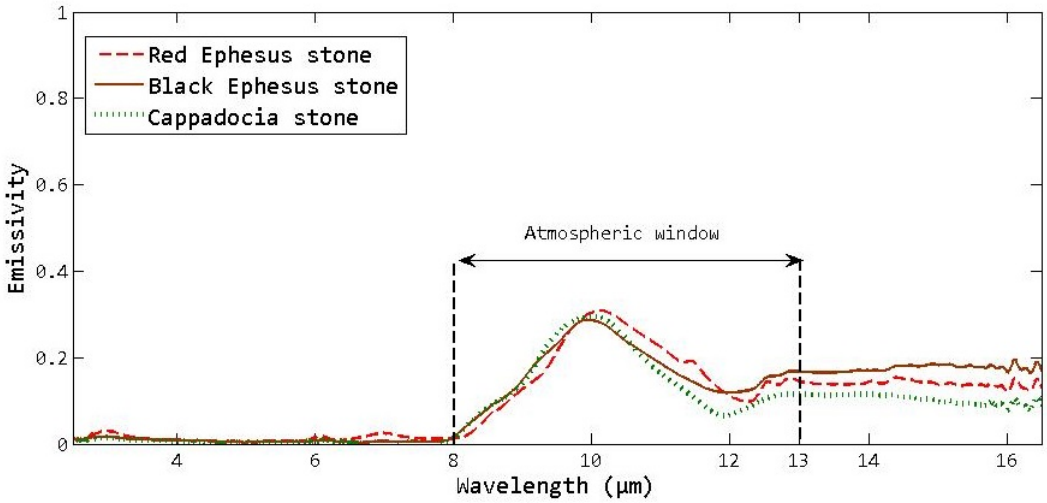

Figure 53: Spectral emissivity of Stone Roof Samples measured by Thermo-Nicolet iS10 FTIR spectrometer. (Performed at Sabanci University, Istanbul, Turkey)

3.4.2 Spectral absorption coefficient results

The absorption spectra of the samples in two series, are presented in Figures 54 and 55. Absorbance or absorptivity (or emissivity) of the samples were measured by FTIR, as explained in the previous section. In the samples considered, the spectral properties, which are essential for radiative cooling calculations were not available at all. The properties in specific experiments had to be measured, which could be compared against the numerical results for validation. Such results, are depicted in Figures 43 and 46. The spectral absorption coefficient κ_λ of the samples can be calculated by [11].

$$\kappa_\lambda = (2.3 \times A_\lambda)/t \tag{10}$$

where A_λ is the spectral absorbance measured from the experiments and t is the thickness of a sample. This equation is based on a direct relationship between the spectral absorptivity and the spectral absorption coefficient. It is noted that high spectral absorption in the atmospheric window yields better performance for radiative cooling, as it was obvious in moss, PPC, and Painted PPC samples.

In the following analysis, the spectral absorption coefficient of the samples was plotted by dividing them into two groups. In the first group, PPC, Painted PPC and moss displayed similar behaviors of increase and decrease in the wavelength range of atmospheric window (8-13 μm). However, for the moss sample, after 11 μm wavelength there was a dramatic increase in the spectral absorption coefficient. A change like that, in the curvature of the absorption coefficient, shows a change in band gap [80]. In the second group of the samples, XPS, black membrane, and red membrane did not show any significant absorption coefficient in the atmospheric window range.

It is noted above that high spectral absorption in the atmospheric window is better for radiative cooling. From the results above, it was obvious that moss, PPC, and Painted PPC samples were better candidates for this application.

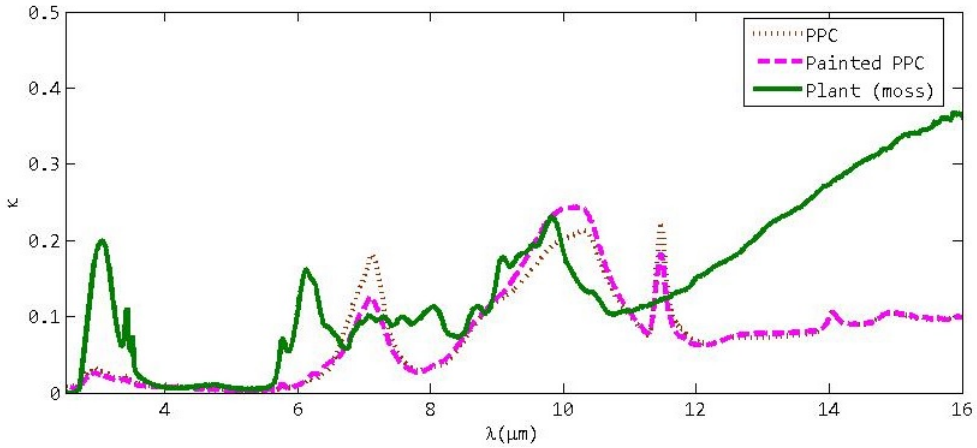

Figure 54: Spectral absorption coefficient (in units of 1/m) of roof materials measured by Thermo-Nicolet iS10 FTIR spectrometer (Performed at Sabanci University, Istanbul, Turkey).

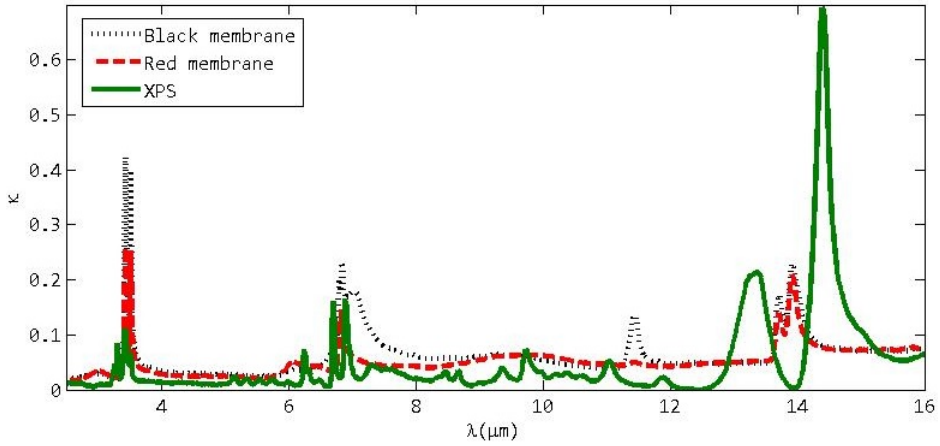

Figure 55: Spectral absorption coefficient (in units of 1/m) of roof materials measured by Thermo-Nicolet iS10 FTIR spectrometer (Performed at Sabanci University, Istanbul, Turkey).

Band Approximation with Stepwise Gray Box Model:

If a medium is semi-transparent, then radiation penetrates the medium. The ability of the materials to absorb thermal radiation might be expressed by the absorption coefficient [81]. Spectral absorption coefficient of a material, dictates how far spectral radiation penetrates into it, and the absorption coefficient depends on the nature of the material [82][83]. The spectral models for the absorption coefficients (in units of 1/m) for six different samples, are presented in Figures 54 and 55. Note that these κ_λ values were determined using the Equation (10) given above.

Three separate spectral intervals (the so-called gray bands) were selected. The solar window, the atmospheric window, and one in between were considered. In Figure 56, PPC, Painted PPC, and moss results are shown. In Figure 57, XPS, black membrane, and red membrane results are presented based on the stepwise gray box model which will be explained in details in the following chapters. Figures 58 to 63 represent the spectral absorption coefficient, calculated experimentally and numerically for each of the six samples.

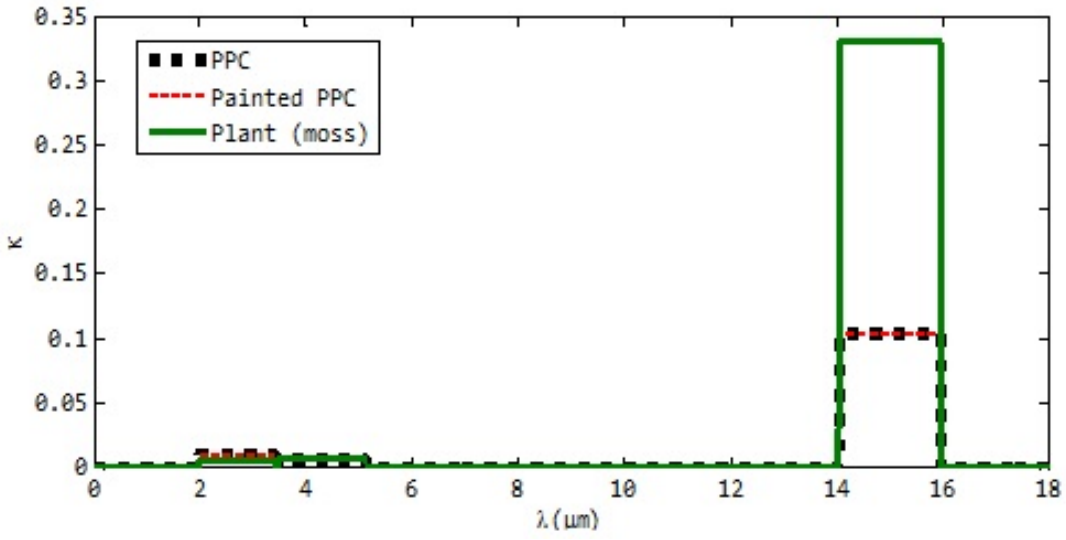

Figure 56: Box model approximation for the absorption coefficient of different roof materials; in units of 1/m, PPC, Painted PPC, and Plant (moss).

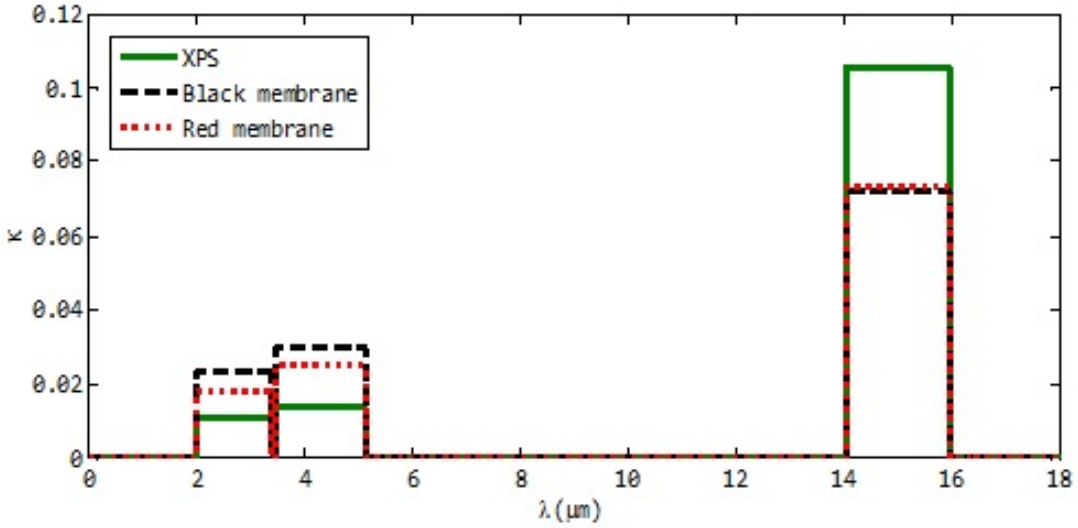

Figure 57: Box model approximation for the absorption coefficient of different roof materials; in units of 1/m, XPS, Black membrane, and Red membrane.

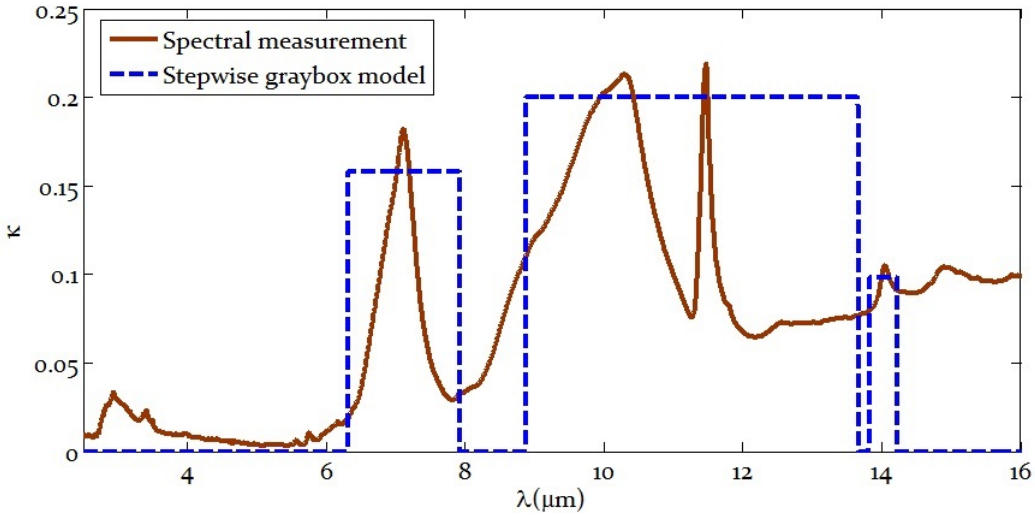

Figure 58: Spectral absorption coefficient of PPC. Comparisons of experimental and numerical results, in units of 1/m.

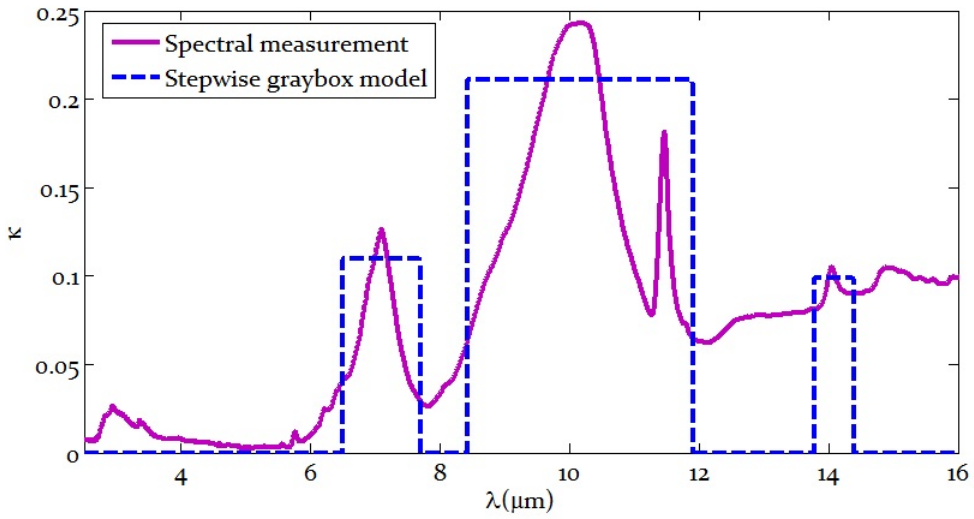

Figure 59: Spectral absorption coefficient of Painted PPC. Comparisons of experimental and numerical results, in units of 1/m.

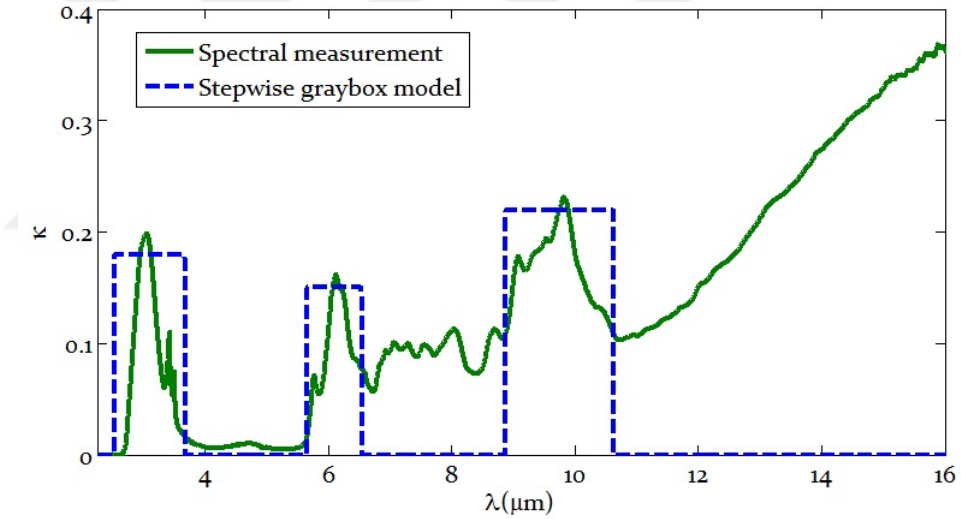

Figure 60: Spectral absorption coefficient of Plant (Moss). Comparisons of experimental and numerical results, in units of 1/m.

As shown in Figure 60, there is a sharp increase in the spectral absorption coefficient for moss at wavelengths longer than 11 μm, which could be related to cutin [84]. In plants, for preventing water loss from internal tissues, cuticles are formed as a barrier and can cover the epidermis leaves, fruits, petals of fruits, and non-lignified stems. Cuticles include mostly intracuticular waxes that are embedded in the cutin matrix, and epicuticular waxes that are deposited on the surface

[79]. The sharp increase was attributed to the presence of cutin in moss.

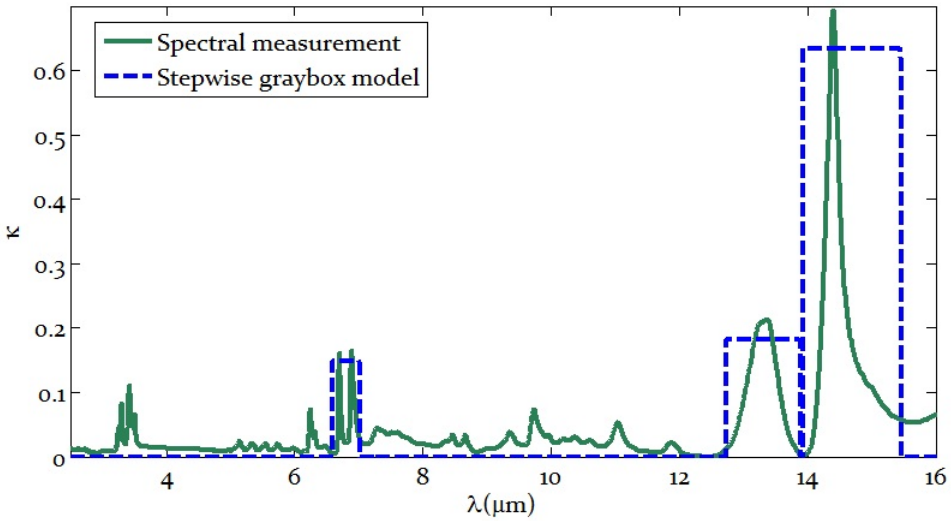

Figure 61: Spectral absorption coefficient of XPS . Comparisons of experimental and numerical results, in units of 1/m..

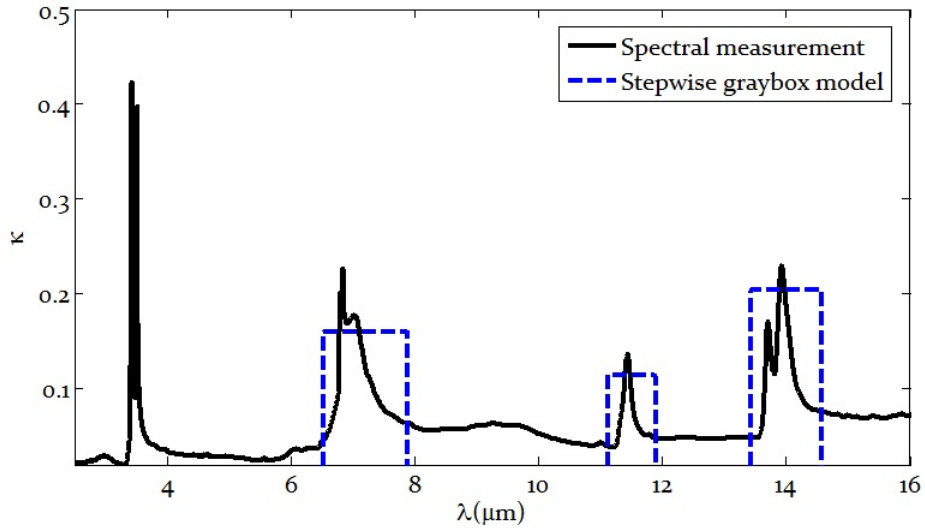

Figure 62: Spectral absorption coefficient of Black membrane . Comparisons of experimental and numerical results, in units of 1/m.

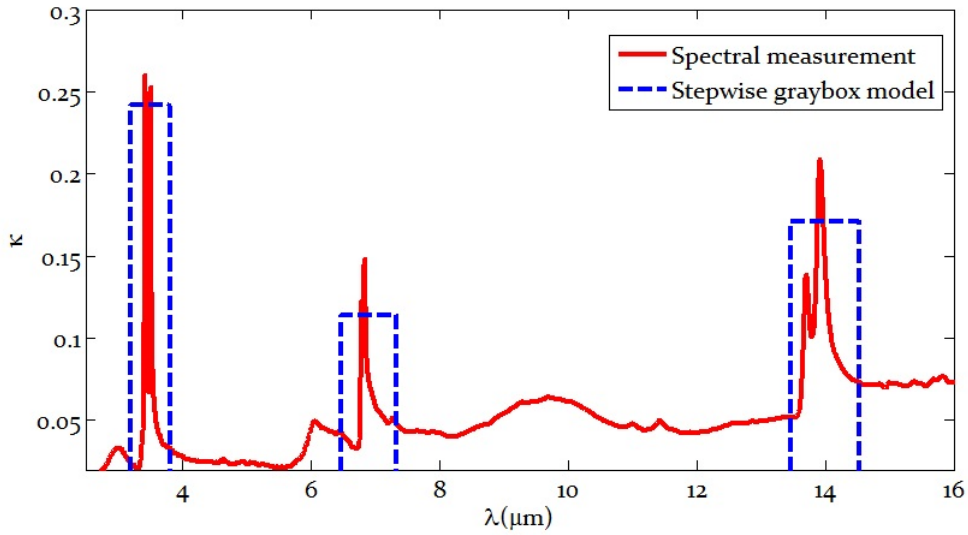

Figure 63: Spectral absorption coefficient of Red membrane . Comparisons of experimental and numerical results, in units of 1/m.

3.5 Description of Reverse Heat Leak Method (RHLM)

How fast a material can conduct the heat is the thermal conductivity and the transfer of heat through solids is conduction. The thickness of the material, temperature difference, and area of the material are the factors that rate of heat flow like the conductivity of the material.

A measurement of a temperature difference that a material resists a heat flow by it, is a heat property which is thermal resistance. Actually, it is the reciprocal of thermal conductivity, but in construction and building, the measurement of how an object per unit area, resists the conductive flow of heat, is called R-value. Therefore, the great the R-value would cause the greater the resistance, and at last the less conductivity which shows the object is better in thermal insulating. The parameters which are significant in R-value are the type of the material, its density, and its thickness.

Materials with high thermal conductivity can be used in heat sink applications and materials with low thermal conductivity in thermal insulation ones [85].

In this study, determination of R-value for materials is significant for quantification of insulation properties and for solving coupled radiation and conduction.

One of the reliable techniques to evaluate the R-value, is the reverse heat leak method (RHLM), which is a major thermal testing method extensively used in the refrigeration industry to test U values of refrigerators [86]. Numerous studies [87][88][89] exist on employing RHLM. While the technique is same, different types of heating elements for simulating the heat load is being used in these studies.

Two prototype samples of dimensions 58 ×58×2 cm were developed. To evaluate the thermal conduction transfer and for solving coupled radiation, R-values should be measured. In this part, the experimental setup which was built consists of the insulation box that was made of Extruded Polystyrene Foam (XPS), test surface, heat load, and the data acquisition system which is composed of thermocouples, a multiplexer, and a data logger. The top is left open as the test surface for testing the fabricated prototype panels whose R-values are to be determined. A commercial software was used for achieving the raw data and real-time monitoring of temperature values. In Figure 64 a schematic of the experimental setup is shown.

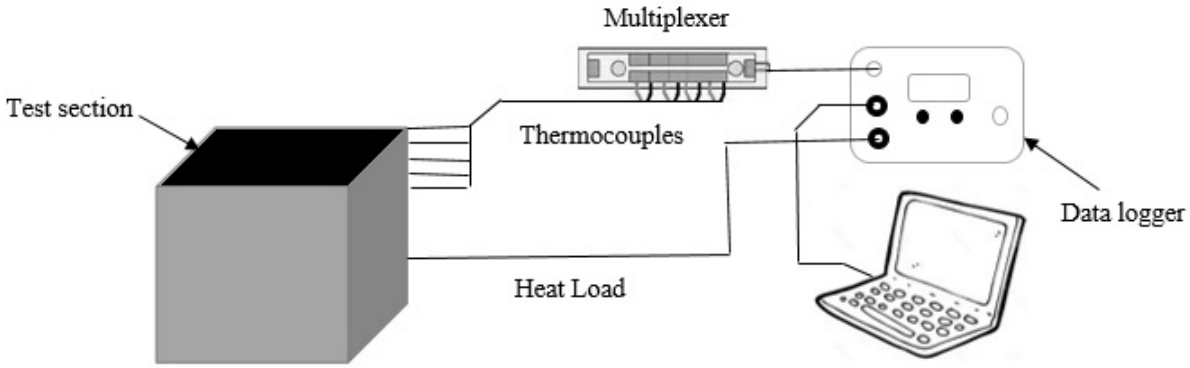

Figure 64: Schematic of the conduction test setup.

In total, 18 T-type thermocouples were calibrated and implemented at selected locations for measuring ambient air, inside air and surface air temperatures. Surface temperatures were measured both on the outer and inner surfaces of each face of the box, centered symmetrically. All thermocouples measuring surface temperatures were covered with 2×2×0.5 cm XPS foam to isolate the thermocouple tips

from the surrounding effects. Inside air temperature was measured at two levels (at one quarter and three-quarters of the inner height) within the box, to get an average inside temperature. Respectively, outside air temperature was measured at four sides of the box. The test box was placed on a hollow galvanized steel stand to ensure that the bottom surface is also completely exposed to outside air. To block the flow of heat through the metal stand, insulative separators were placed between the stand and the box, and rubber strips were used underneath the legs of the stand. The sampling frequency of temperature data collection was one minute. For each test, it was first assured that steady-state was assured, followed by at least one hour of data collection to get at least sixty data at steady state conditions for minimizing the standard deviation. Figure 65 illustrates the reference (XPS) box, along with the heat load (10.5 W light bulb) and thermocouples. The theoretical analysis and the theoretical and experimental R-value results will be explained in the following chapters.

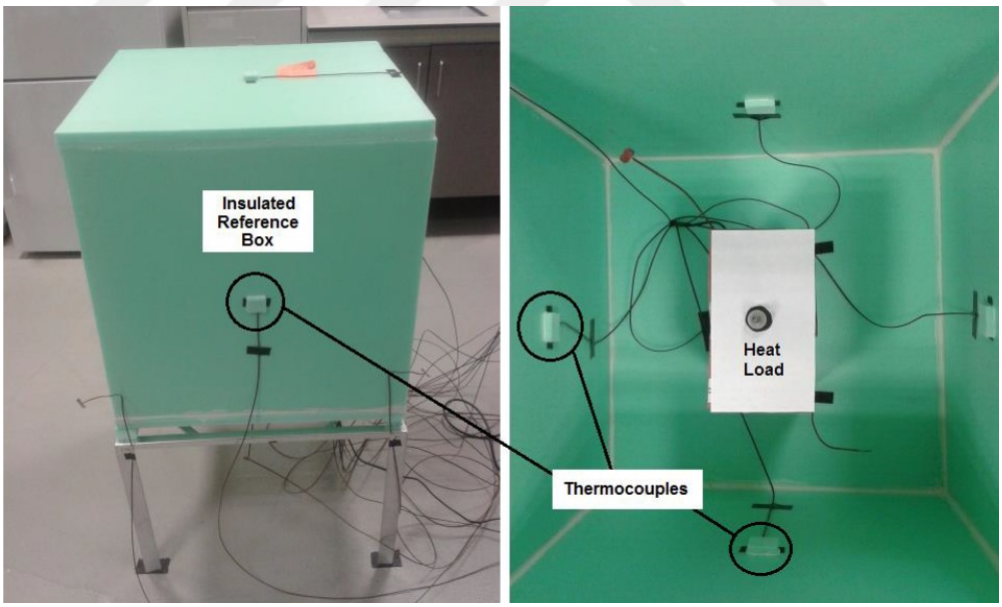

Figure 65: Insulated box with the heat load and thermocouples.

3.6 Discussion

The goal of this study was to evaluate the potential of sustainable materials in radiative cooling, and as the concentration of radiative cooling was in the roofs,

for this the heat conduction and radiation of these materials also was analyzed through the thickness of the roof.

Sustainable materials were used for radiative cooling applications for the first time. For this, in the beginning, the optical properties of them were measured as they were not available in the literatures. In the experimental part,the following attempts have been done.

1. Firstly, a large category of sustainable materials was gathered and the morphology of the surface of them was evaluated under the optical microscope. As these materials have to be used on the surface of the roof like a coating, analyzing the morphology of them is profound. Meanwhile these results can be beneficial for further analysis and also using them in other applications. However for more precise morphology analysis using scanning electron microscopy (SEM) is recommended.

2. Secondly, UV-Visible was done on the samples. UV-Visible wavelength range was not enough for evaluating the samples for radiative cooling, so it was used for selecting the best solar absorber. It was done one two groups of materials. First general materials and second on six selected materials which were sustainable materials and among them the black membrane had the good potential to be a solar absorber. All extra results can be used in other applications as these comparisons have been done for the first time.

3. In the following, FTIR was done for choosing the materials as radiative coolers and among the six selected samples, moss had the highest potential to be a radiative cooler rather than others. Furthermore, FTIR was done on a large group of different materials and their ability to be a good radiative cooler was compared with each other.

Table 2: Cooling behavior of materials.

Material	**Potential as a Solar absorber**	**Potential as a Day time Radiative Cooler**	**Potential as a Night time Radiative Cooler**
PPC	Weak	Good	Good
Painted PPC	Weak	Good	Good
Plant or moss	Weak	Good	Good
Black membrane	Very good	Weak	Weak
Red membrane	Good	Weak	Weak
XPS	Weak	Very weak	Very weak

Generally, Materials with high emissivity in the atmospheric window and low in other bands can be considered as radiative coolers, and the ones with high emissivity in both solar radiation band and atmospheric window range, are candidates for being solar radiators in the daytime and radiative cooler at nighttime. Among the six selected materials in this study, moss, PPC and Painted PPC can be considered as radiative coolers, and black membrane would be a solar absorber, and the summary of them is presented in Table 2.

4. For evaluating the total heat transfer through the roofs, both conduction and radiation is needed and coupled conduction and radiation must be solved. For solving coupled conduction and radiation, conductivity value has to be measured via calculating the R-value. In this study, reverse heat leak method (RHLM) was used and theoretical analysis of it with more details and the results will be explained in the following chapters. This R-value or conductivity value can be fruitful in figuring out which of the mentioned materials is the best heat insulator in the roofs applications.

Chapter IV

NUMERICAL ANALYSIS

4.1 Power of cooling with constant temperature

4.1.1 Introduction and Mathematical Formulations

The phenomenon of "radiative cooling" is obtaining a cooling power by the objects on the surface of the earth, through radiating heat to the cold outer space in the atmospheric window (8-13 μm) [38].

First, a simple analysis of heat balance for buildings surfaces will be provided. Temperature is assumed constant within the medium, and only the radiative energy balance on a surface has been considered. This is called the "power of cooling" analysis. The schematic for the system considered, is shown in Figure 66.

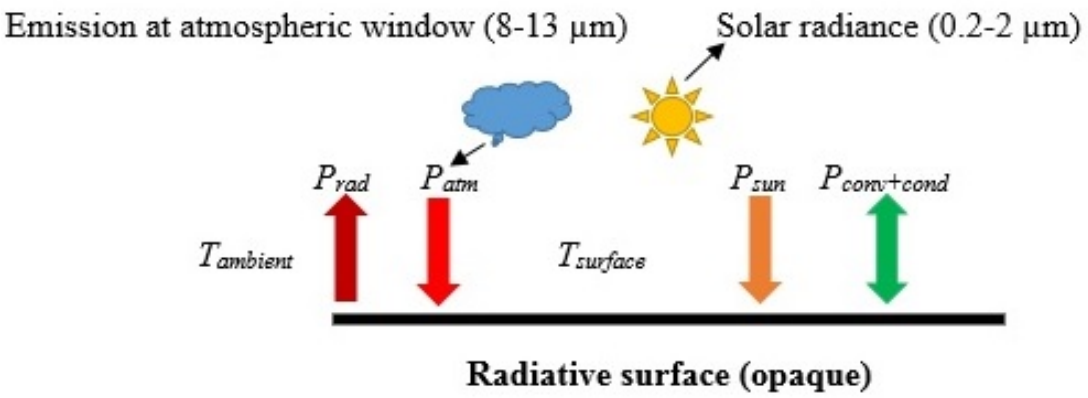

Figure 66: Schematic of radiative cooling based on radiative energy balance on an opaque surface.

T_S, the surface temperature of an opaque surface was constant, with an angular and spectral emissivity $\epsilon(\lambda, \Omega)$. ϵ is the emissivity, λ is the wavelength and Ω is the solid angle.

The structure is subjected to solar irradiance and atmospheric irradiance and is exposed to a clear sky corresponding to an ambient temperature T_{amb}. $P_{net}(T)$

gives the net cooling power of the surface per unit area of the structure.

$$P_{net}(T) = P_{out} - P_{in} \tag{11}$$

$$P_{out} = P_{rad}(T) = Q_{emitted}(T_s) \tag{12}$$

$$P_{rad}(T) = \int d\Omega cos\theta \int_0^{\infty} d\lambda I_{BB}(T,\lambda)\varepsilon(\lambda,\Omega) \tag{13}$$

The radiated energy by the surface per unit area is integrated over all angles,

$$\int d\Omega = \int_0^{\pi/2} d\theta \sin\theta \int_0^{2\pi} d\phi. \tag{14}$$

which provides the angular integral over a hemisphere. The spectral intensity of the Planck blackbody radiation at temperature T is given as [11]

$$I_{BB}(T,\lambda) = \left({}^{2hc^2}/_{\lambda^5}\right) / \left[e^{{}^{hc}/_{(\lambda K_B T)}} - 1\right] \tag{15}$$

which yields,

$$P_{in} = P_{atm}\left(T_{amb}\right) + P_{sun} + P_{cond+conv} \tag{16}$$

$$P_{atm}\left(T_{amb}\right) = \int d\Omega \cos\theta \int_0^{\infty} d\lambda I_{BB}\left(T_{amb},\lambda\right) \varepsilon\left(\lambda.\Omega\right)\varepsilon\left(\lambda,\Omega\right) \tag{17}$$

is the absorbed power per unit area emerging from the atmosphere, and

$$P_{sun} = \int_0^{\infty} d\lambda \varepsilon\left(\lambda,0\right) I_{AM1.5}\left(\lambda\right) \tag{18}$$

is the incident solar power absorbed by the structure per unit area, and for achieving equations (17) and (18), Kirchhoff's Law, $\alpha_{(\lambda,0)} = \epsilon_{(\lambda,0)}$ has been applied for zenith angle of zero, and the angle-dependent emissivity of the atmosphere is given by

$$\varepsilon_{atm}(\lambda, \Omega) = 1 - t(\lambda)^{\frac{1}{\cos\theta}} \tag{19}$$

where t_λ is the atmospheric transmittance in the zenith direction [90]. k_B, λ, h, and c, are the Boltzmann constant, wavelength, Planck constant, and the speed of light, respectively. The solar illumination is represented by AM1.5 Global Tilt spectrum in equation (18), with an irradiance of 964 W/m^2, which represents the average solar conditions of the continental U.S. [12]. Assumed that the structure is facing the sun. Therefore, the term P_{Sun} is without an angular integral, and the structure's emissivity is represented by its value in the zenith direction $\theta = 0$ that would be $\varepsilon(\lambda, 0)$.

$$P_{cond+conv}(T, T_{amb}) = Ah_c(T_{amb} - T) \tag{20}$$

Equation 20 shows the lost power of convection and conduction. $h_c = h_{conv} + h_{cond}$ shows a combined non-radiative heat coefficient. As it was explained before, here, conduction and convection have been neglected for the sake of simplicity.

4.2 Theoretical analysis of heat conduction (R-value)

4.2.1 Introduction and Mathematical Formulations

For solving coupled radiation and conduction, measuring the conductivity value of the samples through R-value is significant.

Conduction heat transfer through the fabricated panels were analyzed to identify the thermal resistance values (R-values) of the samples. Quantification of the R-value of structural components is crucial as it is a direct measure of the insulative performance of these materials. Determination of R-values can be achieved both theoretically and experimentally [91].

Conduction heat transfer through the panel is

$$\int_{y=0}^{y=L} q\frac{dy}{A(y)} = -\int_{T_i}^{T_0} k(T)dT \tag{21}$$

where q is the heat flux (W/m^2), k is the thermal conductivity (W/mk), and T is the temperature. The thermal conductivity k is a function of temperature, in general case. For a uniform medium, Equation (21) is reduced to

$$q = -k\nabla T \tag{22}$$

R-value is related to conductivity k as (l is the thickness and k is the thermal conductivity).

Experimental analysis of the R-value, on the other hand, was carried out using reverse heat leak method (RHLM), as explained with details before.

According to this method, it is assumed that under steady state all the heat from the heat load (10W light bulb) will be leaking through the insulated box that is composed of five reference walls and one test wall under the steady state conditions:

$$q_{panel} = q_{heatload} - \sum q_i \tag{23}$$

where i indicates any wall but the test wall (i = 1, 2, …,5). Heat leaking through these five walls is calculated employing $Fourier's$ law (Applying Fourier's law to the 2-D geometry, a set of following equations are obtained, leading to the R -value of the prototype panel).

The difference, according to Equation 21 gives the heat leak through the sample wall that is being tested. This tested sample panel with a varying cross-sectional area along the path of heat flow is given in Figure 67.

For the sake of simplicity, theory can be applied on one quadrant of the panel, which can be reflected as one half of the drawing in Figure 67 with respect to y-axis. The width of this quadrant is a function of y.

$$a(y) = a_1 + \frac{a_2 - a_1}{L} y \tag{24}$$

$$A\,(y) = (2a)^2 \tag{25}$$

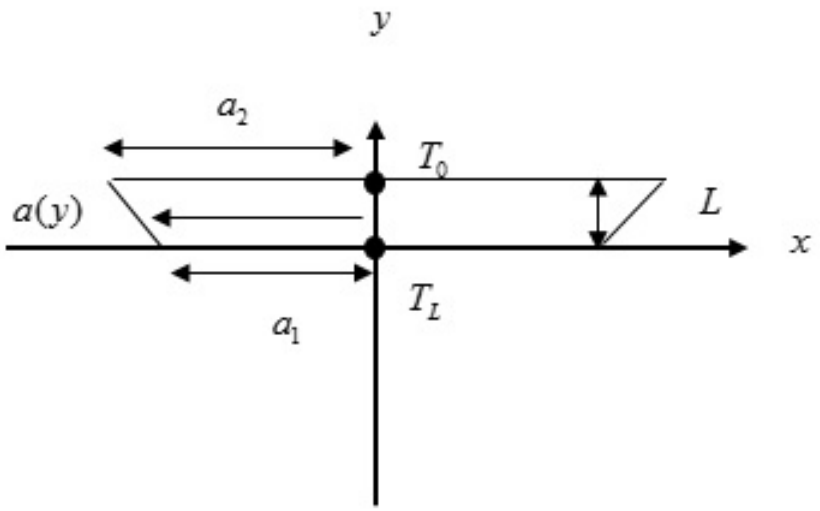

Figure 67: 2-D view of the tested panel with varying cross-sectional area in the direction of heat flow.

$$A\left(y\right) = 4\left(a_1 + \frac{a_2 - a_1}{L} y\right)^2 \tag{26}$$

Embedding Equation (26) into Equation (21) and integrating it gives the heat flow rate of the system and in the following, thermal resistance (R-value) can easily be calculated.

$$q = 4k\frac{a_1 a_2}{L}\left(T_i - T_0\right) \tag{27}$$

$$R_{panel} = \frac{4a_1 a_2 (T_i - T_o)}{q_{panel}} \tag{28}$$

Conduction heat flux through media (Figure 67) is approximated to be 1-D along with a neglect of void and moisture within the medium, so conductivity will be calculated based on Equation 21.

4.2.2 Uncertainty analysis

Uncertainty analysis for the obtained R-values was performed at 95% confidence level (2σ). Temperature, power (heat transfer rate of the heat load), and area measurements were considered in the analysis per the relation is given in Equation 29.

$$R = \frac{(A)(\Delta T)}{q} \tag{29}$$

Total error from all measured quantities can be calculated as in Equation 30 [92].

$$U = \pm\sqrt{U_{Pr^2} + U_{Bi^2}} \tag{30}$$

where U_{Bi} and U_{Pr} are the bias and precision errors, respectively. Then, uncertainties of the R-value measurements for all samples can be calculated using Equation 31.

$$\frac{U_R}{R} = \sqrt{\left(\frac{U_A}{A}\right)^2 + \left(\frac{U_T}{T}\right)^2 + \left(-\frac{U_W}{W}\right)^2} \tag{31}$$

where A, T, and W are measured values of area, temperature, and heat transfer rate, respectively.

4.3 Coupled heat conduction and radiation with temperature profile in one dimensional gray media

4.3.1 Introduction

By considering a thick semi-transparent structure (Figure 68), both the volumetric radiation and conduction heat transfer are accounted for in the analysis. Absorption and emission of radiation are considered from both sides of the surface. In this work, P1 approximation was applied for the solution of radiative transfer equation [93]

The radiative transfer equation (RTE) is an integro-differential equation in five independent variables (two in direction and three in space), which is exceedingly difficult to solve, for this, several approximate methods such as P1 approximation, the Discrete Ordinates Method or the Finite Volume Method, and the Monte Carlo Method are presently used most frequently [94]. Radiative transfer equation is shown in equation 32 and equation 33 shows the source function as well. Equation 34 also shows the optical thickness.

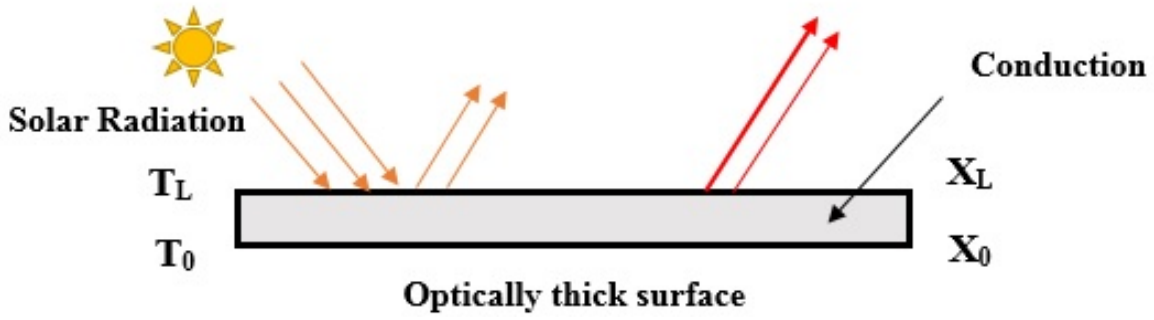

Figure 68: Schematic of an optically thick medium, where both radiation and conduction transfer are considered.

$$\mu\left[\frac{\partial I(\tau,\mu)}{\partial\tau}\right]+I(\tau,\mu)=S(\tau,\mu) \tag{32}$$

$$S(\tau,\mu)=(1-\omega)I_b\left[T(\tau)\right]+(\omega/4\pi)\int_{\phi'=0}^{2\pi}\int_{\mu'=1}^{1}\phi(\mu,\mu')I(\tau,\mu,\mu')d\mu'd\phi' \tag{33}$$

$$\tau=\int_0^y\beta dy \tag{34}$$

For certain problems, one radiation model may be more appropriate than the others. The comparison between different models is mentioned in Table 3.

P1 approximation was selected in this study for solving radiative transfer equation which has enjoyed great popularity because of its compatibility with standard solution methods and relative simplicity [93].

Starting from equation 32 by taking the zeroth and first moments of the equation and integrating equation 34 over all directions after multiplication with μ^0 that is the zeroth moment and μ^1 that is the first moment, intensity moments as equation 35 will be defined [93]

$$\mu\frac{dI}{d\tau}=(1-\omega)I_b-I+\frac{\omega}{2}\int_{-1}^{1}Id\mu,-1<\mu<1 \tag{35}$$

$$I_k=2\pi\int_{-1}^{1}I\mu^k d\mu,k=0,1,... \tag{36}$$

Table 3: Comparison between different models for solving Radiative transfer equation.

Model	Advantages	Disadvantages
Surface-to-surface Model	Simple, good for enclosures, quite fast	No participating media, diffuse surface
Discrete Transfer Radiation	The accuracy depends on the number of rays	No scattering, diffuse surfaces, gray radiation
Discrete-ordinate Model	Capable to deal with wide range of optical regimes	Anisotropic surfaces and non-gray radiation still under development
P-1 Differential Approximation	RTE becomes a simpler advection-diffusion equation	diffuse surfaces, gray radiation, it may over-predict radiation
Rosseland Model	No extra equations: radiation moves directly in energy equation	Optically thick media

which leads to

$$\frac{dI_1}{d_\tau} = (1-\omega)4\pi I_b - I_0 + \omega I_0 = (1-\omega)(4\pi I_b - I_0), \tag{37}$$

$$\frac{dI_2}{d\tau} = -I_1 \tag{38}$$

Here there are two equations in three unknowns, I_0, I_1 and I_2. A closing condition must be found to make the system determine such a relationship between I_0, I_1 and I_2, and It can be assumed that the intensity is isotropic over both the upper and lower hemisphere. Thus,

$$I_k = 2\pi(I^- \int_{-1}^{0} \mu^k d\mu + I^+ \int_{0}^{1} \mu^k d\mu) = \frac{2\pi}{k+1}\left[(-1)^k I^{-1} + I^+\right] \tag{39}$$

$$I_2 = \frac{1}{3} I_0 \tag{40}$$

or

With q=I_1 and G=I_0 equation 40 transforms 37 and 38 to

$$\frac{dq}{d\tau} = (1-\omega)(4\pi I_b - G) \tag{41}$$

$$\frac{dG}{d\tau} = -3q \tag{42}$$

The boundary conditions are leading to

$$\tau = 0 : G + 2q = 4J_1 \tag{43}$$

$$\tau = \tau_L : G - 2q = 4J_2 \tag{44}$$

There is $\frac{dq}{d\tau} = 0$ in the case of radiative equilibrium and, hence, G=$4\pi I_b$. For this case equation 42 reduces to

$$q = \frac{-4\pi}{3}\frac{dI_b}{d\tau} \tag{45}$$

that is the same as for the diffusion approximation though the boundary conditions are different.

4.3.2 Mathematical Formulations

For coupled radiation and conduction problems, the overall energy conservation equation or EE and the radiative transfer equation or RTE should be solved. The overall energy conservation equation which is written with temperature as the initial dependent variable is

$$\rho c_p \frac{\partial T}{\partial t} + \rho c_p U \cdot \nabla T = -\nabla \cdot q^c - \nabla \cdot q^R + \dot{S}_T \tag{46}$$

q^R and q^C are the radiative and conductive heat fluxes, ρ is the fluid density, c_P is the specific heat capacity, U is the fluid velocity vector, and $\dot{S}_T$ shows the source of heat. The conductive heat flux would be given by Fourier law of heat conduction in a single-component fluid.

$$\rho c_p \frac{\partial T}{\partial t} + \rho c_p U \cdot \nabla T = \nabla \cdot (k_c \nabla T) - \nabla \cdot q^R + \dot{S}_T \tag{47}$$

The computation of the radiative heat flux q^R requires the solution of the RTE. By applying the P1 approximation, RTE might be written as [19]

$$\nabla \cdot (\frac{1}{\kappa_\lambda + \sigma_{s\lambda}} \nabla G_\lambda) = -3\kappa_\lambda (4E_{b\lambda} - G_\lambda) \tag{48}$$

based on boundary condition

$$-\frac{2-\varepsilon_\lambda}{\varepsilon_\lambda}\frac{2}{3}\hat{n} \cdot \nabla G_\lambda = (\kappa_\lambda + \sigma_{s\lambda})(4E_{bw\lambda} - G_\lambda) \tag{49}$$

ϵ_λ is the emissivity of the boundary, $\hat{n}$ is the surface normal at the boundary and $E_{b\lambda}$ is the blackbody emissive power. κ_λ and σ_λ are the spectral scattering and absorption coefficients, and G_λ is the spectral incident radiation.

The solution of equation 48 subject to equation 49 was obtained, therefore the divergence of the radiative heat flux can be calculated and solved as equation 47

$$\nabla q^R = \int_0^\infty \kappa_\lambda (4E_{b\lambda} - G_\lambda) d\lambda \tag{50}$$

substitution of equation 50 into 47 gives

$$\rho c_p \frac{\partial T}{\partial t} + \rho c_p U \cdot \nabla T = \nabla \cdot (k_c \nabla T) - \int_0^\infty \kappa_\lambda (4E_{b\lambda} - G_\lambda) d\lambda + \dot{S}_T \tag{51}$$

Equations 48 and 51 present a set of coupled equations.

In the first step, coupled conduction and radiation was solved for a gray sample for checking the validity of the Matlab code, and in the following a more realistic case that would be a non-gray one was solved as well. By applying the assumptions of the one-dimensional gray non-scattering medium which is confined between gray isothermal boundaries, equation 51 might be written as non dimensional form like

$$\frac{d^2\theta}{d\tau^2} = \frac{1}{N}\left(\theta^4 - g\right) \tag{52}$$

Based on the boundary conditions $\theta(0)$=1 and $\theta(\tau_L)$=θ_L, equations 48 and 49 may be written as the following (non dimensional form) [19].

$$\frac{d^2g}{d\tau^2} = -3\left(\theta^4 - g\right) \tag{53}$$

Equations 54 and 55 represent the boundary conditions.

$$\left.\frac{dg}{d\tau}\right|_{\tau=0} + \frac{3}{2}\frac{\varepsilon_0}{2-\varepsilon_0}\left(1 - g(0)\right) = 0 \tag{54}$$

$$\left.\frac{dg}{d\tau}\right|_{\tau=\tau_L} - \frac{3}{2}\frac{\varepsilon_L}{2-\varepsilon_L}\left(\theta_L^4 - g(\tau_L)\right) = 0 \tag{55}$$

τ=κx is the optical thickness from 0 to L. $\theta = {}^{T}/_{T_0}$ is the nondimensional temperature and $g = {}^{G}/_{4\sigma T^4}$ is the incident radiation.

N is the conduction to radiation number and is equal to $N = {}^{k_c\kappa}/_{4\sigma T_0^3}$. Equations 52 and 53 are solved analytically in this work and compared with other studies for validity.

4.4 Coupled heat conduction and radiation with temperature profile in one dimensional non-gray media

4.4.1 Introduction and Mathematical Formulations

The energy conservation equation, which is written based on one-dimensional steady state heat flux for coupled heat conduction and radiation is [95].

$$\frac{dq_{tot}}{dx} = \frac{dq_{con}}{dx} + \frac{dq_{rad}}{dx} \tag{56}$$

q_{rad} and q_{cond} are the radiative and conductive heat flux. The conductive heat flux given by the Fourier law of heat conduction would be [95].

$$\frac{dq_{con}}{dx} = -k\frac{d^2T}{dx^2} \tag{57}$$

The divergence of the radiative heat flux based on stepwise gray box model is written as

$$\frac{dq_{rad}}{dx} = \sum_{k=1}^{N_B+1} \kappa_k (4E_{bk} - G_k) \tag{58}$$

κ_k and G_k are the absorption coefficient and the incident radiation in the k-th spectral box (wavelength interval), and N_B is the number of gray boxes. G_k would be defined as the Equation 59

$$G_k = \int_{\lambda_{k,l}}^{\lambda_{k,u}} G_\lambda d\lambda \tag{59}$$

$\lambda_{k,l}$ and $\lambda_{k,u}$ are the lower and upper boundaries of the k-th gray box. It should be mentioned that in this study, there is a homogeneous medium without any particles (roofs), therefore there is no scattering and the absorption coefficient is equal to the extinction coefficient. The basic idea of the stepwise gray box model is that we divide electromagnetic spectrum into finite intervals. Then we treat the properties of the material in each interval as gray. The intervals usually do not have the same size so for each interval, we need lower bound, upper bound, and value of extinction coefficient. The interval bounds are often chosen manually according to peaks in the extinction spectrum, and we can select them as we like. The important thing is then to determine average gray extinction coefficient for each interval. Usually, the Planck-mean or the Rosseland-mean extinction coefficient is used [96]. The emissive power within the k-th box is given by

$$E_{bk}(T) = \int_{\Delta\lambda_k} E_{b\lambda}(T, \lambda) d\lambda = [f(\lambda_{k,u}T) - f(\lambda_{k,l}T)]\sigma T^4 \tag{60}$$

In equation 60, f is the so called fraction of blackbody and can be calculated according to Howell, Menguc, and Siegel (2016) [11]. Emissive power formula shows how much energy is emitted inside k-th interval.

Substitution of equations 57 and 58 into the equation 56 yields equation 61 that N_B+1 shows the part of the spectrum which is outside of the defined boxes, so called window.

$$k_C \frac{d^2T}{dx^2} = \sum_{k=1}^{N_B+1} \kappa_k (4E_{bk} - G_\lambda) d\lambda \tag{61}$$

If we use spectral extinction coefficient, we should choose one of the nongray methods such as stepwise gray box model, narrow band models, wideband models, weighted-sum-of-gray-gases-models, and recently narrowband k distributions or full spectrum k distributions. As explained in the references [97][19], some of these methods are extremely expensive for ordinary engineering calculations so the gray box model was selected that is simple and effective for nongray calculations. The incident radiation G_λ by omitting scattering can be given by P1 approximation. As mentioned above, nongray, homogeneous non scattering, and one dimensional medium which is confined between isothermal boundaries were the assumptions here. According to boundary conditions which are $T(0) = T_0$ and $T(L) = T_L$ (Figure 64), the governing equations might be written as [93]

$$\frac{d^2G_\lambda}{dx^2} = -3\kappa_\lambda^2 (4E_{b\lambda} - G_\lambda) \tag{62}$$

with the boundary conditions

$$\left.\frac{dG}{dx}\right|_{x=0} + \frac{3}{2}\frac{\varepsilon_{0\lambda}}{2-\varepsilon_{0\lambda}}\kappa_\lambda \left[4E_{b\lambda}(0) - G_\lambda(0)\right] = 0 \tag{63}$$

$$\left.\frac{dG}{dx}\right|_{x=L} - \frac{3}{2}\frac{\varepsilon_{L\lambda}}{2-\varepsilon_{L\lambda}}\kappa_\lambda \left[4E_{b\lambda}(L) - G(L)\right] = 0 \tag{64}$$

Equations 61 and 62 may be written in the matrix form as Mazumder explained [19].

Meanwhile, the equivalent thermal conductivity of the insulating material is evaluated from Equations 65 and 66.

$$q_{total} = -k\frac{dT}{dx} - \sum_{k=1}^{B+1} \frac{1}{3\kappa_k}\frac{dG_k}{dx} \tag{65}$$

$$k_{eq} = \frac{q_{total} L}{T_0 - T_L} \tag{66}$$

4.5 Coupled heat conduction and radiation in Reinforced Concrete (one layer) and Green Roofs (three layers)

4.5.1 Introduction and Mathematical formulations

In this section, two reinforced concrete panels, one plain, and one with moss as a green roof layer were studied both experimentally and theoretically. The objective is to compare one layer roof (which is just concrete one) and two layer roof (which consists of three layers of concrete, soil and moss on it) in thermal radiation and conduction heat transfer.

The corresponding geometry of the green roof is shown in Figure 69.

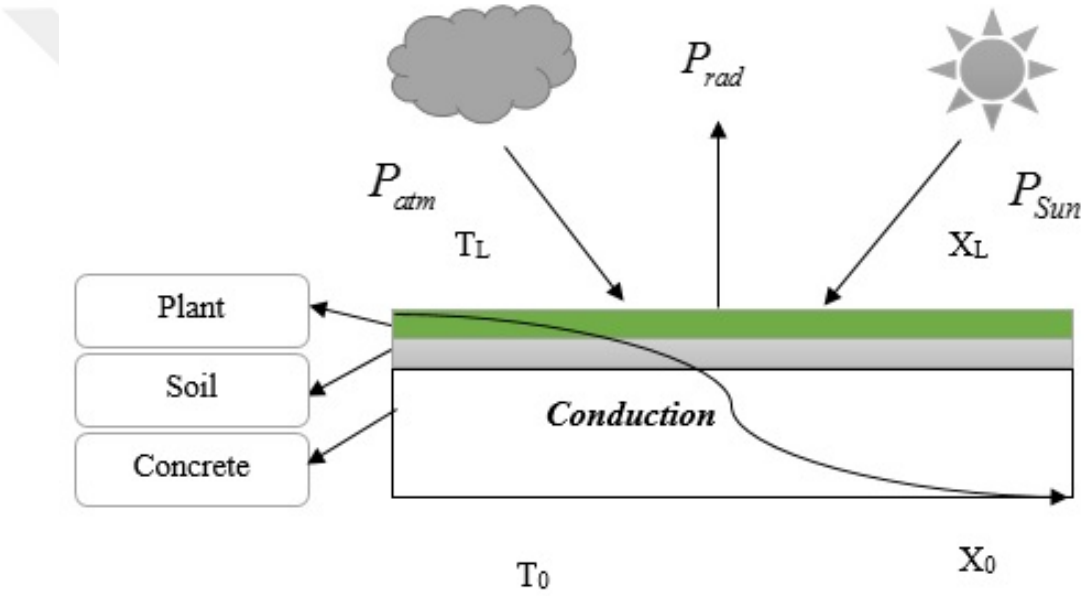

Figure 69: Schematic of the heat transfer through a sample of green roof of a building.

The green roof sample that involves the plant, growth medium (soil), and concrete panel layers can be seen in Figure 70. Theoretical thermal resistance calculation is performed for both reinforced concrete and green sample in this study. It is done based on the homogeneous mixture thermal conductivity determination which is performed employing mass fraction average of the pure species' thermal conductivity (Y) for homogeneous samples:

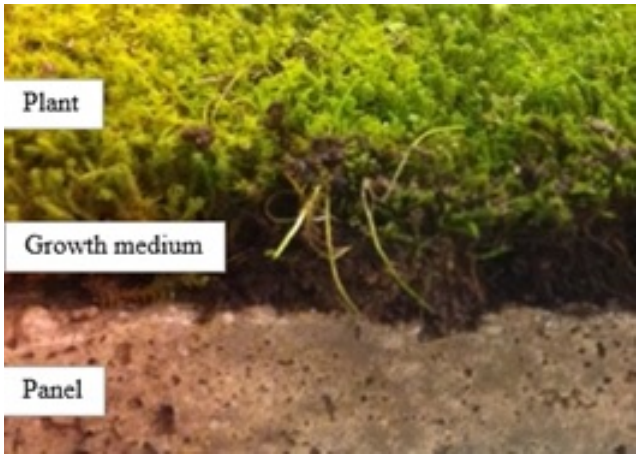

Figure 70: Schematic of the green roof sample.

$$k = \sum_i Y_i k_i \tag{67}$$

Details about calculating the R-value is explained in section 4.2. Energy balance for the plant layer and the soil possesses a more complicated nature due to the interaction between the plant, soil, moisture, and the surrounding air. Equation 68, which accounts for these interactions, was used to obtain the thermal conductivity value

$$\begin{aligned} R_{net,p} + R_{net,g} = \\ (S_p + S_g) + (L_p + L_g) + (P_p + P_g) + Q_{cond} \end{aligned} \tag{68}$$

where S, L, and P pertain to sensible, latent, and precipitation heat fluxes. R_{net} is the net radiation heat flux which is expressed as:

$$R_{net} = R_{SW} + R_{LW} - E \pm R_{exchange} \tag{69}$$

where $R_{exchange}$ is the radiation exchange between the plant layer and the growth medium, and is equal in magnitude and opposite in sign for the layers. Sensible and latent heat fluxes for both the plant canopy and the growth medium can be expressed as

$$S_p = 1.1 LAI \rho_{a,p} c_{p_{air}} h_p U_{a,p} \Delta T \Big|_{a_p,p} \tag{70}$$

$$S_g = \rho_{a,g} c_{p_{air}} h_g U_{a,p} \Delta T \Big|_{a_p,g} \tag{71}$$

$$L_p = l_p LAI \rho_{a,p} h_p U_{a,p} r'' \Delta q \Big|_{a_p,p_{sat}} \tag{72}$$

$$L_g = l_g \rho_{a,g} h_g U_{a,p} \Delta q \Big|_{a_p,g} \tag{73}$$

LAI, $r\ ''$, $U_{a,p}$, h, and q are the leaf area index, surface wetness factor, wind speed of air within the plant canopy, bulk heat transfer coefficient, and mixing ratio for air. It should be mention that the precipitation heat fluxes are negligible.

Chapter V

RESULTS AND DISCUSSIONS

5.1 Power of cooling with constant temperature

Radiative cooling in the new buildings can reduce energy consumption around 70 percent and increase demand in existing in the structures as well. Cooling power or power of cooling is the principle of the radiative cooling [98].

The net radiative cooling power or power of cooling depends on three parameters:

1. The temperature of a surface.

2. The emissivity of a surface.

3. The inclination of the radiator surface from the zenith.

The first and the third properties, are taken as constants in this study. Therefore, the only variable that affects the power of cooling is the spectral emissivity of different samples, which is related to the nature of the material [99].

The net radiative cooling power or power of cooling depends on three parameters: (1) The temperature of a surface; (2) the emissivity of a surface; and (3) the inclination of the radiator surface from the zenith. The first and the third properties, are taken as constants in this study. Therefore, the only variable that affects the power of cooling is the spectral emissivity of different samples, which is related to the nature of the material [60].

An emissivity near to one for most wavelengths in the atmospheric window (8-13 μm), and for most angles of indices, creates a good radiative cooling power, as it increases the power emitted by the structure significantly without influencing the power of the Sun or the power of the atmosphere [100].

To calculate the power of cooling or net power (P_{net}), equations 11 to 19 were solved in MATLAB using the experimental data obtained from the FTIR

measurements (Figure 46).

T_{amb} is considered 30° or 303 K, and $\theta = 0$. Non-radiative heat transfer coefficient hc is assumed negligible, since it is not related to the radiative performance of these samples. Comparisons of the cooling performance of each sample, are presented in Table 4.

Table 4: Comparisons of the characteristics of each surface.

Material ($T_{amb} = 303K$)	**Net Radiative Power** (W/m^2)		
	$P_{rad} = 273K$	$P_{rad} = 283K$	$P_{rad} = 293K$
PPC	12.4	15.4	18.7
Painted PPC	12.9	16	19.4
Plant or moss	23.5	28.6	34.2
Black membrane	8.2	10.4	12.7
Red membrane	7.3	9	11
XPS	6.5	8	9.7
Selective emitter	47.9	60.4	74.5
Broadband emitter	77.6	100	126

In the following, the samples are compared for two ideal cases. What we call as the "ideal sample" is the surface with the most desirable spectral properties. Such a "selective emitter" should have the unit emissivity in the 8-13 μm wavelength range, and zero emissivity in other bands. The second case is referred as the "broadband emitter", which has a unit emissivity in the entire IR region (3$\sim$15 μm) and zero emissivity in the solar radiation spectrum. The schematic of the ideal sample and the broadband emitters are shown in Figures 71 and 72. We also show blackbody emitter on Figure 73, which has the unit emissivity at all wavelengths.

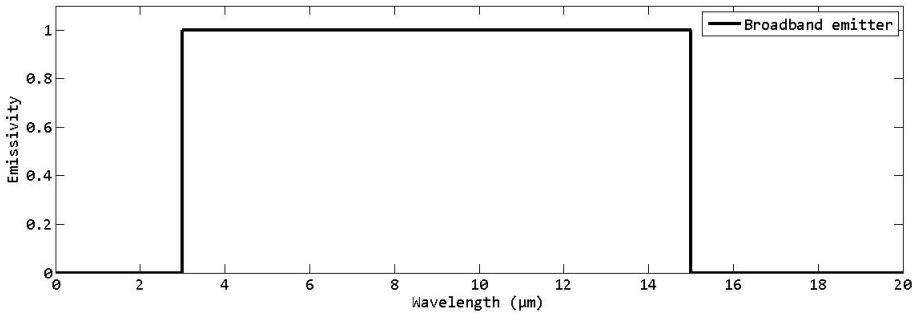

Figure 71: Emissivity curve for Broadband emitter.

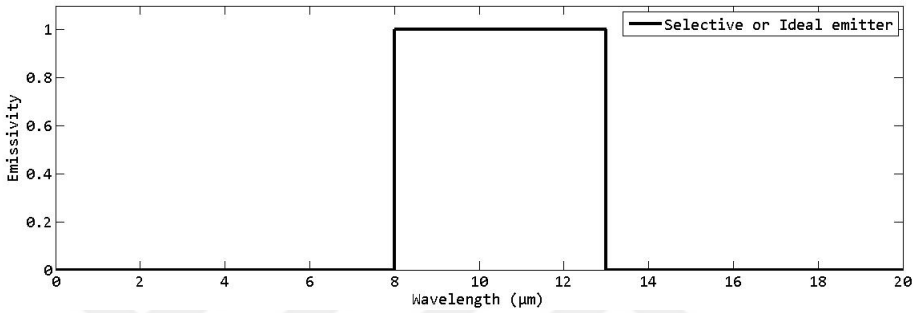

Figure 72: Emissivity curve for Selective emitter.

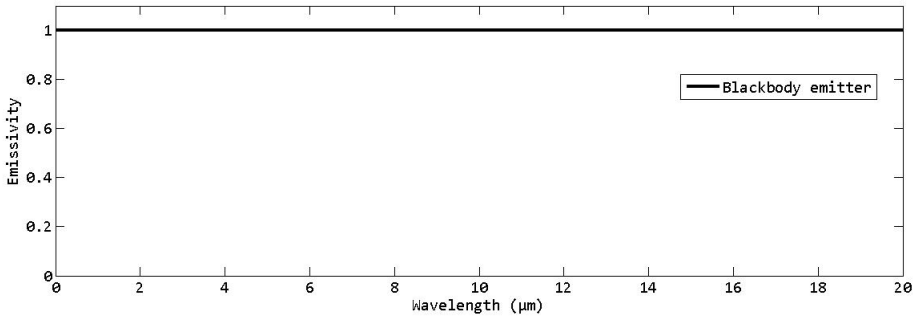

Figure 73: Emissivity curve for Blackbody emitter.

Based on Table 4 and the comparison of the power of cooling, the moss sample has the highest cooling power of 34.2 W/m^2 at a surface temperature of 293 K and ambient temperature of 303 K. Under the same conditions, the broadband emitter and the selective emitter have cooling powers of 126 W/m^2 and 74.5 W/m^2. White painted PPC and PPC have the highest cooling power after moss sample with cooling powers of 19.4 W/m^2 and 18.7 W/m^2. For the remaining samples, the cooling power is lower than these values.

Silicon oxide, which is essentially glass, is also suggested to be used as a possible radiative cooler; its properties as a selective radiator and corresponding power of cooling were reported [99]. In Table 5, the power of cooling of silicon oxide is compared to the moss sample, which had the highest power of cooling in this study. It was clear that moss could be a better radiative cooler, rather than the silicon oxide, and grows naturally. Moss is a sustainable material, which can be easily used in green-roof applications.

Table 5: Comparisons of the cooling characteristics of Moss and silicon oxide surfaces.

Material ($T_{amb} = 303K$)	Net Radiative Power (W/m^2)
Plant or moss	34.2
Silicon oxide	27.5

The change in the radiative cooling power of the samples at the ambient temperature of 30°C (303 K) in the daytime and 20°C (293 K) at nighttime was modeled and showed. Figure 74 shows the radiative cooling of the samples in the summer at daytime and nighttime for different surface temperatures. These calculations were done based on the Equations 11 to 19 and in Matlab codes.

The radiative cooling power becomes zero when each surface reaches its equilibrium temperature. Furthermore, the ideal composite surface always has the highest cooling powers when the ambient temperature is higher than the surface temperature. In that sense, the broadband emitter has the highest power of cooling and the ideal emitter is the second.

Moss in comparing with other samples has high radiative cooling power, and finally both PPC and white painted PPC show similar cooling performance since their spectral emissivities are similar. Totally when there is a low difference between the surface temperature and ambient temperature, and surface temperature reaches ambient temperature, the power of the cooling increases. In comparison with daytime and nighttime for the summer case, there is a reduction in cooling power in the nighttime for all of the samples. This means that these samples have a better power of the cooling for daytime applications.

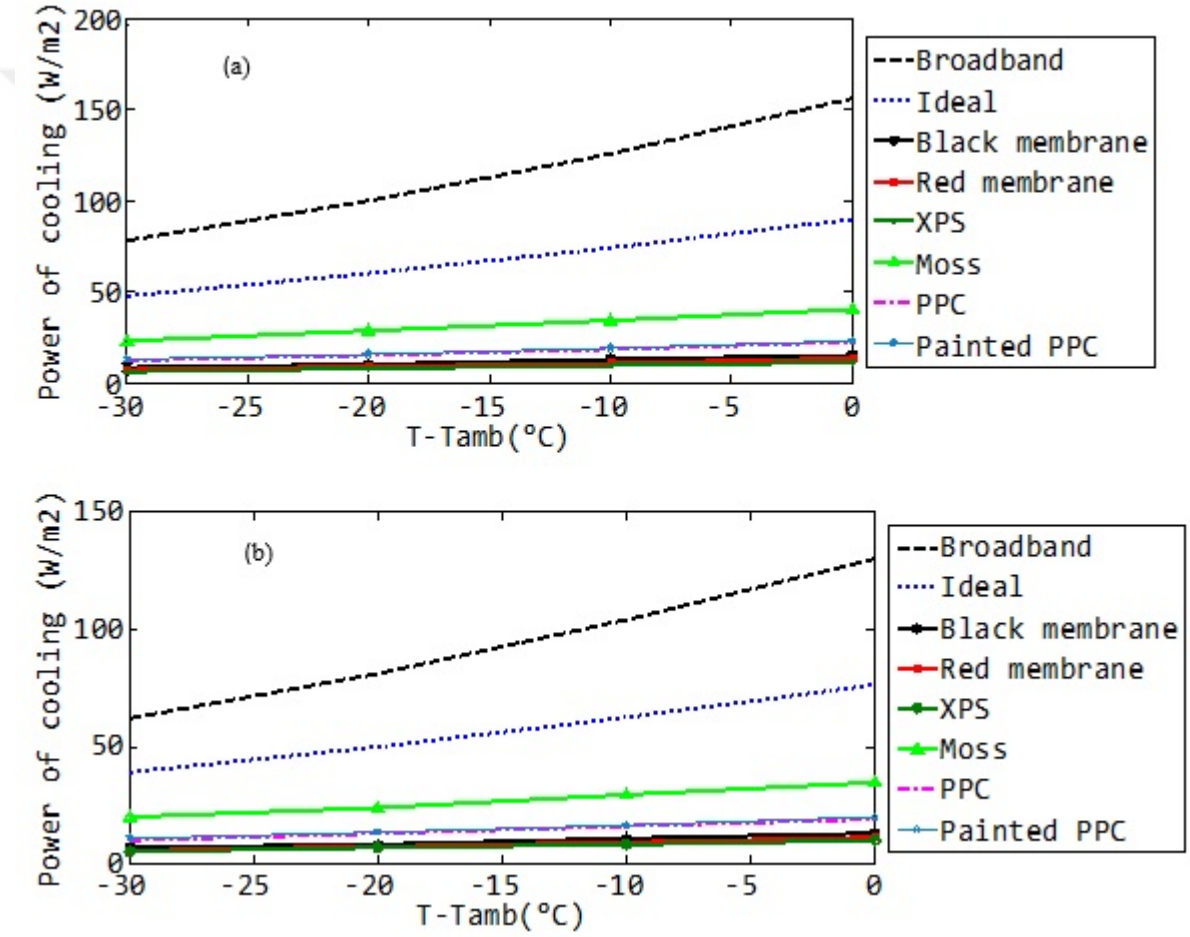

Figure 74: Change in radiative cooling power of the samples in summer time with surface temperatures at ambient temperature of (a) 30°C Daytime and (b) 20°C Nighttime.

The change in the radiative cooling power of the samples at the ambient temperature of 10°C (283 K) in the daytime and 0°C (273 K) in the nighttime for winter time was shown in Figure 75 (based on Equations 11 up to 19). The same procedure is used for winter times and summer times. The Broadband emitter, the Ideal emitter, and the moss sample have the highest cooling power.

In the comparison between summer time and winter time, in the summer time at daytime there was the highest cooling power in all of the samples, and at the highest ambient temperature that was T=30°C=303 K, there was the highest power of the cooling.

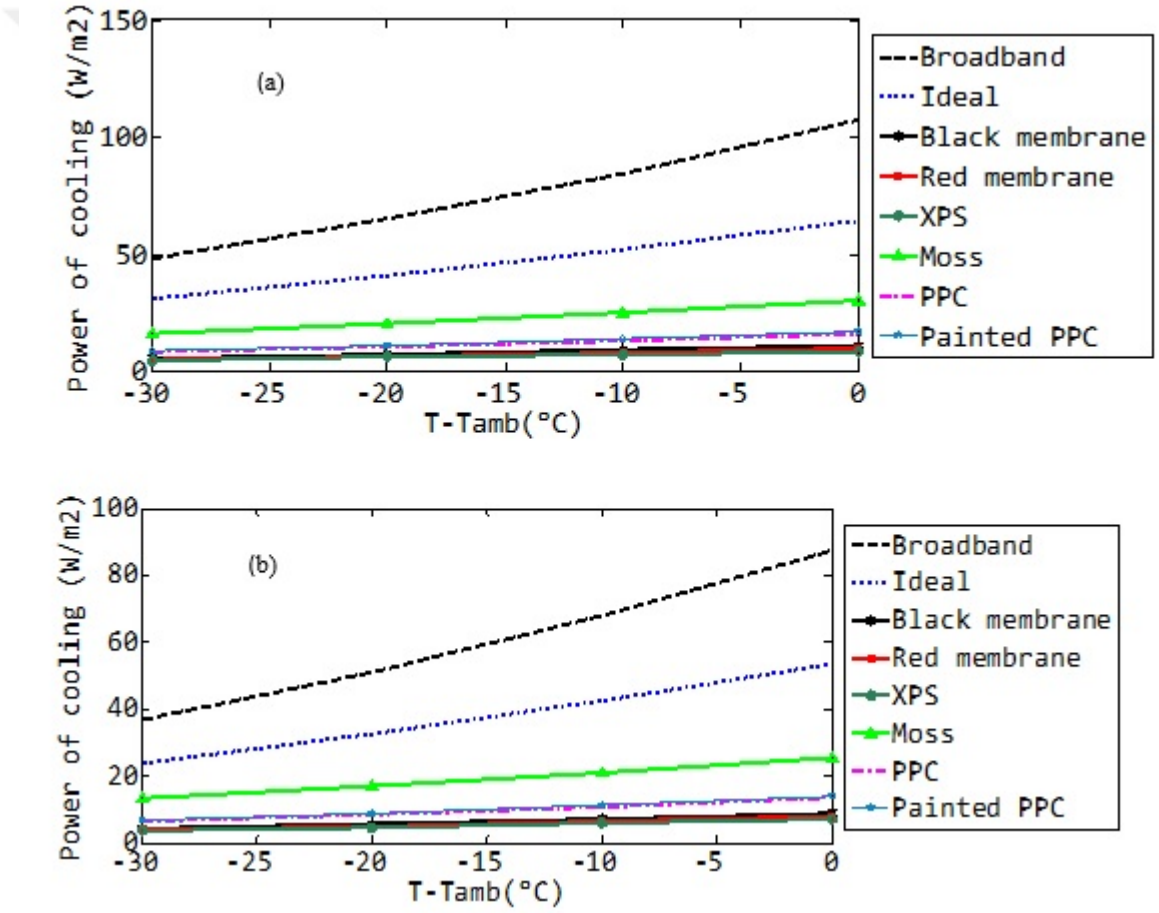

Figure 75: Change in radiative cooling power of the samples in winter time with surface temperatures at ambient temperature of (a) 10°C Daytime and (b) 0°C Nighttime.

It could commented that for summer daytime cooling, moss was better than all other samples.

5.2 Theoretical analysis of heat conduction (R-value)

The measure of resistance to heat flow through a certain thickness of material, is R-value. For this, the higher the R-value, the higher thermal resistance the material has, hence the material has the better insulating properties.

R-value is equal to the thickness of the material (L) divided by its thermal conductivity (K); (R=L/K), therefore higher R-value shows less thermal conductivity in the insulating material. Thermal conductivity generally increases profoundly with increasing temperature and it does not change with the geometry [101].

In the conduction heat transfer calculations, the thermal conductivities of the samples were needed. These values can be determined from the experimentally measured resistance, R-values. Therefore, the Reverse Heat Leak Method (RHLM) was used, which was discussed before in section 3.5 [102][103]. They are listed in Table 6.

Table 6: Thermal conductivities of the materials .

$Name$	$R-value(K.m^2/W)$	$k(W/m.K)$
PPC	0.222	2.25
Painted PPC	0.282	1.77
Plant or moss	0.261	1.91
Black membrane	0.253	1.98
Red membrane	0.077	6.49
XPS	0.826	0.96

Although these conductivity values were measured for calculating coupled conduction and radiation in this study, but their potential for being a good insulation also can be evaluated. Among these six selected materials, XPS has the lowest thermal conductivity so its the best insulator, and red membrane with the highest conductivity is the worst candidate as being an insulation structure.

5.3 Coupled heat conduction and radiation with temperature profile in one dimensional gray media

Emission from a semitransparent solid or liquid or a gas is a volumetric phenomenon, but emission from liquid or an opaque solid is a surface phenomenon (Figure 76), for this radiative transfer equation (RTE) is not an accurate solution for modeling the heat transfer through the roofs.

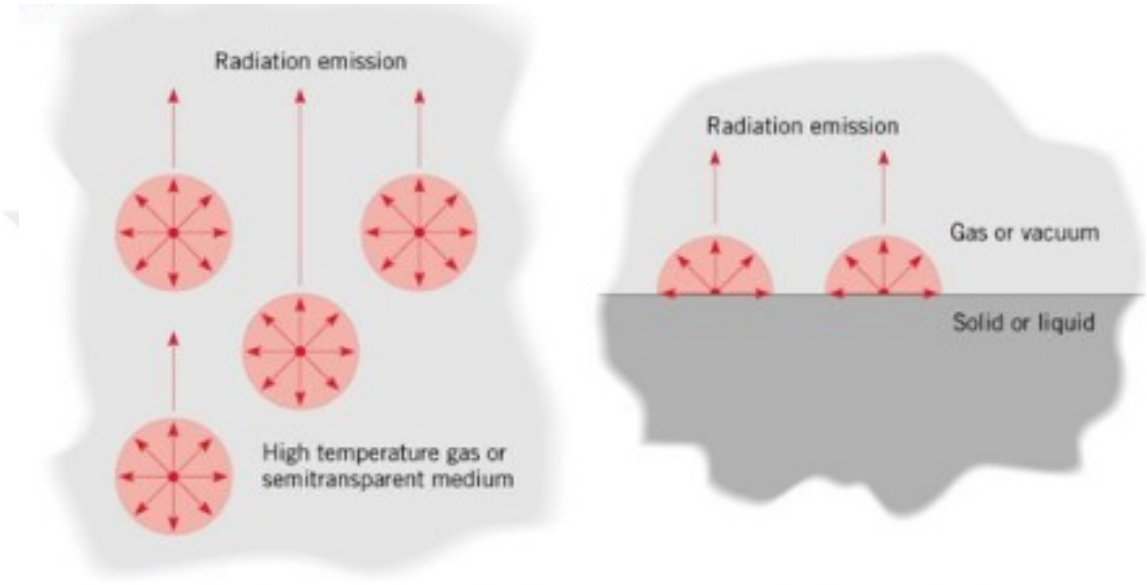

Figure 76: Emitted radiation for solid or liquid as a surface phenomenon [104].

In the first step of evaluating the heat transfer in the roofs, RTE was solved by P1 approximation method as explained before from equation 32 to 45. The result for a general case (One dimensional gray slab) is shown in Figure 77.

Single-scattering albedo is the ratio of scattering efficiency to total extinction efficiency. According to Figure 77, when there is just radiation heat transfer, by increasing the scattering albedo the non-dimensional solar flux will increase as well. As this work focused on bulk materials without particles in them, therefore scattering will be eliminated.

Establishing a more realistic model would be coupled radiation and conduction for a gray case that the schematic of it is shown in Figure 78.

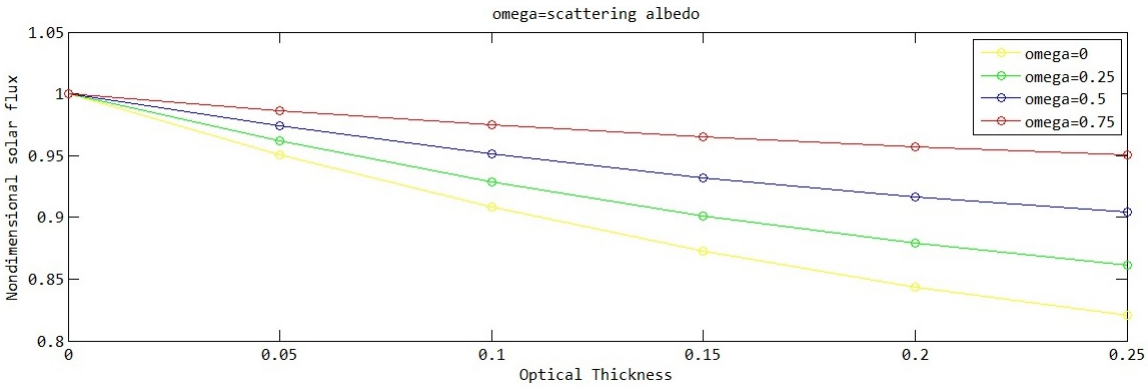

Figure 77: Solving radiative transfer equation for a one-dimensional gray case with different scattering albedo.

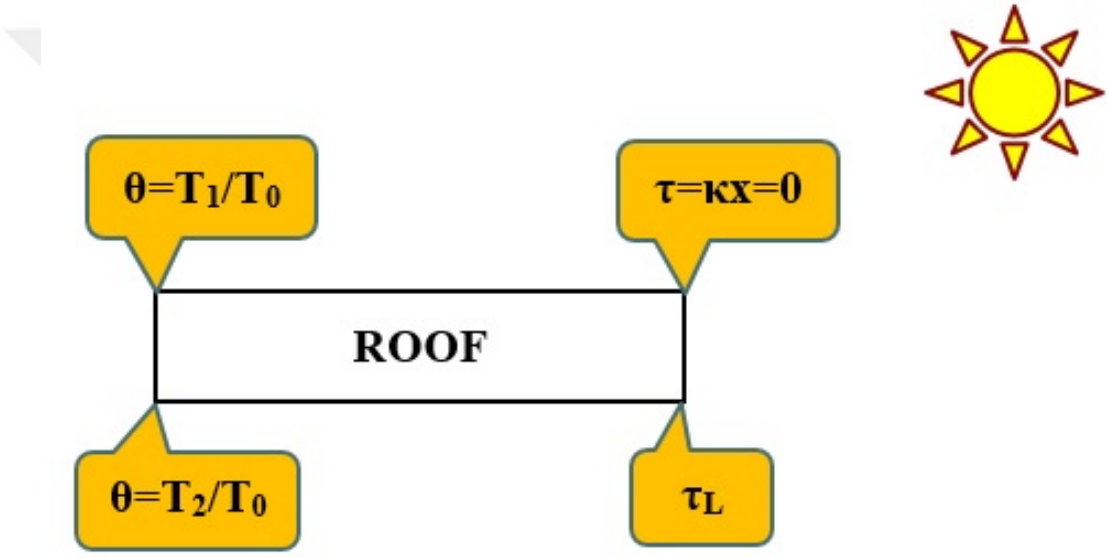

Figure 78: Schematic of coupled radiation and conduction energy balance (for the gray case in this study).

The temperature profiles for 1D media were determined from a coupled conduction and radiation analysis, as discussed before. These profiles depicted a nonlinear behavior because of radiative absorption within the medium. The nonlinear temperature profile is due to the volumetric absorption of incident radiation by the slab [97]. Figure 79 shows the temperature profiles for a gray case, which is plotted to evaluate the validity of the codes. Conduction-Radiation for one-dimensional gray media was solved analytically and the result had 100% agreement with other studies [93][19].

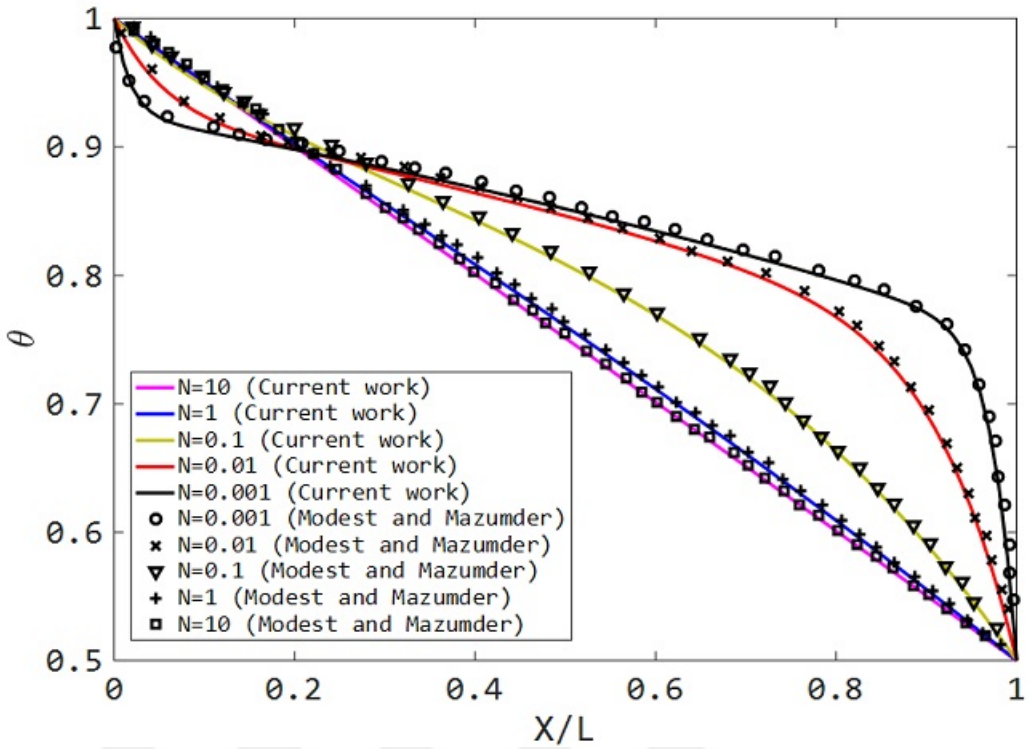

Figure 79: Validation of the numerical analysis for non-dimensional temperature profiles for combined radiation and conduction transfer in a gray slab (comparisons are made against Modest book [93] and Mazumder paper [19]).

Figure 80 also represents the coupled radiation and conduction for a gray case comparing with just radiation in a gray model. In the following, the non-dimensional temperature profile of the selected samples in the gray case were compared with each other and is presented in Figure 81.

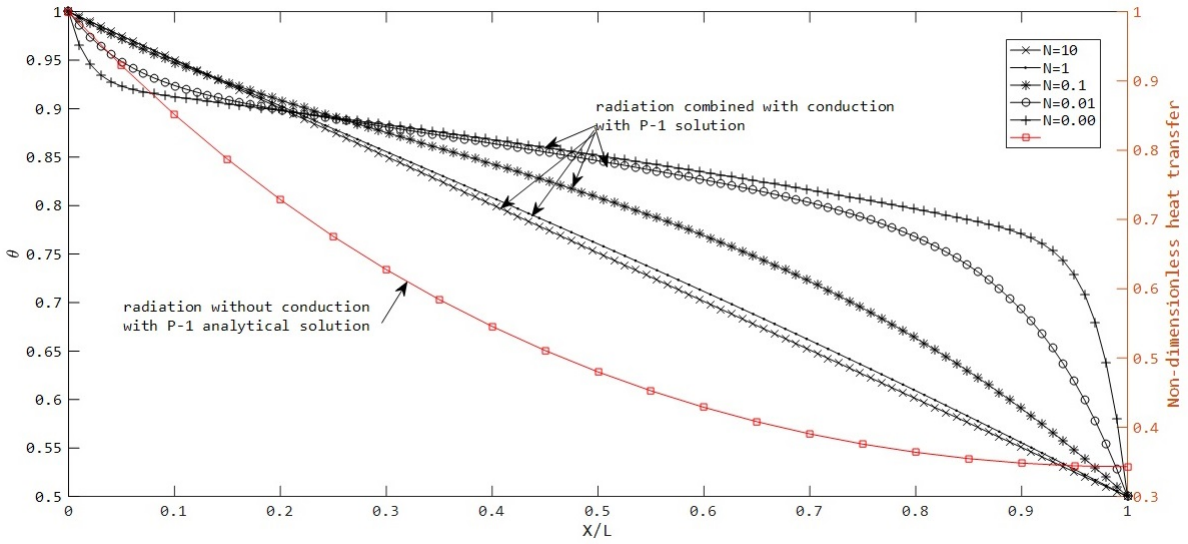

Figure 80: Non-dimensional temperature profiles for combined radiation and conduction in a gray slab comparing with radiative transfer.

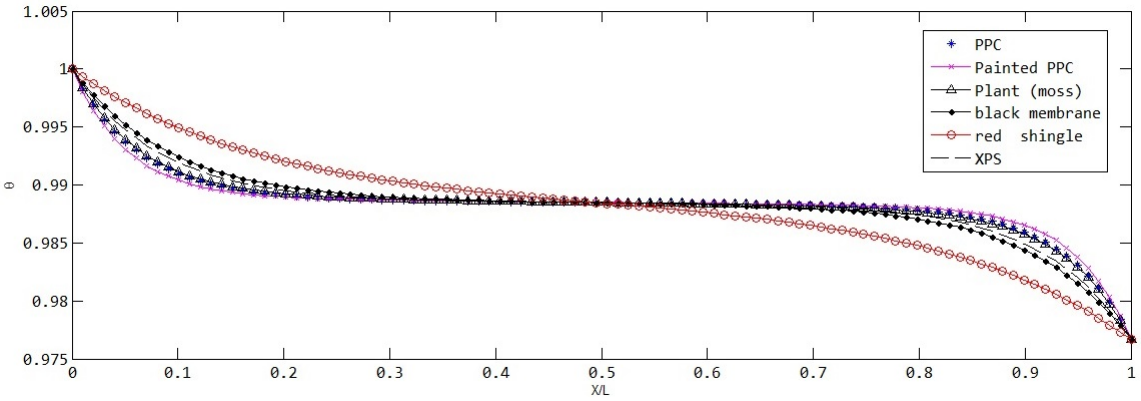

Figure 81: Effect of different sustainable materials on temperature profile.

Figure 81 displays that on the surface of the media up to 0.1, for higher conduction to radiation number (N=10), the non-dimensional temperature is higher too, but in the following (from 0.1-1), for lower conduction to radiation value, the non-dimensional temperature is high that it can be related to surface phenomenon of radiation in conduction-radiation heat transfer. Additionally, radiation without conduction presents descending slope through the media as well.

As the aim of this study was radiative cooling and in radiative cooling the wavelength range is significant, so gray model is not a valid model for this study

and in the following coupled radiation and conduction was solved for a non-gray model.

5.4 Coupled heat conduction and radiation with temperature profile in one dimensional non-gray media

In this section, the results for a non-gray medium with the temperature gradient will be discussed. This case is closely related to the thermal transfer phenomena at roofs. The schematic of coupled conduction and radiation for a non-gray case is presented in Figure 82.

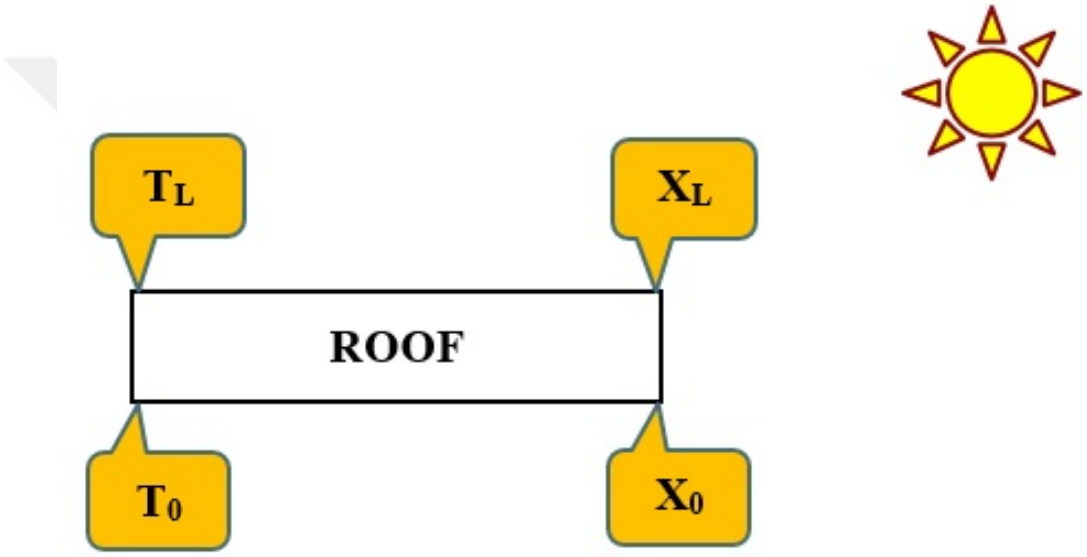

Figure 82: Schematic of coupled radiation and conduction energy balance (for the non-gray case in this study).

Here, the effect of convection had been omitted for the sake of simplicity. Numerical experiments for a non-gray case were performed based on the six different materials which introduced before, with the data presented in Table 7. The stepwise gray model was used to show the spectrum consisted of three boxes (based on Mazumder work [19]). Thermal conductivities of the samples were calculated and measured as explained in the previous chapters.

Optical properties of these materials were not available in the literature, so their emissivities and absorption coefficients were taken from the experimental work in this study (3.4). Determination of R value for the materials was significant.

Table 7: Summary of the parameters used in the analysis.

T_0	T_L	L	λ_1	λ_2	λ_3
293K	300K	5cm	2.7μm	4.3μm	15μm

For this, the Reverse heat leak method (RHLM) which was discussed before, was used (Section 3.5) and the results were shown in Table 6.

The temperature profiles for 1D media were determined from a coupled conduction and radiation analysis, as discussed before. These profiles depicted a nonlinear behavior because of radiative absorption within the medium. The nonlinear temperature profile is due to the volumetric absorption of incident radiation by the slab [97].

Figure 83 shows the temperature profiles obtained from simulations for different materials. The results showed the nonlinear steady-state temperature profile for homogeneous media, where the conduction to radiation parameter was lower than one, as already explained in References [11][81][93][105].

In the next set of simulations given below, the walls were considered to be at the same temperature. By doing so, we focused only on the effect of material emissivity. The predicted temperature profiles are shown in Figure 83 in non-dimensional fashion, although they correspond to a wall thickness 50 cm. It should be mentioned that this physical size was just an assumption and the code could be applied for any physical sizes.

It can be seen from Figures 79 and 83 that the higher temperatures (non-dimensional temperature θ near 1) are in the near-wall region. In this region, which was the surface of the roof for our model, the radiation mechanism was more significant, as radiation is a surface phenomenon. As mentioned in Reference [106], when the boundaries are opaque, the temperature peaks can only appear at the heated surface, as the radiative energy might not transfer to the inside of the medium directly but can only heat the surface. Consequently, the energy is transferred inside from the heated surface.

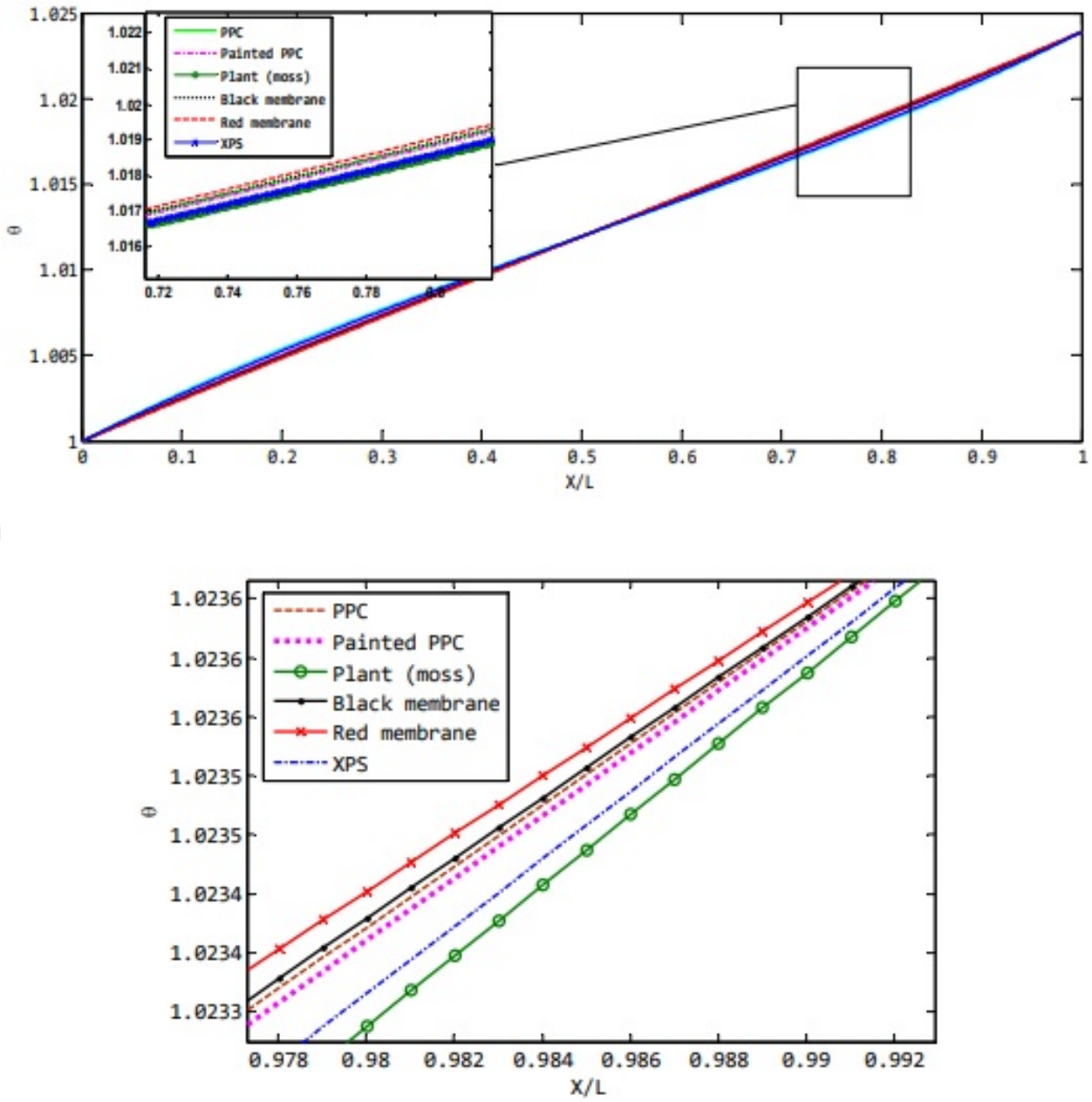

Figure 83: (a) Temperature profile using the non-gray formulations for different roof materials; and (b) Right part zoomed.

In Figure 83, from the surface through the sample, red membrane is on the top with high non-dimensional temperature, as it has the highest conductivity among all samples. Therefore, it shows that heat conduction was dominant in this sample. On the other hand, XPS and moss had the lowest non-dimensional temperature in comparison with other samples. XPS as mentioned before, is a good insulator, with the lowest conductivity, and its spectral emissivity is also low in mentioned bands.

Moss sample had average conductivity and high spectral emissivity. Radiation transfer was more dominant in moss, rather than conduction, and it has a higher potential to be a radiative cooler.

5.5 Comparison of coupled heat conduction and radiation in Reinforced Concrete (one layer) and Green Roofs (three layers)

In this section, two reinforced concrete panels; one plain, and one with moss as a green roof layer were investigated for potential passive cooling applications. In addition, two other types of plants (cactus and leaf) were also investigated in comparing with the moss.

Fourier transform infrared spectroscopy (FTIR) measurements were performed to measure the emissivity of new plant samples at infrared wavelengths and the results were compared with the moss (green roof model) and PPC (reinforced concrete roof model) samples which were measured before.

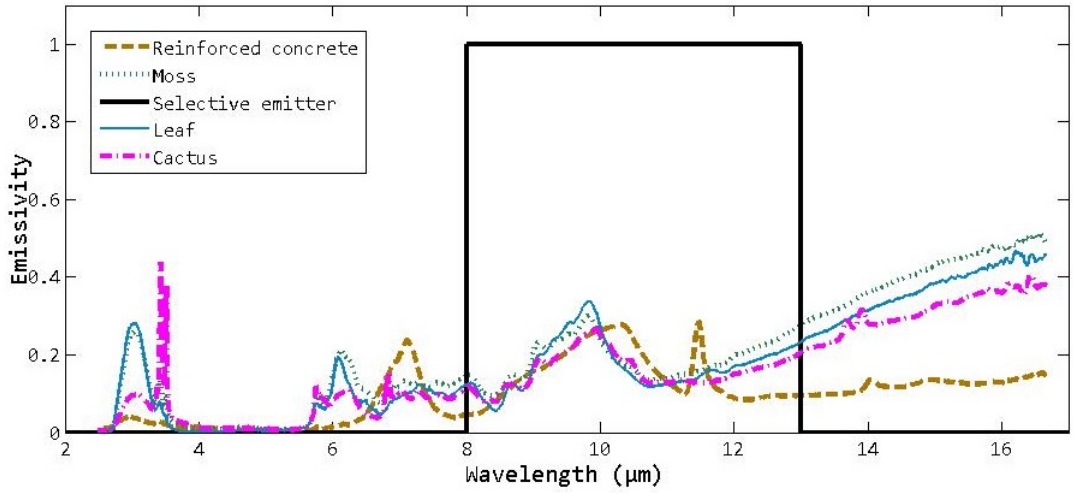

Figure 84: Spectral emissivity of reinforced concrete and green samples measured by Thermo-Nicolet iS10 FTIR spectrometer (Performed at Sabanci University, Istanbul, Turkey).

Figure 84 shows the spectral emissivity of the concrete roof (with PPC) and green roof (moss, leaf or cactus) with the ideal case for radiative cooling. As explained before, for radiative cooling "atmospheric window" range is significant.

A material with high emissivity in this range (8-13 μm) and low in other bands can emit the solar irradiance more in daytime and be a good radiative cooler for the roofs.

In comparing all materials (PPC, moss, leaf and cactus), it is clear that moss has a little higher spectral emissivity in the atmospheric window and all of them have the same spectral emissivity in other bands. The sharp increase of emissivity after atmospheric window in green samples is related to cuticles in plant samples which explained before [79].

Power of the cooling of the samples were calculated based on equations 11 to 19 and the results are shown in Table 8. Theoretical calculation was performed at surface temperature of 293 K.

Table 8: Power of the cooling of Reinforced concrete and Green sample.

Sample	Power of the cooling at 293K (W/m^2)
PPC	18.71
Moss	34.23
Leaf	30.90
Cactus	27.33
Ideal emitter	74.5

For these power of cooling calculations the following assumption have been made. First, the ambient temperature of 303 K was assumed. Second the non-radiative heat transfer is negligible here. The spectral emissivity was taken from the measurements and the data related to the Sun and the atmosphere was taken from the literatures [12].

Results in Table 8 shows that although the samples properties are far from the Ideal or selective emitter, but the cooling performance of the moss sample is higher than other type of plants and PPC or reinforced concrete roof.

The spectral models for the absorption coefficients (in units of 1/m) for all samples (PPC and three plant types) are presented in Figures 85 to 88. It should be mention that that this value (absorption coefficient) are determined by $(2.3 \times A)/t$,

which A is the absorbance and t is the thickness, and there is a direct relationship between absorptivity and absorption coefficient, so high spectral absorption coefficient in the atmospheric window shows better performance of the materials in radiative cooling which is clear in the moss sample.

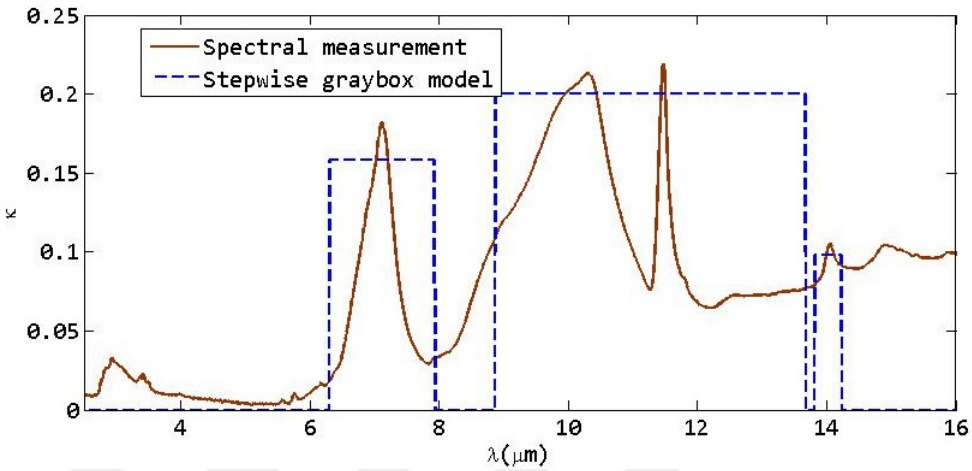

Figure 85: Spectral absorption coefficient of PPC. Comparisons of experimental and numerical results, in units of 1/m.

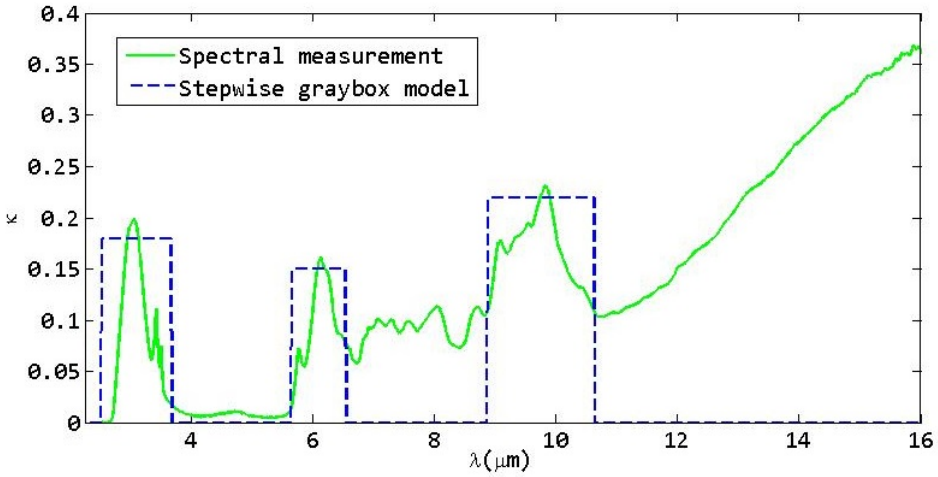

Figure 86: Spectral absorption coefficient of moss. Comparisons of experimental and numerical results, in units of 1/m.

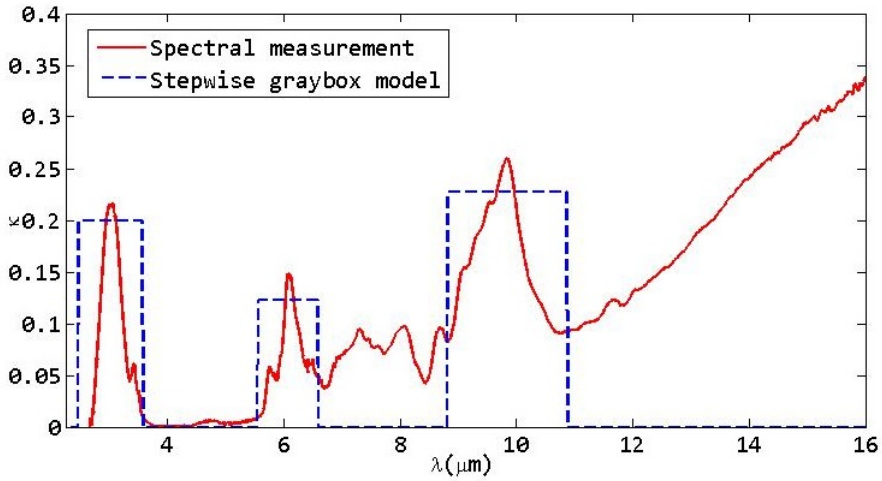

Figure 87: Spectral absorption coefficient of leaf. Comparisons of experimental and numerical results, in units of 1/m.

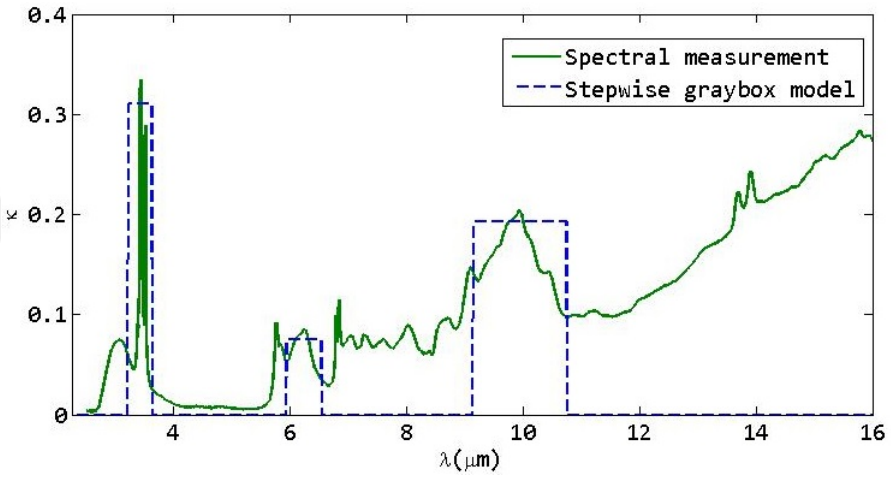

Figure 88: Spectral absorption coefficient of cactus. Comparisons of experimental and numerical results, in units of 1/m.

For solving the coupled radiation and conduction in the non-gray body, stepwise gray box model was used as explained in the previous chapters. Figure 89 shows the temperature profile of both models of reinforced concrete roof (with PPC) and green roof (PPC with moss) in non-gray case. Here, in this Figure, just moss was evaluated as a plant for green roof model.

For the calculation of temperature, equation $k\frac{d^2T}{dx^2} = \sum_{k=1}^{N_B+1} \kappa_k(4E_{bk} - G_\lambda)d\lambda$ should be discretized and the value of the temperature gradient at the faces of the

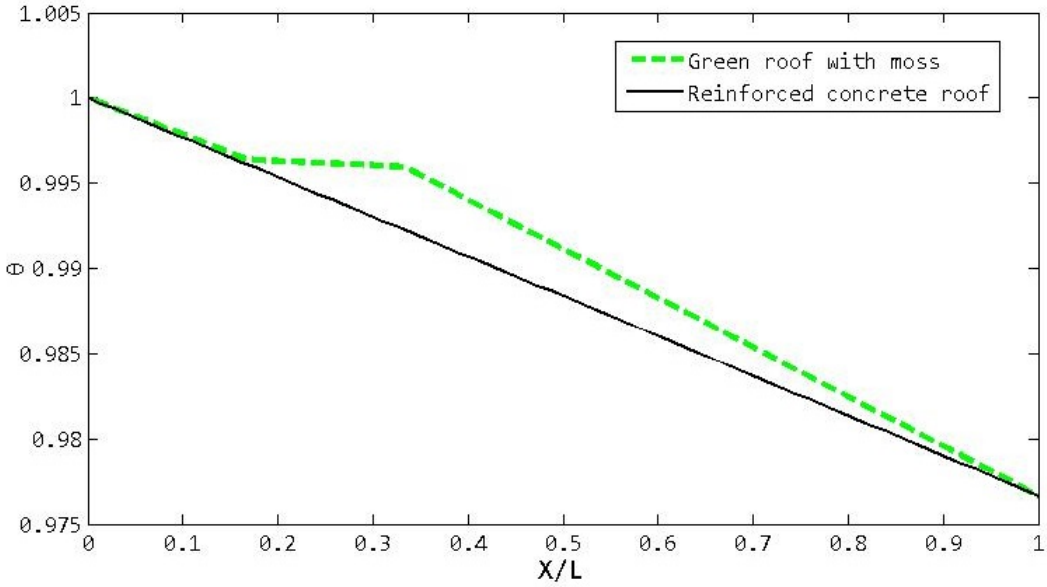

Figure 89: Temperature profiles for Reinforced concrete roof and Green Roof calculated from equations 61 and 62.

control volume is needed.

Temperature profile in one-dimensional semitransparent media which is transferring heat by radiation and conduction is commonly a nonlinear function, but here, the variation of the ratio with position seems linear as the difference between the boundary temperatures was low. The ratio in the Figure 89 has a rising trend from right to left because of the increasing temperature in that direction.

The equivalent thermal conductivity which is the most significant property of insulating material, is evaluated from Equations 65 and 66. [97]. Figure 90 shows the comparison of the equivalent thermal conductivity between the two models. Figure 91 represents the ratio of radiative flux to total flux for both reinforced concrete roof model and green roof model.

Radiative flux is the second term in Equation 65 which is the total flux. The high difference of the Ratio of radiative flux to total flux on the surface of the green model is related to the dependence of the spectral emissivity to radiative heat flux, which is higher in the moss sample rather than the PPC one.

In thick materials the ratio of radiative to total heat flux would not be constant

along the position as the radiation is a surface phenomenon and the conductive heat flux and the radiative heat flux in optically thick materials are proportional to the negative gradient of the temperature (-∇T).

In the following, coupled radiation and conduction was solved for two other types of plants; leaf and cactus, for comparing with the moss sample for evaluating the heat transfer (conduction and radiation) among these samples.

Figure 92 depicts the temperature profile in the moss, cactus and leaf. As it is clear from the Figure 92, the non-dimensional temperature of leaf and cactus are too close too each other and the moss has the lower temperature profile in comparing with them.

Figure 93 represents the equivalent conductivity in three plant samples. Leaf and cactus have the same value of equivalent conductivity and the moss sample has the lower value in comparing with them. At last, in comparing the various plant samples, Figure 94 shows the ratio of radiative flux to total flux which leaf has the highest ratio and the moss sample has the lowest one. It should be mentioned that the thickness for this section was 2 cm for concrete and 1 cm for the soil and plant.

Mosses are small flowerless plants which typically grow in dense green mats or clumps, often in shady or damp locations. This contrasts with the pattern in all vascular plants, as they do not have vascular tissue (special kind of plant tissue that is used to transport nutrients and water through the plant). Because of that, mosses lack stem, root, and flowersMosses have such characteristics that distinguish them from other plants. They have a root-like subterranean tissue (multicellular rhizoid) that absorbs water and nutrients from the soil. These can be the reasons that the moss show different thermal behavior in comparing with leaf and cactus which are vascular plants [91].

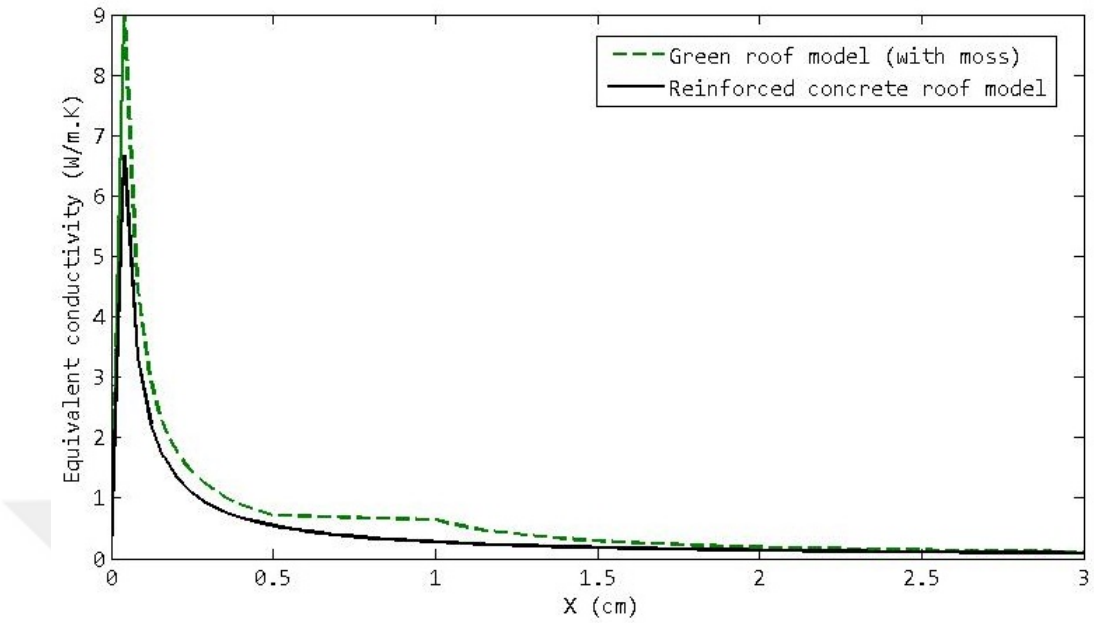

Figure 90: Equivalent thermal conductivities of both models (green roof with moss and reinforced concrete calculated from equations 65 and 66).

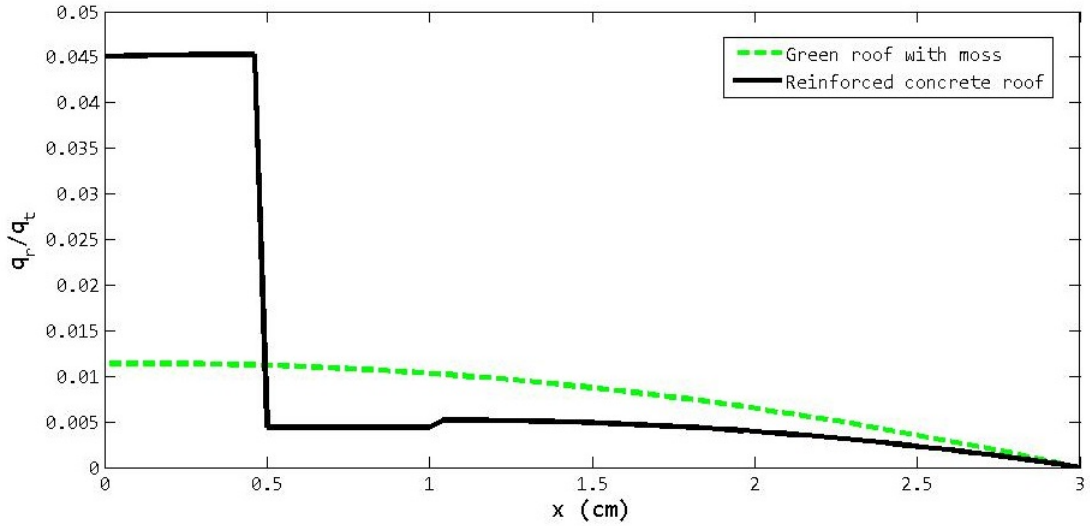

Figure 91: Ratio of radiative flux to total flux calculated from equation 65.

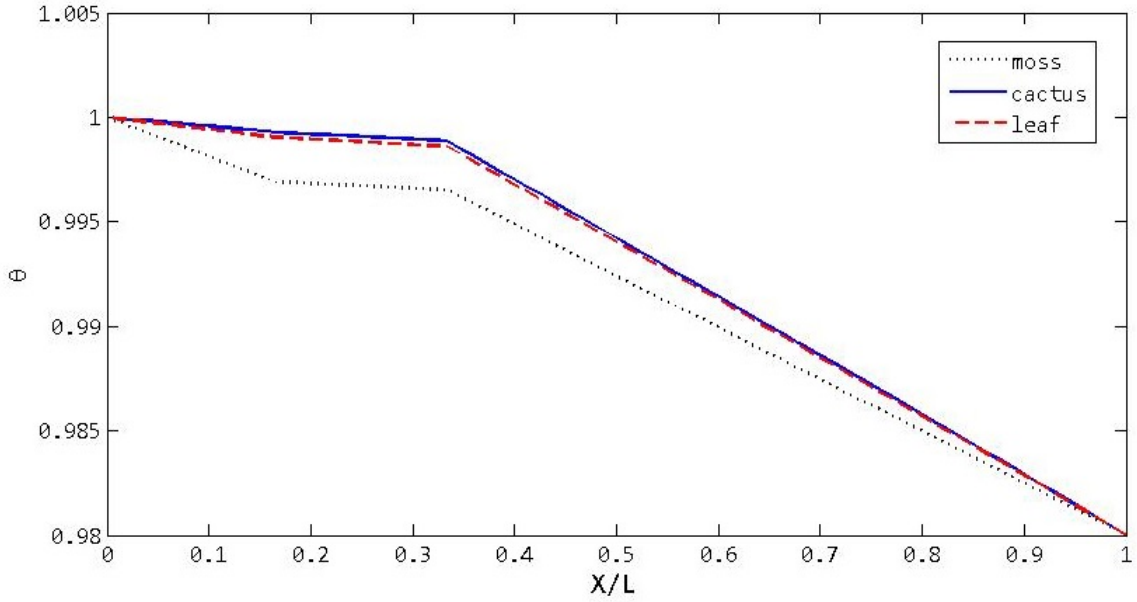

Figure 92: Temperature profiles for plant samples calculated from equations 61 and 62.

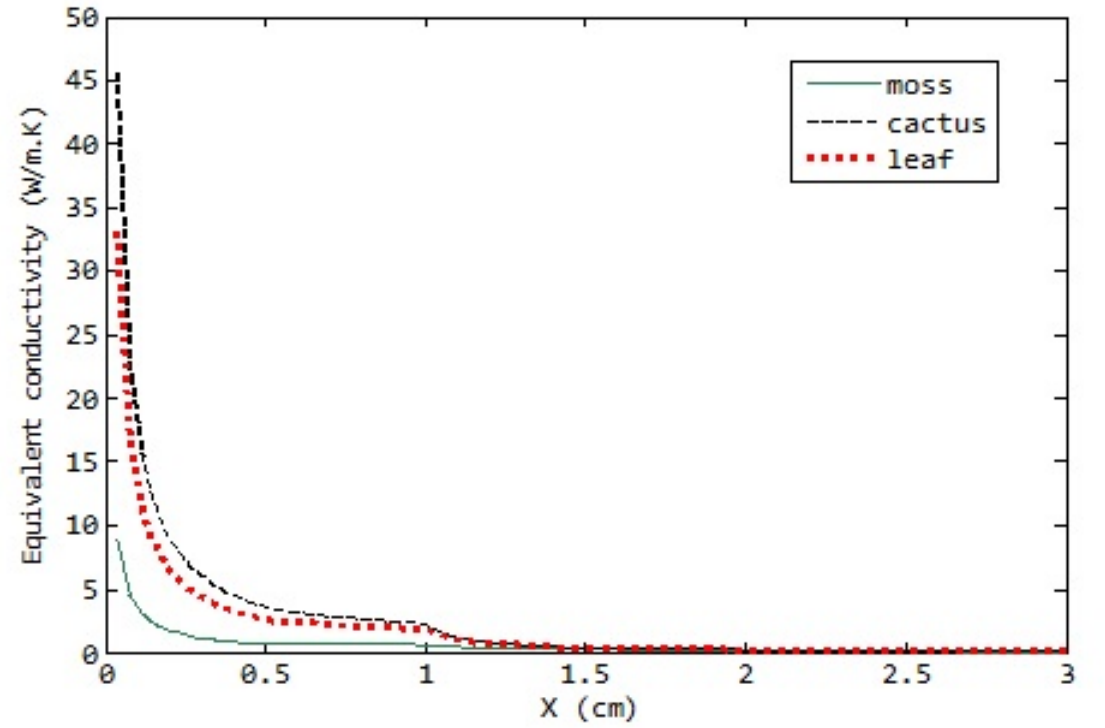

Figure 93: Equivalent thermal conductivities of plant samples calculated from equations 65 and 66.

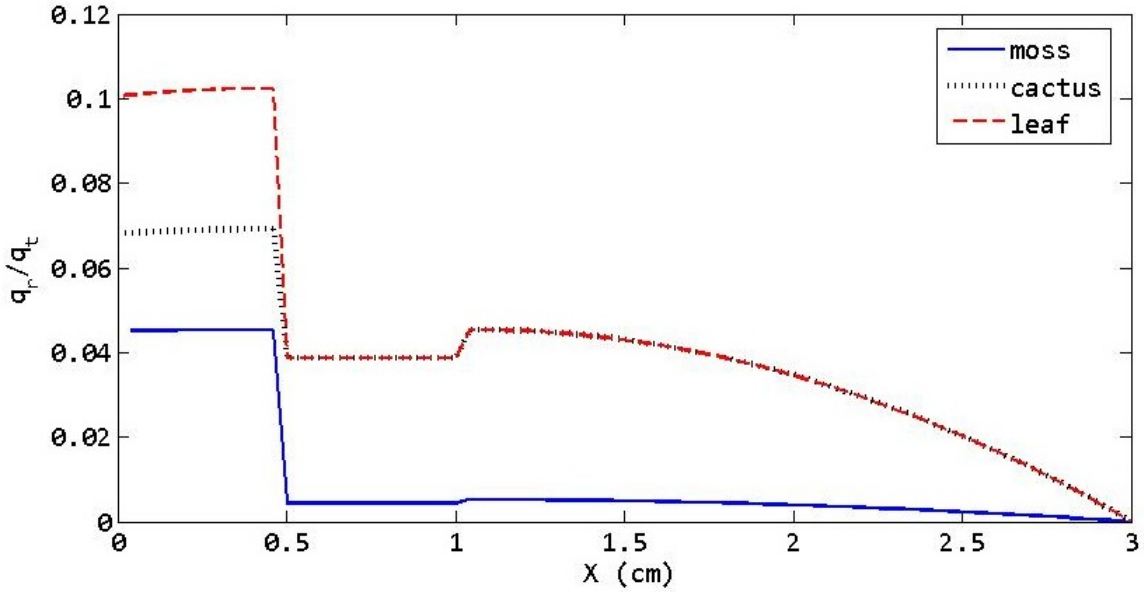

Figure 94: Ratio of radiative flux to total flux of plant samples calculated from equation 65.

Chapter VI

CONCLUSIONS AND FUTURE WORK

6.1 Conclusions

In this study, several sustainable materials were analyzed to explore their radiative heating and cooling potentials. These materials have several environmental benefits, such as being non-toxic, reusable, and renewable; and they can enhance the cooling performance of the roofs and walls of buildings in an inexpensive way. When choosing the materials for this study, the emphasis was on the following criteria:

1. Materials which have high spectral emissivity in both solar band (0.2–2 μm) and atmospheric window (8–13 μm) were considered; these materials are good candidates as solar collectors at daytime, and solar emitters or radiator coolers at night time.

2. Materials which have high spectral emissivity in the atmospheric window (8–13 μm) and low spectral emissivity outside of this window were considered; radiative cooling can be achieved on the surface of these materials, and they are good candidates as radiative coolers at daytime.

3. Materials which have high spectral emissivity at solar band and low spectral emissivity in other bands were considered; as they are good candidates for solar energy absorption.

Based on these criteria, red membrane, black membrane, XPS, PPC, painted PPC, and moss were considered. These materials were available and abundant in Turkey, where the study was conducted. Among these, moss, PPC, and painted PPC could be considered as radiative coolers, and black membrane would be a solar absorber.

As the optical properties of the materials were not available in the literature,

as a first step, the experimental analyses for all samples were carried out and their spectral emissivity and reflectivity were measured using an FTIR spectrometer and UV-Visible spectrophotometer. These results were later converted to spectral absorption coefficient data.

Meanwhile, Optical image of the materials with some other sustainable materials for morphology analysis is shown. In addition, the spectral emissivity of a category of different materials for future studies has been presented.

In numerical analysis, the power of cooling for the opaque samples at constant temperature was calculated (for 6 selected materials). Results were compared against an ideal selective emitter and broadband emitter. The best sample for potential radiative cooling purposes was deemed to be moss, whose power of cooling was even higher than Silicon oxide samples. Power of cooling was also calculated for all samples, for summer and winter daytime and nighttime performances, and then they were compared against those of a selective ideal emitter and broadband emitter.

Radiation transfer is usually a volumetric phenomenon, as such a coupled conduction and radiation analysis was also carried out for semi-transparent materials. A numerical model was developed and solved with MATLAB, using the experimental spectral absorption coefficient and thermal conductivity data obtained from the experiments (for 6 selected samples). In order to validate the codes, the coupled conduction and radiation problem was first solved for a gray case, and then compared against the data available in the literature. These coupled analyses were then extended to non-gray materials using stepwise gray box models.

Among all materials considered, moss was deemed to be the best candidate as a sustainable material to be used as a radiative cooler for outside surfaces of buildings. However, its conductivity was higher than a sample like XPS, for being a good insulator. Therefore, moss should be grown on a better insulator surface to have the highest possible benefit from it. A summary of the findings of the present study for different materials considered, is presented in Table 2 to help the reader

to make a quick comparison between them.

In the last section, a one dimensional model of heat transfer by radiation and conduction was developed in two different roofs (reinforced concrete roof and reinforced concrete with a green layer of on the surface). The present method provides evaluating the radiation for outside of the building through measuring spectral emissivity and calculating the power of the cooling for the sake of radiative cooling. Meanwhile, this method evaluated the total heat transfer (coupled radiation and conduction) through the roofs.

In the first step, as it was shown before the spectral emissivity of the green roof (with moss on the surface) was higher than the reinforced concrete roof (with PPC on the surface), so green model would be a better radiative cooler.

In the next step, in comparing to other approaches in coupled radiation and conduction and also in heat transfer studies through the roofs, heat conduction and radiation for a non-gray case via stepwise gray box model was solved, at last, it was admitted that the green roof model is more effective in radiative cooling rather than reinforced concrete roof.

Eventually, the moss was substituted with two other types of plants; leaf and cactus in power of cooling, and coupled conduction and radiation heat transfer, which demonstrated that the moss is the best plant material on the surface of the building roofs.

6.1.1 Key Findings

1. Materials which was used for radiative cooling in other studies were expensive such as different oxides and non-oxides ceramics but in this study a model was derived for any material including sustainable materials in any conditions.

2. Models for radiative cooling applications generally used for solar panels but in this work, a new model established for roofs in the buildings.

3 .Models which were defined for radiative cooling were only established for radiation on the surface assuming a thin layer but in this work a realistic model was developed considering coupled conduction and radiation.

4. Coupled conduction and radiation for a non-gray case was solved and the relation between it with selecting the best radiative cooler was shown.

5. Coupled conduction and radiation was solved for a real green roof (concrete with soil and moss on the surface of it), it compared with the reinforced concrete roof in radiative cooling. In addition, three types pf plants which were; leaf, cactus and moss were compared for selecting the best plant as a radiative cooler.

6.2 Future Work

1. This study was developed for radiative cooling and radiation and conduction heat transfer through the roofs, it can be developed for other applications as well with this procedure.

2. In this study for the first time, there was a look to sustainable materials and inexpensive materials in radiative cooling, with these results new group of materials can be introduced for this application.

3. A morphology and spectral emissivity of a lot of sustainable materials are presented in this study for the first time. The power of the cooling and coupled conduction and radiation of them can be calculated for comparing with the selected materials.

4. This model was developed for bulk materials which are ideal, the future work can be analyzing the impacts of porosity on radiative cooling and heat transfer via coupled radiation and conduction through the roofs, new category of composite materials also can be substituted instead of the materials in this study (in one layer or more layers).

5. This study was defined for a defined parameters. In the future, this study can be done with new parameters and the results can be compared with this study. For example: Conduction and convection were neglected in power of the cooling part, so they can be added.

6. Experimental temperature measurement test on the surface with measuring the ambient temperature and irradiation was not done, it can be done in different atmospheric situations.

Bibliography

[1] M. A. Kamal, "An Overview of Passive Cooling Techniques in Buildings: Design Concepts and Architectural Interventions," *Acta Technica Napocensis: Civil Engineering & Architecture*, vol. 55, no. 1, 2012.

[2] IEA, "Energy and Climate Change," *World Energy Outlook Special Report*, pp. 1–200, 2015.

[3] A. K. Elsadig, *Energy Efficiency in Commercial Buildings*. PhD thesis, University of Strathclyde 2005.

[4] M. S. McClaren, "Energy Efficiency and Conservation Attitudes: An Exploration of a Landscape of Choices," *ProQuest Dissertations and Theses*, p. 210, Prtlan State University 2015.

[5] K. Ashley Shell, "Analysis of Energy Efficiency Strategies in Residential Buildings Thesis," The Ohio State University 2010.

[6] D. H. C. Toe, "Application of Passive Cooling Techniques to Improve Indoor Thermal Comfort of Modern Urban Houses in Hot-Humid Climate of Malaysia," *Graduate School for International Development and Cooperation of Hiroshima University*, no. September, 2013.

[7] B. B. Naghshine and A. Saboonchi, "Optimized thin film coatings for passive radiative cooling applications," *Optics Communications*, vol. 410, pp. 416–423, 2018.

[8] X. Lu, P. Xu, H. Wang, T. Yang, and J. Hou, "Cooling potential and applications prospects of passive radiative cooling in buildings: The current state-of-the-art," *Renewable and Sustainable Energy Reviews*, vol. 65, no. 4800, pp. 1079–1097, 2016.

[9] C. Y. Tso, K. C. Chan, and C. Y. Chao, "A field investigation of passive radiative cooling under Hong Kong's climate," *Renewable Energy*, vol. 106, pp. 52–61, 2017.

[10] M. M. Hossain and M. Gu, "Radiative cooling: Principles, progress, and potentials," *Advanced Science*, vol. 3, no. 7, pp. 1–10, 2016.

[11] J. R. Howell, M. P. Menguc, and R. Siegel, *Thermal Radiation Heat Transfer*. CRC Press: Boca Raton, FL, USA; Taylor & Francis: Didcot, UK; Abingdon, UK, 6th ed., 2016.

[12] L. Zhu, A. Raman, and S. Fan, "Color-preserving daytime radiative cooling," *Applied Physics Letters*, vol. 103, no. 22, p. 223902, 2013.

[13] R. Dunkle, "Thermal Radiation Characteristics of Surfaces," *Theory and Fundamental Research in Heat Transfer*, pp. 1–31, 1963.

[14] D. F. Hall and F. A. A., "Thermal control coatings performance at near geosynchoronous altitude," *JTHT*, vol. 6, no. 4, pp. 665–671, 1992.

[15] A. Poullikkas, I. Hadjipaschalis, and G. Kourtis, "A comparative overview of wet and dry cooling systems for Rankine cycle based CSP plants," *Trends in Heat and Mass Transfer*, vol. 13, no. January 2013, pp. 27–50, 2013.

[16] J. H. Henninger, "Solar Absorptance and Thermal Emittance of Some Common Spacecreaft Thermal Control Coatings," *Nasa Reference Publication*, vol. 1121, 1984.

[17] X. Wang, D. Jiang, and X. Lang, "Future extreme climate changes linked to global warming intensity," *Science Bulletin*, vol. 62, no. 24, pp. 1673–1680, 2017.

[18] T. Ekström, R. Bernardo, and A. Blomsterberg, "Cost-effective passive house renovation packages for Swedish single-family houses from the 1960s and 1970s," *Energy and Buildings*, vol. 161, pp. 89–102, 2018.

[19] S. Mazumder, "A new numerical procedure for coupling radiation in participating media with other modes of heat transfer," *Journal of Heat Transfer*, vol. 127, no. 9, pp. 1037–1045, 2005.

[20] M. F. Rose, P. Adair, and K. Schroeder, "Selective emitters for thermophotovoltaic power systems for use in aerospace applications," *Journal of Propulsion and Power*, vol. 12, pp. 83–88, 1996.

[21] S. Wijewardane and D. Y. Goswami, "A review on surface control of thermal radiation by paints and coatings for new energy applications," *Renewable and Sustainable Energy Reviews*, vol. 16, no. 4, pp. 1863–1873, 2012.

[22] A. Licciulli, D. Diso, G. Torsello, S. Tundo, A. Maffezzoli, M. Lomascolo, and M. Mazzer, "The challenge of high-performance selective emitters for thermophotovoltaic applications," *Semiconductor Science and Technology*, vol. 18, no. 5, 2003.

[23] B. D. Reed, J. Biglow, and S. Schneider, "Engineering Issues of Iridium Coated Rhenium Rockets," *Materials and Manufacturing Processes*, vol. 13, no. 5, 1998.

[24] A. Sentenac and J. Greffet, "Design of surface microrelief with selective radiative properties," *IJHMT*, vol. 37, no. 4, pp. 553–558, 1994.

[25] J. J. Greffet and C. Henkel, "Coherent thermal radiation," *Contemporary Physics*, vol. 48, no. 4, pp. 183–194, 2007.

[26] C. G. Granqvist and A. Hjortsberg, "Radiative cooling to low temperatures: General considerations and application to selectively emitting SiO films," *Journal of Applied Physics*, vol. 52, no. 4205, 1981.

[27] C. G. Granqvist, "Radiative heating and cooling with spectrally selective surfaces," *Appl. Opt.*, vol. 20, no. 15, pp. 2606–2615, 1981.

[28] M. G. Meir, J. B. Rekstad, and O. M. Lovvik, "A study of a polymer-based radiative cooling system," *Solar Energy*, vol. 73, no. 6, pp. 403–417, 2002.

[29] K. D. Dobson, G. Hodes, and Y. Mastai, "Thin semiconductor films for radiative cooling applications," *Solar Energy Materials and Solar Cells*, vol. 80, no. 3, pp. 283–296, 2003.

[30] M. Benlattar, E. M. Oualim, M. Harmouchi, A. Mouhsen, and A. Belafhal, "Radiative properties of cadmium telluride thin film as radiative cooling materials," *Optics Communications*, vol. 256, no. 1-3, pp. 10–15, 2005.

[31] M. Benlattar, E. M. Oualim, T. Mouhib, M. Harmouchi, A. Mouhsen, and A. Belafhal, "Thin cadmium sulphide film for radiative cooling application," *Optics Communications*, vol. 267, no. 1, pp. 65–68, 2006.

[32] H. Gonome, M. Baneshi, J. Okajima, A. Komiya, and S. Maruyama, "Controlling the radiative properties of cool black-color coatings pigmented with CuO submicron particles," *Journal of Quantitative Spectroscopy and Radiative Transfer*, vol. 132, pp. 90–98, 2014.

[33] G. B. Smith, A. Gentle, P. D. Swift, A. Earp, and N. Mronga, "Coloured paints based on iron oxide and silicon oxide coated flakes of aluminium as the pigment, for energy efficient paint: Optical and thermal experiments," *Solar Energy Materials and Solar Cells*, vol. 79, no. 2, pp. 179–197, 2003.

[34] J. A. Johnson, J. J. Heidenreich, R. A. Mantz, P. M. Baker, and M. S. Donley, "A multiple-scattering model analysis of zinc oxide pigment for spacecraft thermal control coatings," *Progress in Organic Coatings*, vol. 47, no. 3-4, pp. 432–442, 2003.

[35] W. E. Vargas, A. Amador, and G. A. Niklasson, "Diffuse reflectance of TiO2 pigmented paints: Spectral dependence of the average pathlength parameter and the forward scattering ratio," *Optics Communications*, vol. 261, no. 1, pp. 71–78, 2006.

[36] R. Levinson, P. Berdahl, H. Akbari, W. Miller, I. Joedicke, J. Reilly, Y. Suzuki, and M. Vondran, "Methods of creating solar-reflective nonwhite surfaces and their application to residential roofing materials," *Solar Energy Materials and Solar Cells*, vol. 91, no. 4, pp. 304–314, 2007.

[37] H. Gonome, M. Baneshi, J. Okajima, A. Komiya, and S. Maruyama, "Controlling the radiative properties of cool black-color coatings pigmented with CuO submicron particles," *Journal of Quantitative Spectroscopy and Radiative Transfer*, vol. 132, pp. 90–98, 2014.

[38] M. Hu, G. Pei, L. Li, R. Zheng, J. Li, and J. Ji, "Theoretical and Experimental Study of Spectral Selectivity Surface for Both Solar Heating and Radiative Cooling," *International journal of photoenergy*, vol. 2015, 2015.

[39] C. N. Suryawanshi and C. T. Lin, "Radiative cooling: Lattice quantization and surface emissivity in thin coatings," *ACS Applied Materials and Interfaces*, vol. 1, no. 6, pp. 1334–1338, 2009.

[40] H. Bao, C. Yan, B. Wang, X. Fang, C. Y. Zhao, and X. Ruan, "Double-layer nanoparticle-based coatings for efficient terrestrial radiative cooling," *Solar Energy Materials and Solar Cells*, vol. 168, no. November 2016, pp. 78–84, 2017.

[41] P. C. Hsu, A. Y. Song, P. B. Catrysse, C. Liu, Y. Peng, J. Xie, S. Fan, and Y. Cui, "Radiative human body cooling by nanoporous polyethylene textile," *Science*, vol. 353, no. 6303, pp. 1019–1023, 2016.

[42] A. M. Baldridge, S. J. Hook, C. Grove, and G. Rivera, "The ASTER spectral library version 2.0," *Remote Sensing of Environment*, vol. 113, pp. 711–715, 2009.

[43] E. Rephaeli, A. Raman, and S. Fan, "Ultrabroad band Photonıc structures-Fan group," *Nano Letters*, vol. 13, pp. 1457–1461, 2013.

[44] A. P. Raman, M. A. Anoma, L. Zhu, E. Rephaeli, and S. Fan, "Passive radiative cooling below ambient air temperature under direct sunlight," *Nature*, vol. 515, no. 7528, pp. 540–544, 2014.

[45] K. Zhang, D. Zhao, X. Yin, R. Yang, and G. Tan, "Energy saving and economic analysis of a new hybrid radiative cooling system for single-family houses in the USA," *Applied Energy*, vol. 224, no. March, pp. 371–381, 2018.

[46] R. Family and M. P. Menguc, "Materials for Radiative Cooling: A Review," *Procedia Environmental Sciences*, vol. 38, pp. 752–759, 2017.

[47] S. H. Mousavi-Nasab and A. Sotoudeh-Anvari, "A new multi-criteria decision making approach for sustainable material selection problem: A critical study on rank reversal problem," *Journal of Cleaner Production*, vol. 182, pp. 466–484, 2018.

[48] K. Fic, A. Platek, J. Piwek, and E. Frackowiak, "Sustainable materials for electrochemical capacitors," *Materials Today*, vol. 21, no. 4, pp. 437–454, 2018.

[49] B. Panda, S. Chandra Paul, and M. Jen Tan, "Anisotropic mechanical performance of 3D printed fiber reinforced sustainable construction material," *Materials Letters*, vol. 209, pp. 146–149, 2017.

[50] J. R. Wunsch, "Polystyrene – Synthesis, Production and Applications," *iSmithers Rapra Publishing*, p. 15, 2000.

[51] J. GmbH, "What is XPS (extruded polystyrene foam)," tech. rep., Foam Technology, 2001.

[52] M. C. Pumping, "Foam Pouring Concrete: Making High Performance homes With Sustainability.," tech. rep., 2016.

[53] V. Vaou and D. Panias, "Thermal insulating foamy geopolymers from perlite," *Minerals Engineering*, vol. 23, no. 14, pp. 1146–1151, 2010.

[54] A. Benk and A. Coban, "Possibility of producing lightweight, heat insulating bricks from pumice and (H_3PO_4) or NH_4NO_3-hardened molasses binder," *Ceramics International*, vol. 38, no. 3, pp. 2283–2293, 2012.

[55] L. Gündüz, "The effects of pumice aggregate/cement ratios on the low-strength concrete properties," *Construction and Building Materials*, vol. 22, no. 5, pp. 721–728, 2008.

[56] M. Alam, H. Singh, S. Brunner, and C. Naziris, "Experimental characterisation and evaluation of the thermo-physical properties of expanded perlite - Fumed silica composite for effective vacuum insulation panel (VIP) core," *Energy and Buildings*, vol. 69, pp. 442–450, 2014.

[57] J. Chen, W. Huang, S. Jiang, X. Y. Li, Y. An, C. Li, X. L. Gao, and H. B. Chen, "radiation resistance crossmark," *Radiation Physics and Chemistry*, vol. 130, no. September 2016, pp. 400–405, 2017.

[58] S. Kültür and N. Türkeri, "Assessment of long term solar re fl ectance performance of roof coverings measured in laboratory and in fi eld," *Building and Environment*, vol. 48, pp. 164–172, 2012.

[59] M. P. Brennan, A. L. Abramase, R. W. Andrews, and J. M. Pearce, "Solar Energy Materials & Solar Cells Effects of spectral albedo on solar photovoltaic devices," *Solar Energy Materials and Solar Cells*, vol. 124, pp. 111–116, 2014.

[60] K. Wattanavatee, M. Krmar, and T. Bhongsuwan, "A survey of natural terrestrial and airborne radionuclides in moss samples from the peninsular Thailand," *Journal of Environmental Radioactivity*, vol. 177, pp. 113–127, 2017.

[61] X. Liu, Z. Li, K. Zhong, Y. J. Chao, P. Miraldo, and Y. Shi, "Generic distortion model for metrology under optical microscopes," *Optics and Lasers in Engineering*, vol. 103, pp. 119–126, 2018.

[62] C. V. Vo, F. Bunge, J. Duffy, and L. Hood, "Advances in thermal insulation of extruded polystyrene foams," *Cellular Polymers*, vol. 30, no. 3, pp. 137–156, 2011.

[63] P. Klõšeiko, K. Varda, and T. Kalamees, "Effect of freezing and thawing on the performance of "capillary active" insulation systems: A comparison of results from climate chamber study to HAM modelling," *Energy Procedia*, vol. 132, pp. 525–530, 2017.

[64] A. Oushabi, S. Sair, Y. Abboud, O. Tanane, and A. E. Bouari, "An experimental investigation on morphological, mechanical and thermal properties of date palm particles reinforced polyurethane composites as new ecological insulating materials in building," *Case Studies in Construction Materials*, vol. 7, no. February, pp. 128–137, 2017.

[65] R. Dylewski and J. Adamczyk, "The comparison of thermal insulation types of plaster with cement plaster," *Journal of Cleaner Production*, vol. 83, pp. 256–262, 2014.

[66] A. Y. Katukiza, M. Ronteltap, C. B. Niwagaba, F. Kansiime, and P. N. L. Lens, "A two-step crushed lava rock filter unit for grey water treatment at household level in an urban slum," *Journal of Environmental Management*, vol. 133, pp. 258–267, 2014.

[67] M. Aufaristama, Höskuldsson, I. Jónsdóttir, and R. Ólafsdóttir, "Mapping and Assessing Surface Morphology of Holocene Lava Field in Krafla (NE Iceland) Using Hyperspectral Remote Sensing," *IOP Conference Series: Earth and Environmental Science*, vol. 29, no. 1, 2016.

[68] D. Ricci, F. Bassetti, and S. Savastano, "Beneficial effects of dry bottom ash extraction and recycling in modern PCF power plants," *Fuel*, vol. 215, pp. 13–21, 2018.

[69] N. Cesar, C. Universidade, R. Grande, K. Salvagni, H. Universidade, and R. Grande, "Coal Bottom Ash As a Geomaterial : Influence of Particle Morphology on the Behavior of Granular Materials," *SOILS AND FOUNDATIONS*, no. 2, pp. 361–373, 2015.

[70] Y. Li and R. W. Babcock, "Green roofs against pollution and climate change. A review," *Agronomy for Sustainable Development*, vol. 34, no. 4, pp. 695–705, 2014.

[71] R. S. Khandpur, *Handbook of Analytical Instruments*. Tata McGraw-Hill, third ed., 1989.

[72] M. Hu, G. Pei, Q. Wang, J. Li, Y. Wang, and J. Ji, "Field test and preliminary analysis of a combined diurnal solar heating and nocturnal radiative cooling system," *Applied Energy*, vol. 179, pp. 899–908, 2016.

[73] F. V. Silva, S. Resende, A. N. Araújo, and J. A. Prior, "Determination of pKa(s) of nilutamide through UV-visible spectroscopy," *Microchemical Journal*, vol. 138, no. 2017, pp. 303–308, 2018.

[74] T. Aziz, M. Waters, and R. Jagger, "Analysis of the properties of silicone rubber maxillofacial prosthetic materials," *Journal of Dentistry*, vol. 31, no. 1, pp. 67–74, 2003.

[75] D. Wang and G. P. Bierwagen, "Sol-gel coatings on metals for corrosion protection," *Progress in Organic Coatings*, vol. 64, no. 4, pp. 327–338, 2009.

[76] P. Bermel, J. Lee, J. Joannopoulos, I. Celanovic, and M. Soljacic, "Selective Solar Absorbers," *Annual Review of Heat Transfer*, pp. 231–254, 2012.

[77] T. Rymsza, E. A. Ribeiro, L. F. d. C. e. de Carvalho, T. Bhattacharjee, and R. de Azevedo Canevari, "Human papillomavirus detection using PCR and ATR-FTIR for cervical cancer screening," *Spectrochimica Acta - Part A: Molecular and Biomolecular Spectroscopy*, vol. 196, pp. 238–246, 2018.

[78] P. R. Griffiths, J. A. De Haseth, and J. D. Winefordner, *Fourier Transform Infrared Spectrometry*. 2nd ed., 2007.

[79] B. L. Hernández Velasco, D. Arrieta-Baez, P. I. Cortez Sotelo, J. V. Méndez-Méndez, B. M. Berdeja Martínez, and M. B. Gómez-Patiño, "Comparative studies of cutins from lime (Citrus aurantifolia) and grapefruit (Citrus paradisi) after TFA hydrolysis," *Phytochemistry*, vol. 144, pp. 78–86, 2017.

[80] N. M. Ravindra, P. Ganapathy, and J. Choi, "Energy gap – refractive index relations in semiconductors – An overview," vol. 50, pp. 21–29, 2007.

[81] M. P. Menguc, "Heat Transfer in a Radiating Laminar Flow between Parallel Plates," 1980.

[82] J. S. Cheong, A. N. A. P. Baharuddin, J. S. Ng, A. B. Krysa, and J. P. R. David, "Solar Energy Materials & Solar Cells Absorption coe ffi cients in AlGaInP lattice-matched to GaAs," vol. 164, no. September 2016, pp. 28–31, 2017.

[83] C. Proctor, B. Lu, and Y. He, "Remote Sensing of Environment Determining the absorption coef fi cients of decay pigments in decomposing monocots," *Remote Sensing of Environment*, vol. 199, pp. 137–153, 2017.

[84] B. Ribeiro da Luz and J. K. Crowley, "Spectral reflectance and emissivity features of broad leaf plants: Prospects for remote sensing in the thermal infrared (8.0-14.0 μm)," *Remote Sensing of Environment*, vol. 109, no. 4, pp. 393–405, 2007.

[85] H. Haiming and E. Collaboration, "The status of R value measurement at BESIII," in *Nuclear and Particle Physics Proceedings*, vol. 287-288, pp. 61–64.

[86] G. Huelsz, F. Gomez, M. Pineirua, J. Rojas, M. de Alba, and V. Guerra, "Evaluation of refrigerator/freezer gaskets thermal loads," *HVAC&R Research*, vol. 17, no. 2, pp. 133–143, 2011.

[87] C. Hermes, C. Melo, and F. Knabben, "Alternative Energy Test Method for Frost-Free Refrigerators and Freezers," *International Refrigeration and Air Conditioning Conference*, pp. 1–9, 2012.

[88] J. M. Goncalves, C. Melo, C. J. L. Hermes, and J. R. Barbosa Jr, "Experimental Mapping of the Thermodynamic Losses in Vapor Compression Refrigeration Systems," *Journal of the Brazilian Society of Mechanical Sciences and Engineering*, vol. 33, no. 2, pp. 159–165, 2011.

[89] V. Parenti and H. Kramer, "PASCAL TM Technology: A Novel Breakthrough Polyurethane Foaming Technology for Domestic Appliance Insulation,"

[90] S. D. Lord, "A New Software Tool for Computing Earth's Atmospheric Transmission of Near- and Far-Infrared Radiation," tech. rep., NASA Technical Memorandum 103957, IR Transmission Spectra, Gemini Observatory, 1992.

[91] S. Frankenstein and G. Koenig, "FASST Vegetation Models," tech. rep., US Army Corps of Engineers Technical Report, TR-04-25, 2004.

[92] R. J. Moffat, "Describing the Uncertainties in Experimental Results," *Experimental Thermal and Fluid Science*, vol. 1, pp. 3–17, 1988.

[93] M. F. Modest, *Radiative Heat Transfer*. Academic Press: Cambridge, MA, USA, 3rd ed., 2003.

[94] M. F. Modest and S. Lei, "The simplified spherical harmonics method for radiative heat transfer," *Journal of Physics: Conference Series*, vol. 369, no. 1, 2012.

[95] S. Whitaker, *Fundamental Principles of Heat Transfer*. Pergamon, 1977.

[96] R. Viskanta and M. P. Menguc, "Radiation heat transfer in combustion systems," *Progress in Energy and Combustion Science*, vol. 13, no. 2, pp. 97–160, 1987.

[97] P. Ferkl, R. Pokorný, M. Bobák, and J. Kosek, "Heat transfer in one-dimensional micro- and nano-cellular foams," *Chemical Engineering Science*, vol. 97, pp. 50–58, 2013.

[98] R. Family and M. P. Menguc, "Analysis of Sustainable Materials for Radiative Cooling Potential of Building Surfaces," *Sustainability*, vol. 10, 2018.

[99] S. N. Bathgate and S. G. Bosi, "Solar Energy Materials & Solar Cells A robust convection cover material for selective radiative cooling applications," vol. 95, pp. 2778–2785, 2011.

[100] A. Hervé, J. Drevillon, Y. Ezzahri, K. Joulain, A. Hervé, J. Drevillon, Y. Ezzahri, and K. Joulain, "Radiative cooling by tailoring surfaces with microstructures To cite this version : HAL Id : hal-01680256 Radiative cooling by tailoring surfaces with microstructures," 2018.

[101] C. G. Somana, "Evaluation of Aerogel Composite Insulations by Characterization and Experimental Methods," University of Kansas 2012.

[102] S. Celik, R. Family, and M. P. Menguc, "Analysis of perlite and pumice based building insulation materials," *Journal of Building Engineering*, vol. 6, pp. 105–111, 2016.

[103] S. Celik, R. Family, and M. P. Menguc, "Thermal evaluation of Perlite and Pumice based building insulation materials using reverse," *First Thermal and Fluids Engineering Summer Conference*, pp. 1–8, 2015.

[104] F. P. Incropera, D. P. DeWitt, T. L. Bergman, and A. S. Lavine, *Fundamentals of Heat and Mass Transfer*. 6th ed., 2006.

[105] M. Menguc, Y. Yener, and M. N. Ozisik, "Interaction of Radiation and Convection in Thermally Developing Laminar Flow in a Parallel-Plate Channel," in *Proceedings of the ASME National Heat Transfer Conference*, (Seattle, WA, USA), 1983.

[106] P. Wang, H. Tan, L. Liu, and T. Tong, "Coupled radiation and conduction in a scattering composite layer with coatings," *Thermophys. Heat Transfer*, vol. 14, pp. 512–522, 2000.

VITA

Roxana Family was born in Tehran, Iran. After getting the diploma in Mathematics and Physics, she enrolled in two Bachelors in the university simultaneously. She received her Bachelor of Science in Materials and Metallurgical engineering (Ceramics) from Islamic Azad University in 2006. She worked in Shahed University Research Center (Nanotechnology and Dentistry Center) as a researcher for two years. She got her second Bachelor of Art in English Language Interpretation and Translation in this period of time. In 2008, she started her Master of Science in Materials and Metallurgical engineering (Ceramics) in Islamic Azad University (Science and Research branch in Tehran). In 2011, she finished her MS with one ISI, two ISC, two international conference, and three national conference papers with an Iranian patent. Then she joined Islamic Azad University (Shahrood branch) as a lecturer in the Materials engineering department for three semesters before joining Ozyegin University. In 2013, she started her Ph.D. in Mechanical engineering in Ozyegin University, and in 2014, she joined Professor Pinar Menguc group (ECEM/CEEE) and started her work under his supervision in "Radiative cooling by spectrally selective materials for buildings". She published papers in three international conferences and three ISI journals in the duration of her Ph.D.